2008

Three dimensional finite element modeling of stacked geotextile tubes for embankment stabilization

Mark Wayne McElroy
Lehigh University

McElroy, Mark Wayne, Jr.

Three Dimensional Finite Element Modeling of Stacked Geotextile Tubes...

January 2008

Three Dimensional Finite Element Modeling of Stacked Geotextile Tubes for Embankment Stabilization

by

Mark Wayne McElroy Jr.

A Thesis

Presented to the Graduate and Research Committee

of Lehigh University

in Candidacy for the Degree of

Master of Science

in

Civil and Environmental Engineering

Lehigh University

January 2008

This thesis is accepted and approved in partial fulfillment of the requirements for the Master of Science.

October 24, 2007

Date

Thesis Advisor

Chairperson of Department

Acknowledgements

I would like to thank my two co-advisors, Mesut Pervizpour and Sibel Pamukcu, for their consistent support throughout my research. Sibel Pamukcu provided me with the opportunity to pursue a research topic of my own choosing. She helped me to initially develop my research goals and continued to guide me as my work progressed. I cannot express enough appreciation for all of the time and effort Mesut Pervizpour put into helping me with this project. He spent countless hours getting directly involved with my work and helping me through problems. He was instrumental in my development as researcher and as a modeler. And finally, I would like to thank my family for their continued support and encouragement throughout my education.

Table of Contents

List of Tables

List of Figures

Abstract

The use of geotextile tubes for flood mitigation, retaining systems and possibly in containment and storage applications is gaining much attention in construction of temporary and permanent geotechnical facilities. Although there have been many successful applications of geotubes in these capacities, further work is needed in prediction of their performance.

In this study, three-dimensional finite element models of stacked geotubes in ABAQUS are used to investigate their application as soil retaining structures. The geotubes are modelled as flexible membranes filled with an elasto-plastic soil material. A single geotube's geometry, obtained from ABAQUS, is validated by comparison to the available experimental results in the literature. The verified model of a single tube is then used as a starting point for stacked formations.

Various designs composed of stacked geotubes lining the face of an embankment, were modelled using finite elements in order to investigate their impact on the sliding stability due to gravity and surcharge loads. The stability of the system is investigated for two slope angles, 45 and 55 degrees, as the proximity of the surcharge load to the top of the embankment was also varied.

Four different designs of the stacked tube retaining structures were modelled using finite elements (FEM). The first demonstrated a reduction in lateral movement of

the embankment, but the model lacked the desired level of realism with the imposed boundary of a rigid wall against the bottom tube. The second design proved to be too difficult to model with finite elements when a geotextile blanket was integrated with the stacked tubes. The third design, with evenly spaced stakes against the bottom tube increased lateral movement of the embankment, but slightly reduced plastic strains and shear stresses. The fourth and final design, which employed variable size tubes increasing from top to bottom, was more stable than others, but it increased deformation, shear stress, and plastic strain in the embankment.

1 Introduction

A wide range of methods is available for designing and constructing soil retention structures that have been proven effective and efficient. Most of them, such as reinforced concrete and modular walls, require design and construction expertise. In an effort to develop a soil retention structure that can be constructed inexpensively, quickly, and possibly by untrained labour, several designs of stacked soil filled geotextile tubes are investigated. The only synthetic construction material required for a structure of this nature is the geotextile. The tubes can potentially be filled with on site soil or slurry. In the construction of these facilities, some experience will certainly improve the installation however the need for skilled labour may be minimal. This allows stacked geotube soil retention structures to be erected virtually at any location by local work force in an inexpensive and timely fashion.

There have been numerous studies conducted concerning the use of single or stacked geotubes to be used as breakwaters and water retention structures [3, 4, 10, 11, 13, 16, 17, 20]. These studies have used physical, analytical, and finite element models to predict behaviour and feasibility of such structures. Less research has been conducted in the area of using geotube structures for soil retention. The following is an attempt to further the ability to predict the behaviour of geotextile tube soil retention structure designs using a finite element model. Specifically, a design of an embankment stabilization structure consisting of stacked tubes lining the face of an unstable slope, subject to various surcharge loads is considered.

Conceivably, the simplest design for a geotube retaining wall would be a single tube filled with soil laying on a stiff foundation with the soil slope on one side. The effectiveness and stability of such a design could be determined analytically with minimal effort. However, when more complicated designs involving variations such as multiple stacked tubes, sloping or unstable foundations, tube straps, tube anchors, or dynamic loads, it becomes difficult to predict performance and reliability without a physical model. It also may prove to be challenging to predict and prevent possible failure modes.

Analytical or finite element models are possible alternatives to physical models. Analytical models can become complex and unmanageable as the complexity of the structure increases. Finite element models (FEM) can be difficult to construct and

may require a certain level of expertise, however they can accommodate designs of higher complexity. They also provide the ability to fine-tune a design by making small modifications until desirable results are achieved, as was exploited in this work.

2 Background

2.1 Geotextile tube description

A geotextile tube can be described as a permeable geotextile wrap that is filled with sand or dredged slurry material. The diameter of the tube depends on its application and site conditions [1]. Its length also depends on these factors but in general can be unlimited [11]. The term "geotube" can be synonymous with the term "geotextile tube" and is the name of a copyrighted product by TenCate (originally by Nicolon). Dating back to 1957, when the first sand filled flexible tubes were made, geotubes have since been put to many uses. They have been used successfully in applications such as breakwaters, shoreline protection, island creation, sand dune cores, wetland creation, groynes, jetties, and dikes [8]. They also can be used for dewatering fine grained soils, industrial sludges, sewage treatment sludges, and agricultural farm waste [12].

In construction, the geotextile tube arrives on site rolled up on a tube [8]. The tube is then laid flat at the location of installation. Sand or dredged material slurry, often

from on site or local quarry, is then pumped into the tube through inlets spaced along the length of the tube. The geotextile then acts as a cheese cloth letting the slurry water to drain out but retaining the soil. Depending on the geotextile permeability and soil particle size within the tube, the inlets should be close enough so the water does not drain out before it can transport the soil evenly between the inlets [15].

One of the primary advantages to geotube structures lies in their construction. As was previously mentioned, the only construction material needed to be manufactured and brought to the construction site is the geotextile. The tubes can be constructed in challenging site conditions such as underwater or in wetlands. The process has a minimal impact on the surroundings due to fewer personnel, materials, and construction equipment normally needed than other types of construction for similar functionality.

There are several factors of safety regarding different aspects of the product that must be taken into consideration when selecting a geotextile to use as a geotube. The first three deal with the strength of the geotextile; an installation damage factor of safety, a seam strength factor of safety, and an ultimate strength factor of safety [15]. During installation there could be unusual excessive loads caused by irregularities in pumping rate and pressure. During the tube's lifetime the ultimate strength of the material certainly is important as it will govern when it begins to tear, however the seams of the tube are the weak links. A creep factor of safety should also be considered. The geotextile will undergo creep behaviour resulting in a

reduction in ultimate strength over time [15]. Other factors of safety to consider are for biological degradation, chemical degradation, and degradation caused by ultra-violet radiation [15]. Specifically, the geotextile should be resistant to salts, alkalis, and acids [8].

Apparent opening size is another important aspect of geotextile selection. The material must be such that water is allowed to escape, but all of the soil particles are retained. A perfect retention is not as important for geotube used in structures as it is for tubes used for filtration applications [15]. Different design and test methods for selecting an effective apparent opening size and permeability for a geotextile can be found in text by Koerner [12]. This consideration is important if an on site soil is used to fill the tubes.

2.2 Recent Background on Geotextile Tube Modelling

In 1981, Gen S. Liu defined and solved the governing differential equations predicting the shape of a geotube filled with sand or cement slurry [16]. Liu also gathered experimental data to verify the numeric model [16]. Liu studied the use of the geotubes as breakwaters in a surf zone along the coast.

Since Liu's experiments, other researchers such as, Silvester, Carroll, Kazimierowicz, and Leshchinsky have presented numerical approaches to geotube

design considering geometry, stresses, and internal and external pressure factors [6, 10, 14, 15, 20].

Adama Engineering, offers GeoCoPS (Geosynthetics Containing Pressurized Slurry), a software package used for geotube design. The software is supplemented by a complete numeric explanation as well as discussion regarding materials and construction procedures [14]. Results from GeoCoPS for specific tubes are compared to results for the same tube from methods presented in the past by Liu, Silvester, Carroll, and Kazimierowicz [6, 10, 16, 20].

Nicolon, now part of TenCate, is also a manufacturer of geosynthetics and commissioned Delft Hydraulilcs in 1994 to conduct physical modelling and research on the use of submerged geotubes and geocontainers as breakwaters [4]. The research involved various stacking formations and their stability when subjected to waves. The two factors that were varied were significant wave height and water depth over the crest of the structure.

Seay [18] presents a three dimensional finite element model of a section of a geotube. Various tube sizes were modelled using shell elements with small bending stiffness. The tubes, initially empty and flat, were inflated with an internal hydrostatic pressure. Variations, such as altering the internal pressure, were made in the models. The effects on tube height, ground contact length, and shell stresses were observed.

Klusman developed a numerical model of a few geotube stacking configurations [11]. His model predicted that a 2:1 pyramid stacking formation when loaded with water on one side would remain stable when triangular wedges are placed at the base of the tubes to prevent sliding of the stack. Mohler and co workers [17] conducted work on a physical model of three-tube stacking formation of water filled tubes for levee construction. The study showed that sliding was a prominent failure mode and that strapping the tubes together was an essential part of the structural stability.

Cantre developed a two-dimensional finite element model of a geotube cross section [5]. This model investigated the effects of consolidation and loads from other stacked tubes on tube geometry.

2.3 Case Studies

Since 1967 flexible plastic fabric tubes have been used as a means of coastal protection along the German North Sea coast [7]. From 1967 to 1986 there were five types of geotextiles used. These tubes were constructed for groynes on tidal flats, retaining dikes in tidal flats, stabilization of beach nourishment, and an emergency closing of a dike breach. In 1979 geotextile samples that were both exposed to the sun and hidden from the sun were taken from tubes. The samples protected from the sun showed a 10% reduction in tensile strength. The samples exposed to sunlight showed reductions in tensile strength up to 56%. These studies showed that

geotubes can be used successfully in coastal applications protected or unprotected from sunlight for time periods ranging from 1 to 2 decades.

In 1990 a series of storms threatened the historic house Kliffende on the western shore of the Isle of Sylt, Germany [9]. Perched atop a coastal cliff, erosion brought the edge of the cliff only 5.4 m away from the building, whereas when the house was built in the 1920's the cliff was 80 m away. Due to the site's location in a nature reserve, "hard" structures such as concrete blocks and rock revetments were not desirable. A terraced system of geotextile tubes 8 m high was constructed to protect the coastal region directly in front of the house. The structure has performed well and since construction has weathered storm surges with waves up to 5 m high.

At the Naviduct in Enkhuizen, Netherlands, geotubes are used as the core for guide dams. The Naviduct can be thought of as a cross between an aqueduct and a bridge. It is a water way suspended over land for boats where automobile traffic can pass underneath. In construction of the Naviduct, the excavation material was directly used to fill the tubes, resulting in a sustainable construction process. Unless confined in an innovative way, such as a geotube, the excavated soil there would have been too fine to use in dam construction. The tubes were laid where the dam was to be and then covered with a rock layer for protection [21].

The Amwaj Island off the coast of Bahrain in the Arabian Gulf was created using geotubes [8]. The 2.79 million square meter island was created to provide land for

houses, hotels, commercial real estate, and marinas. A two tube staggered stack creates a perimeter for the island that is filled with locally dredged sand. The height of the two tubes reaches 4.6 meters. After filling the tubes, they are covered with rock in some areas and sand in other areas to create beaches. The two tube stacking of Amwaj Island formation is similar to the design discussed in this study.

3 Analysis

3.1 Scope

The primary challenge in the finite element modelling of geotubes is the difficulty of capturing the influence of their construction stages on the time dependant and hence behaviour. Typically, the construction process starts with a permeable geotextile tube that is laid empty on the ground at the desired location. It is then filled by pumping in a soil-water slurry mix. The water then seeps out through the pores in the geotextile leaving a packed saturated mass of soil inside the tube. The tube solidifies as the viscous slurry inside looses its water over time. During the tube's viscous phase, the equilibrium shape of the geotube cross-section is determined as a function of the pumping pressure and the unit weight of the slurry [14, 15]. Once the tube has drained and is solid, it possesses the shear and compressive strength needed to function as a self-standing stable structure.

Establishing a finite element model that incorporates these fundamental material and geometric changes occurring simultaneously proves to be demanding. This challenge can be overcome by creating a series of "sub-models", each simulating a different stage of the tubes. The results from each of these sub models can then be used as initial conditions for the subsequent one, resulting in an integrated model describing the behaviour of the finished structure.

The geotube stack design presented here is intended to stabilize the slopes of an embankment that is subject to a surcharge load from a road at the top of the embankment. Two slope angles are considered: 45 and 55 degrees. The slopes are prone to failure along a computed toe-slip plane as shown in Figure 3.1.1. The stack of tubes, as shown in Figure 3.2.1, is used to restrain lateral movement. Various models for each slope angle with surcharges placed at several positions in proximity to the top of the bank are investigated.

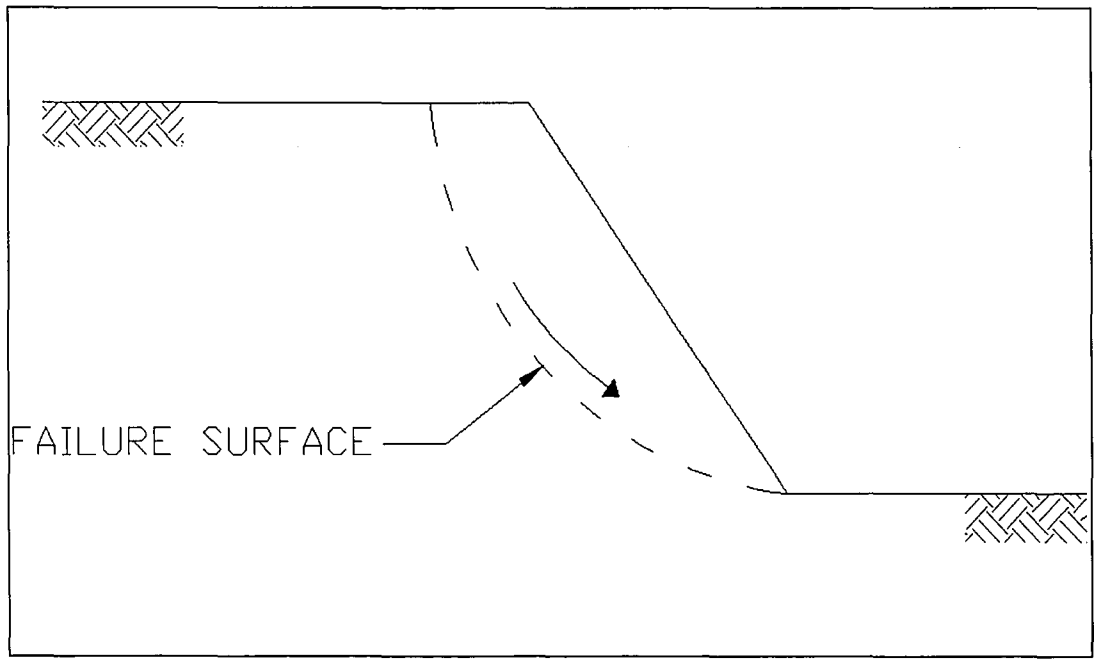

Figure 3.1.1. Failure Surface.

3.2 Modelling Approach

ABAQUS 6.7 was used in the development of finite element models of stacked geotextile tubes. A typical design involved the three tubes resting on a deformable embankment, as seen in Figure 3.2.1.

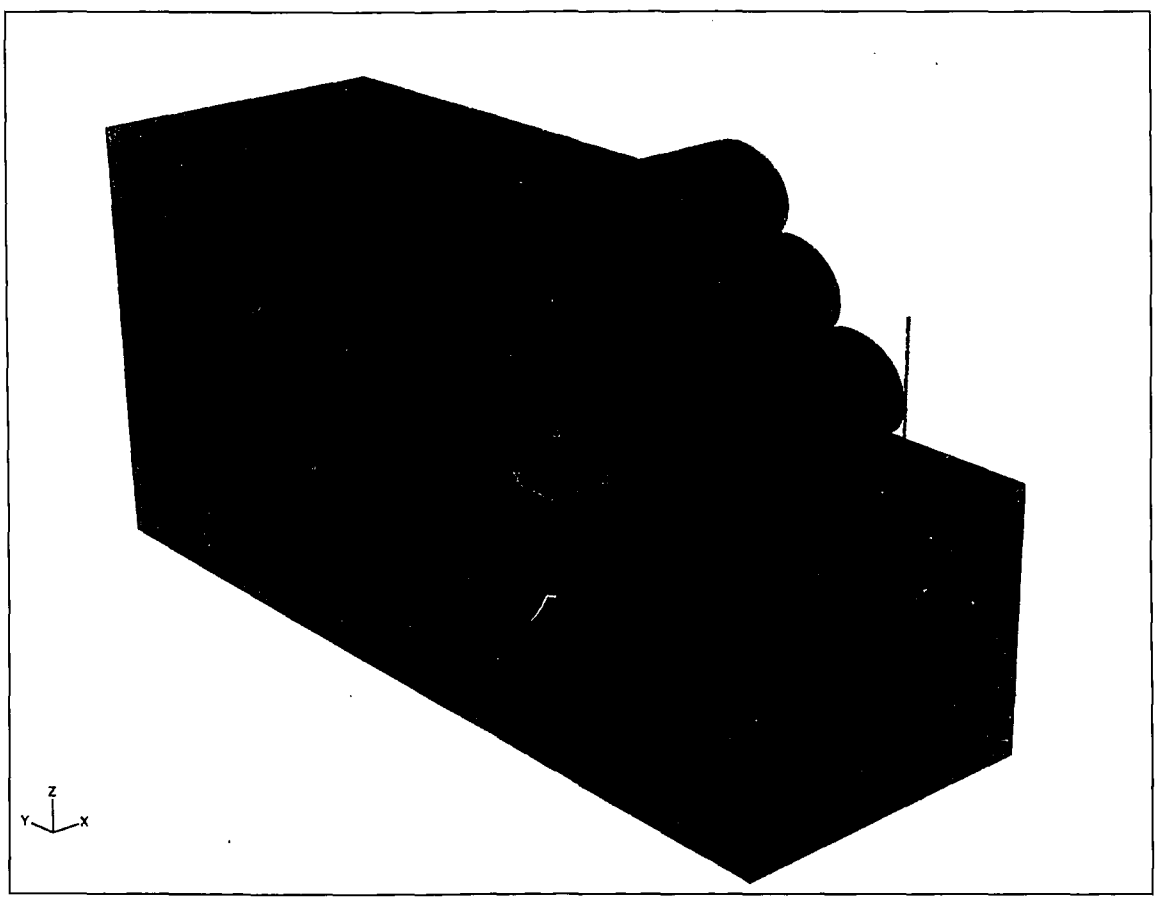

Figure 3.2.1. Typical stacking formation (depicted with boundaries of Design 3).

While there was an evolutionary process in developing an effective and realistic design, the modelling procedures and techniques were the same for all of the models. All of the designs modelled, depicted typically in Figure 3.2.1, were similar enough

3.2 Modelling Approach

ABAQUS 6.7 was used in the development of finite element models of stacked geotextile tubes. A typical design involved the three tubes resting on a deformable embankment, as seen in Figure 3.2.1.

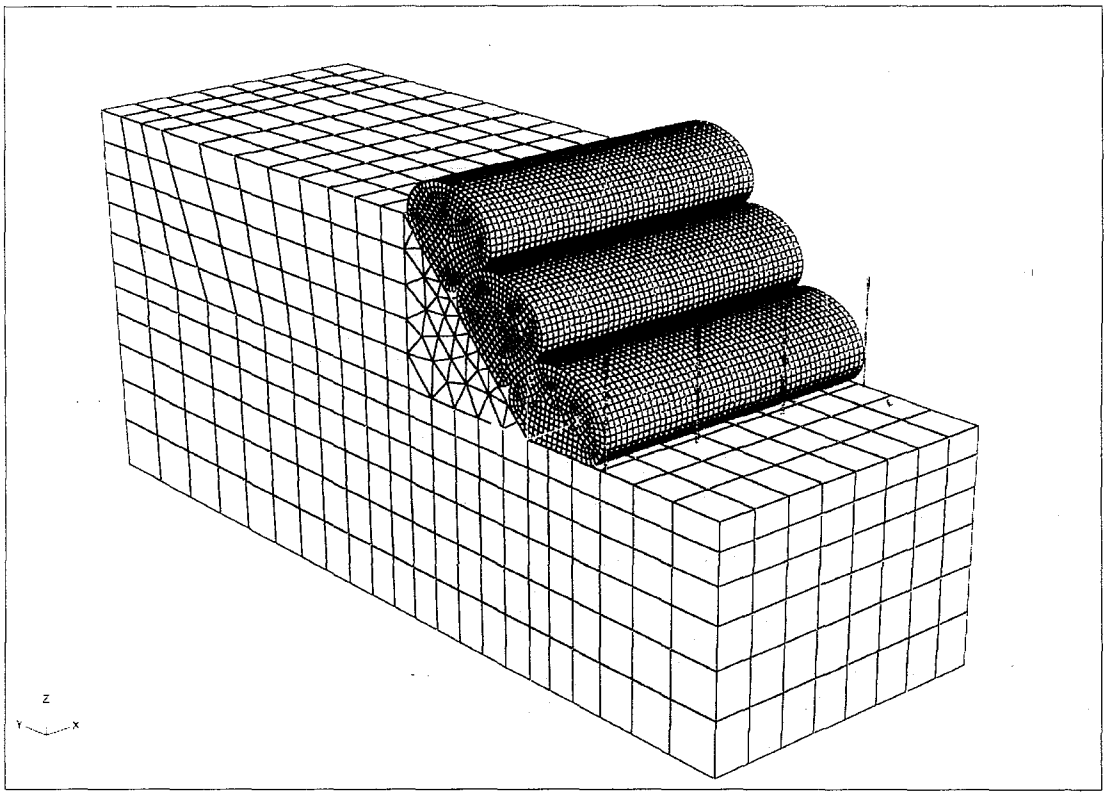

Figure 3.2.1. Typical stacking formation (depicted with boundaries of Design 3).

While there was an evolutionary process in developing an effective and realistic design, the modelling procedures and techniques were the same for all of the models. All of the designs modelled, depicted typically in Figure 3.2.1, were similar enough

so that the sub-modelling process was the same for all of them. The first sub-model consisted of only one tube, the bottom tube in the stack, represented as a hollow membrane resting on a rigid surface of the embankment slope under consideration. In this sub-model, only the viscous stage of the tube's life is modelled. This stage provides the initial tube geometry.

In the first sub-model, the tube is initially a uniform cylinder with zero bending stiffness that rests on a flat surface, with the embankment slope on one side. It is subjected to an internal hydrostatic pressure simulating the liquid slurry load that the tube would experience in the pumping process. The tube then deforms on the surface until it reaches its equilibrium shape. The tube was originally positioned so that it would deform onto the embankment creating a contact surface.

The final geometry from the first sub-model serves as the initial shape of the bottom tube in the stacked formation. In the next sub-model, the bottom tube is replaced by a solid mass of soil in the shape determined from the first sub-model. This solid tube is surrounded by a thin skin acting as the geotextile. A hollow cylindrical membrane tube, identical to the initial tube in the first sub-model, is then placed on top wedged against the slope. The goal here is to determine the geometry of the second tube in the stack. The same process is used to obtain the geometry of the top tube.

Once the geometry of all three tubes is determined and the solid tubes are in place, the flat surface the tubes were resting on and deforming against is replaced by a deformable solid embankment.

The hollow membrane tubes essentially represent mass-less hydrostatically loaded tubes internally. It is for this reason, that they are only used for determination of geometry. Once the solid tubes are in place, they posses the internal shear resistance developed in the soil that contributes directly to the structure's load carrying capacity. It is this shear resistance, combined with the compressive strength of soil and the friction interactions between the tubes and the foundation that allow the stack to retain its shape and carry load.

During the sub-modelling process, it became evident that the structure would fail by means of sliding. The bottom tube would not remain in place when the other two were loaded with gravity thus causing the whole structure to slide down the embankment. A simple solution to this is to restrain the bottom tube from sliding. This turned out to be the primary design challenge in getting the structure to perform correctly. However, initially in all of the sub-models, a boundary condition was imposed on the bottom tube that prevented it from sliding. This was done in order to obtain all of the initial tube geometries without having to consider structural stability and performance until later when the stack and foundation were assembled together.

Other potential failure modes, besides sliding, are overtopping, rolling of individual tubes, or foundation soil bearing failure. It is likely that if any of these failure modes were to occur in the model, the ABAQUS solver simply would produce an error for the modelled section indicating that a solution for the stiffness equations behind the model did not converge. This most likely would be due to excessive deformations and stresses. The models created in this study are limited by the fact that ABAQUS cannot simulate these failure modes. If a solution to a model does not converge, it can be inferred that one of the possible failure modes may be occurring. Adjustments can then be made to the design in the model to obtain structural stability, but the exact nature of the failure may not be known for sure from these models.

3.3 Assumptions

The following assumptions were made when modelling the tubes.

- The effects of soil consolidation on tube geometry and tube strength are small.
- The geotextile strength is not exceeded.
- Effects of seams and local imperfections in the geotextile on tube geometry and tube strength are neglected.
- The geotextile does not slide relative to the soil inside the tube once filled.
- Bearing capacity failure does not occur.

4 Initial Slope Stability Analysis

4.1 Classical Analysis

Before any results from the finite element models of the different designs can be of use, the initial state of stability for the slope itself should be obtained. For this, Slope/W™ (GeoStudio, 2004) was used for this purpose. A slope stability analysis was conducted on 45 and 55 degree slopes modelled with the same geometry and material properties that were to be used in the ABAQUS models. The height of the 45 degree slope embankment model was selected 3.2 meters, while the 55 degree slope embankment height was 3.5 m. These heights were based on the height of three stacked tubes. The soil in Slope/W™ was defined as a Mohr-Coulomb material with total unit weight of 19.26 kN/m^3, φ = 35.3°, and c = 1.484 kPa. The soil friction angle and cohesion values, φ and c, relate to the β and d parameters that ABAQUS uses as for the Cap Drucker-Prager soil model, as shown in equations 1 and 2 below.

$$\tan(\beta) = \frac{6\sin(\varphi)}{3-\sin(\varphi)} \quad (1) \qquad\qquad d = \frac{18c\cos(\varphi)}{3-\sin(\varphi)} \quad (2)$$

A factor of safety of 1.1 was determined for the 45 degree slope according to both the Bishop's method and the Morgenstein-Price method. The 45 degree slope at 3.2-meter height is stable only by a small margin. This state serves as the reference state

representing the stresses and strains at the verge of failure. These will be compared to the resulting stress and strain levels when the stacked tubes are mounted in place.

For the 55 degree slope, a factor of safety of 0.87 was determined again using both the Bishop's method and the Morgenstein-Price method. According to this analysis, the slope at the height of 3.5 meters, is unstable and would fail. A second analysis of the same slope at 3.0-meter height was carried out. This yielded a 1.00 factor of safety according to Bishop's method and a 0.99 factor of safety according to the Morgenstein-Price method. The maximum stable height for this soil in a 55 degree slope is 3 meters. A model of this slope was also run in ABAQUS. The expected outcome of the ABAQUS analysis was the reduction of stresses and strains for these critical slope configurations with the application of the geotube structures.

Originally a failure criterion was adopted by considering the critical slope stresses and strains "safe" and if they were exceeded in models with the tubes in place, the slope could be considered to have failed. However, the weight of the tubes changed the deformation behaviour of the embankment making it difficult to directly compare stresses and strains to the stable slope. For example, the maximum strain might be greater in a case with the tubes in place, but this strain could be at a location in the embankment that has a minimal effect on the slope's stability. To overcome this incompatibility, it was decided to compare specific stress and strain components at several selected locations in the embankment. In doing so, the geotube structure's affect on the stability of the slope can be gained only through the improvement of

stress and strain fields at critical locations, but an exact quantitative analysis of the slope's stability can not be carried out.

The strains used in the comparisons are *maximum principal plastic strain vectors*, *lateral strains*, and *plastic strain magnitudes*. For the slopes with no tubes, the plastic strain vectors provide information on the location and the possible mechanism of failure. The lateral strain component is considered as a representation of the magnitude of movement of the slope. This is relevant since one of the main goals of the tube structure is to prevent or reduce lateral movement of the slope.

The plastic strain magnitudes throughout the embankment give a general indication of how the tubes affect plastic deformation behaviour. This is relevant because, while plastic strain may or may not mean failure, it nevertheless provides an idea of where the failure will most likely occur. Based on that information, values for stress and strain can be compared between models at the locations that have been identified as important or critical. These critical locations can, of course, be correlated and verified with other results such as lateral deformation and maximum stresses.

The stress used for comparison purposes is the x-y shear stress. This is the shear stress that has a vertical and horizontal component when looking at the x-y cross-section of the embankment. It is the resisting shear component that provides strength when the slope is deforming laterally. It also is associated directly with the lateral strains compared between models. However the x-y shear stress may not be the

maximum shear component present at a given location. It is likely that the maximum shear stress orientation varies with location.

Since the 3.2-meter high 45 degree slope was determined to be stable with a factor of safety of 1.1, the ABAQUS was expected to demonstrate how the stability would be affected by tube placement. The original 3.5 meter high 55 degree slope was determined to be unstable. Its height had to be reduced to 3.0 meters in order to get a factor of safety of 1.0 in Slope/W™.

4.2 Finite Element Analysis

Slope/W™ was used to determine of the critical slope geometry. The same slopes were modelled in ABAQUS to obtain actual stress and strain values within the embankment, including the critical slip surface area. ABAQUS analysis results of stress and strain distributions within the soil mass in the embankment were used to compare the slope behaviour with and without the geotubes, both configured at the critical geometry. ABAQUS could be used to predefine failure in the embankment along with the selected cap plasticity soil model. Hence, the stable slope models' results (from ABAQUS) are important because they serve as the baseline for the occurrence of failure when comparing results from models with the tube structure in place.

Cap Plasticity is selected as the constitutive model to represent the expected behaviour of the soil in the embankment and inside the tubes. Tables 4.2.1 and 4.2.2 contain the soil parameters used to define Cap Plasticity behaviour in ABAQUS. The representative parameters used in this model were experimentally determined by Shoop et al [19] for Lebanon Sand.

Table 4.2.1. Elastic and Plastic parameters for Lebanon Sand [19].

Elasticity	
Young's Modulus	E = 8.5 MPa
Poisson's Ratio	v = 0.45
Mass Unit Weight	$\gamma = 75\ kg/m^3$
Plasticity	
Cohesion	d = 10,000 Pa
Angle of Friction	$\beta = 55.8°$
Cap Eccentricity	$R = 0.45$
Initial Yield Surf. Position	$\varepsilon_o = 0$
Transition Surf. Radius	$\alpha = 0$
Flow Stress Ratio	K = 1

Table 4.2.2. Cap hardening data for Lebanon Sand [19].

Yield Stress (Pa)	**Volumetric Plastic Strain**
8200	0
38900	0.009
76000	0.022
163900	0.038
365500	0.054
720100	0.072

The embankment is modelled as a block of soil. It is composed of the same Cap Plasticity soil that fills the tubes (Tables 4.2.1 and 4.2.2).

The following results are presented in sections of three dimensional finite element models of each embankment under consideration. The typical embankment configuration is shown in Figure 3.2.1, with the exact dimensions varying with slope angle and height for specific models. The sections are six meters thick and are intended to be representative of a much longer embankment. The sides and ends of the embankment in the model are restrained to movement within their own plane. The base of the embankment is restrained from movement in all directions. Three dimensional stress elements with reduced integration are used. The mesh size is about 0.3 m in the zone near the slope and increases to about 0.6 m elsewhere. Only gravity loads are applied in the stable slope models.

The first slope modelled in ABAQUS was the 45 degree slope with a factor of safety of 1.1. Figure 4.2.1 illustrates this slope with the initial and deformed geometries superimposed. Displacements have been scaled up by a factor of 10 to show the slope's movement more effectively. Figure 4.2.1 shows that the top of the slope is moving to the left and the bottom is moving to the right. Meanwhile, all locations are moving downwards. Similar deformation behaviour occurs in the 55 degree slope. Figures 4.2.2 and 4.2.3 illustrate maximum principle plastic strain vectors due to a gravity load in the 45 and 55 degree slopes.

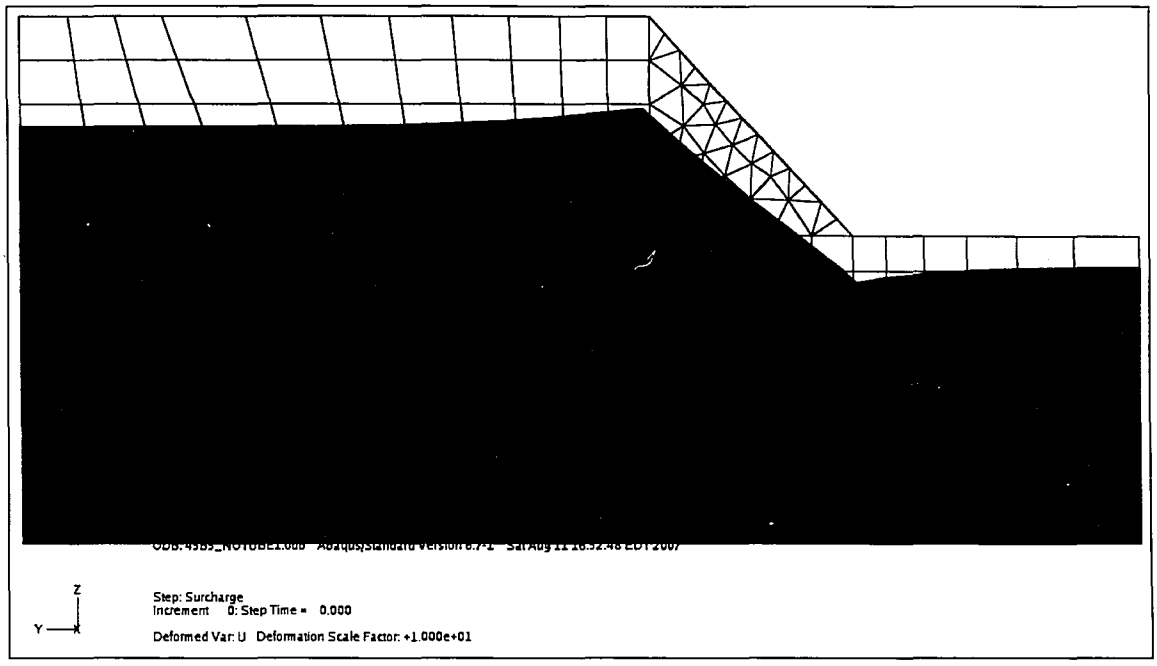

Figure 4.2.1. Deformed 45 degree slope scaled up ten times.

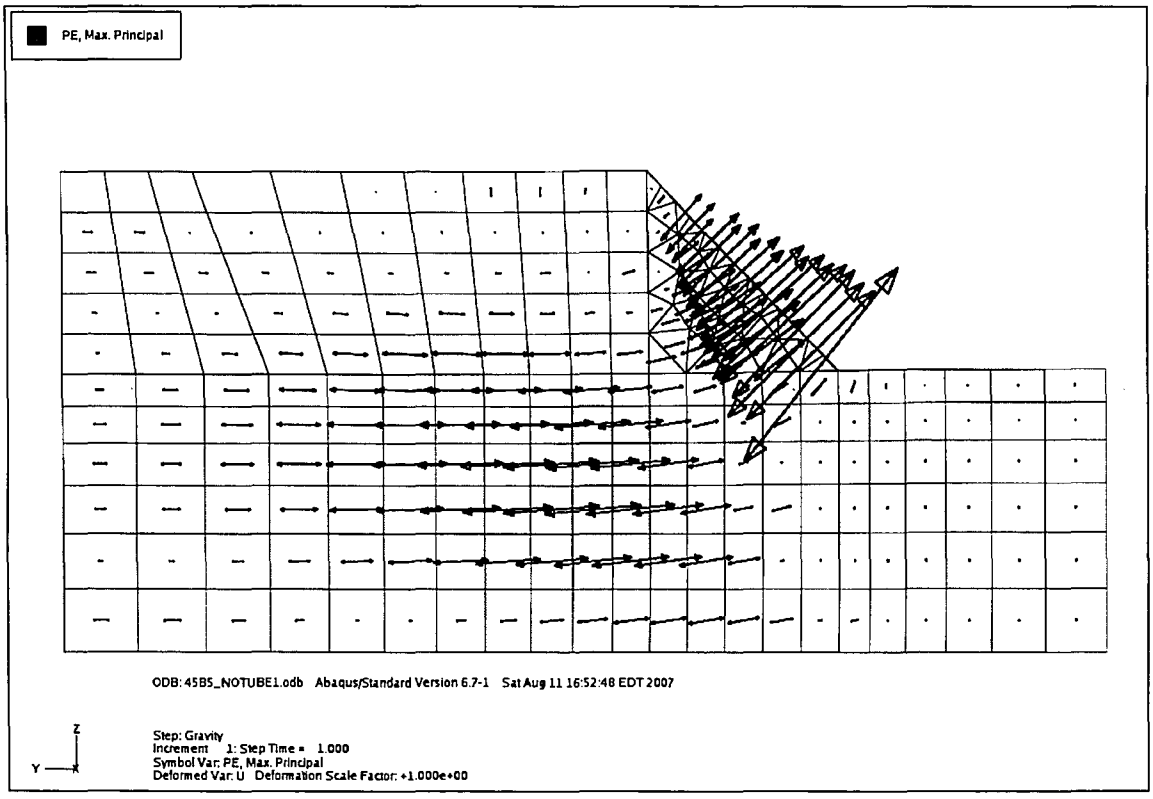

Figure 4.2.2. Plastic strain vectors for 45 degree, 3.2 meter high stable slope.

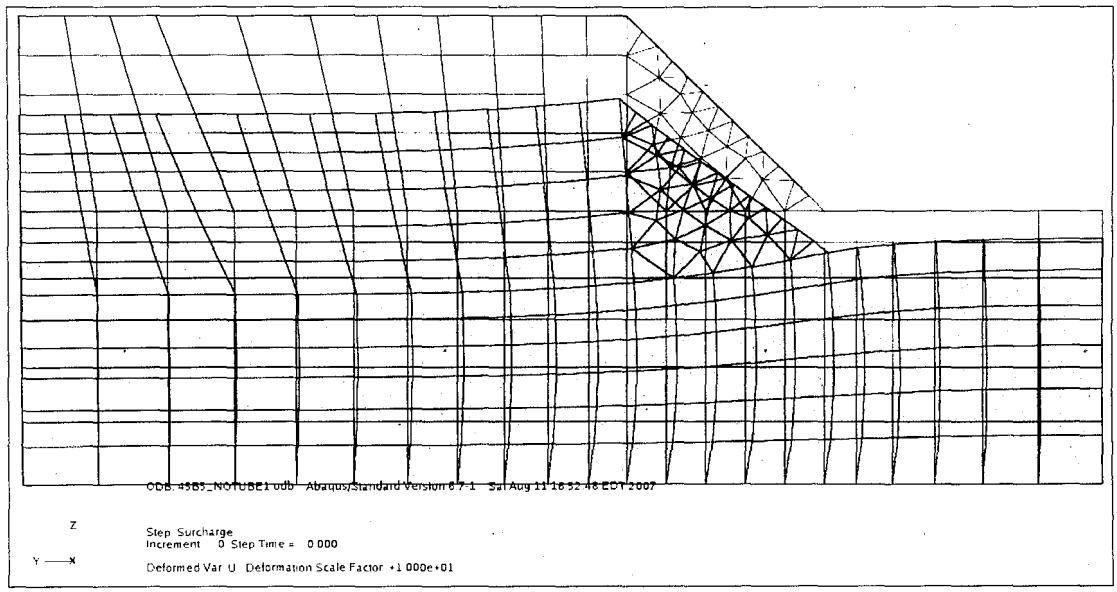

Figure 4.2.1. Deformed 45 degree slope scaled up ten times.

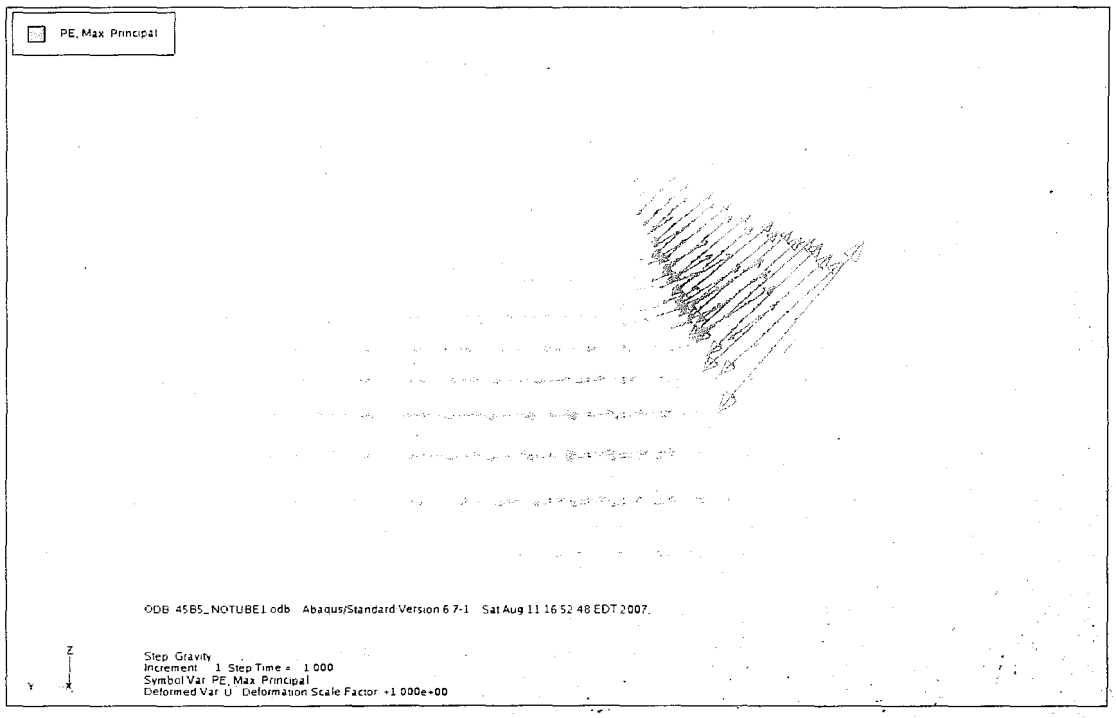

Figure 4.2.2. Plastic strain vectors for 45 degree, 3.2 meter high stable slope.

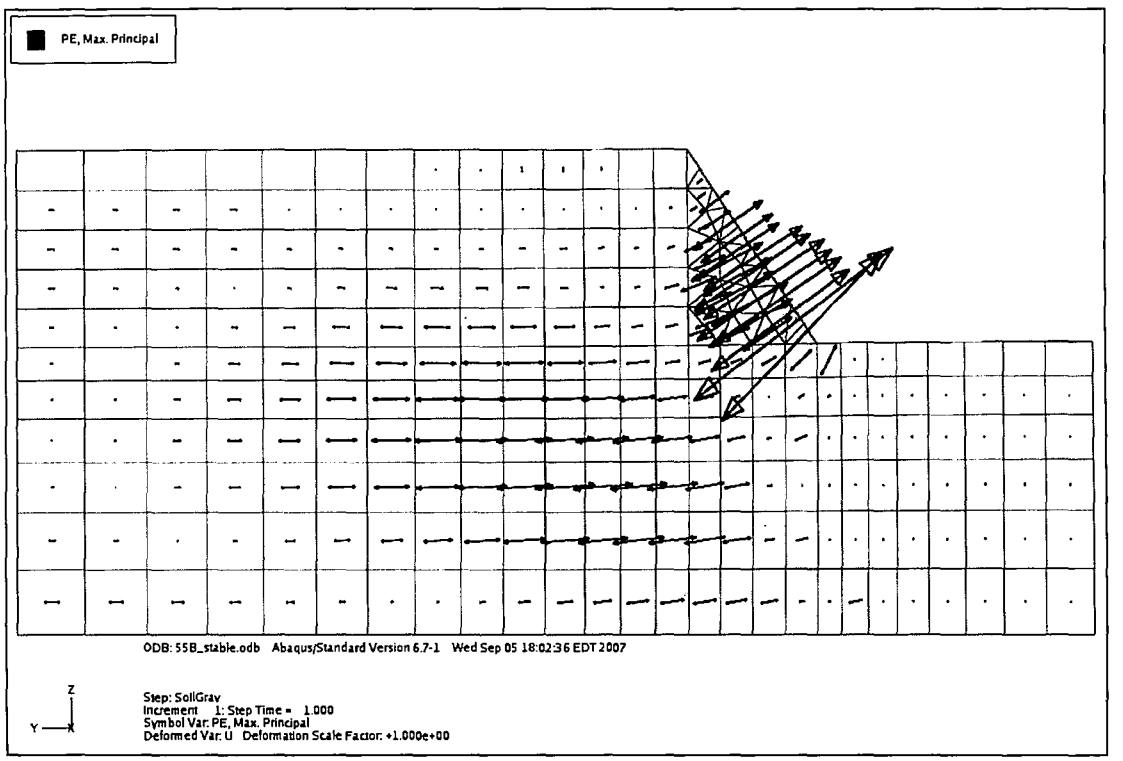

Figure 4.2.3. Plastic strain vectors for 55 degree, 3.0 meter high stable slope.

The vectors show that the slope deforms most plastically near the surface of the slope and about the toe as expected. One of the goals of using the stacked tubes will be to reduce these plastic strains at the toe.

Figures 4.2.4 and 4.2.5 show the plastic strain magnitude contours for the two slopes respectively. These figures can help to identify critical or high strain locations in the embankment and confirm other inferred behaviour about the embankment's deformation.

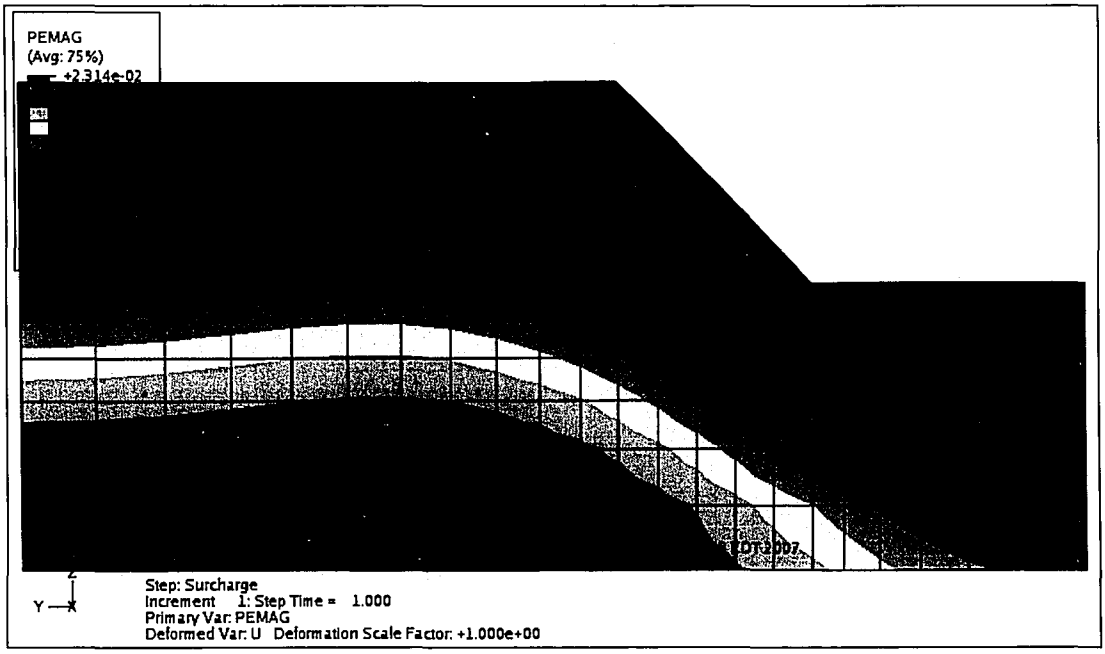

Figure 4.2.4. Plastic strain magnitudes in 45 degree stable slope, H=3.2 m.

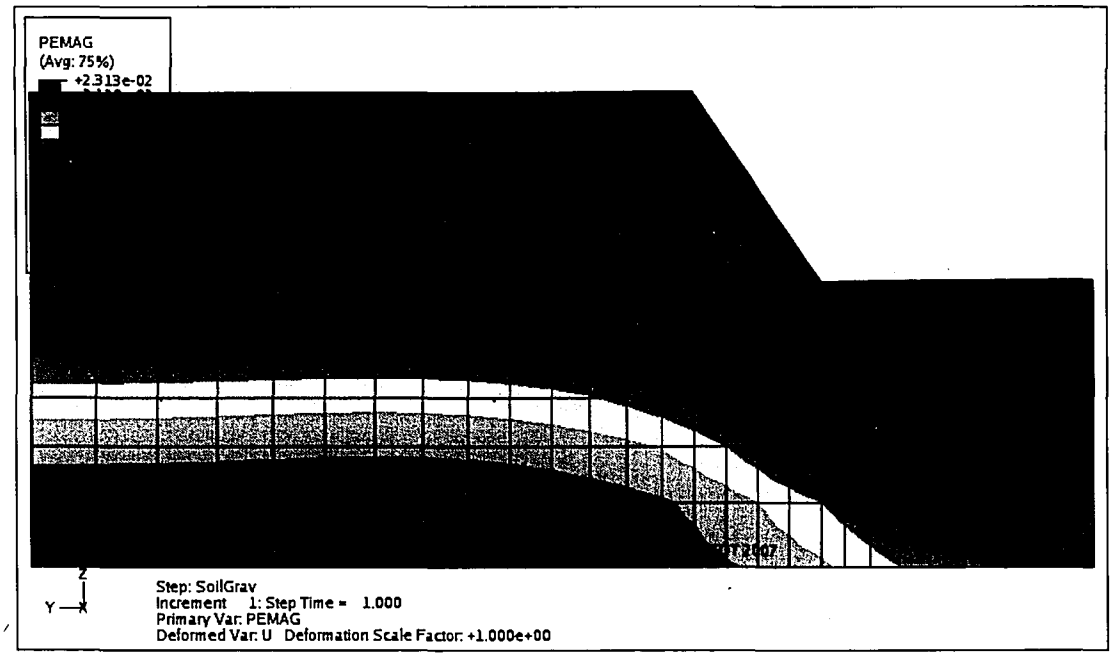

Figure 4.2.5. Plastic strain magnitudes in 55 degree stable slope, H=3.0 m.

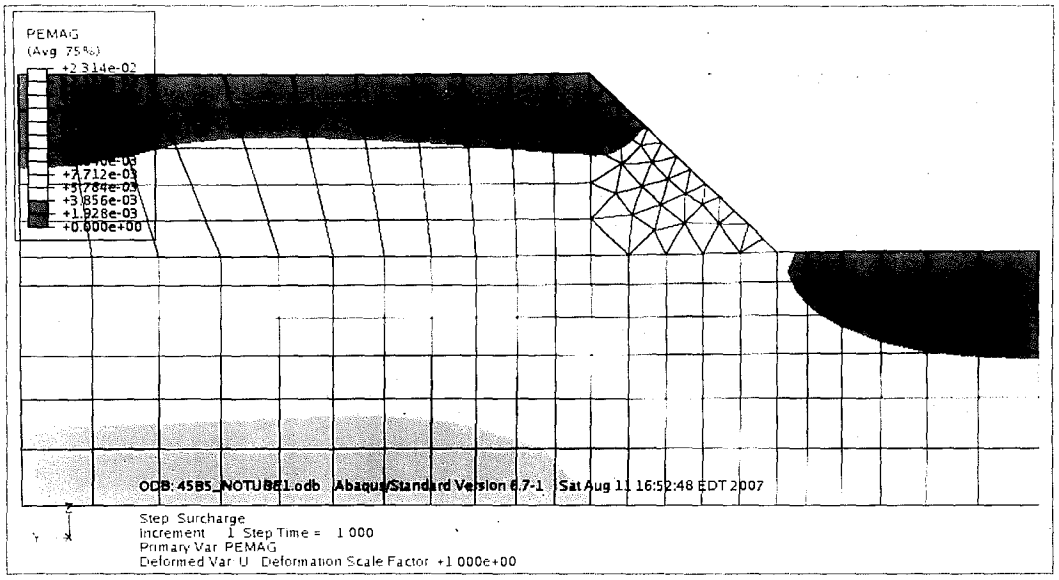

Figure 4.2.4. Plastic strain magnitudes in 45 degree stable slope, H=3.2 m.

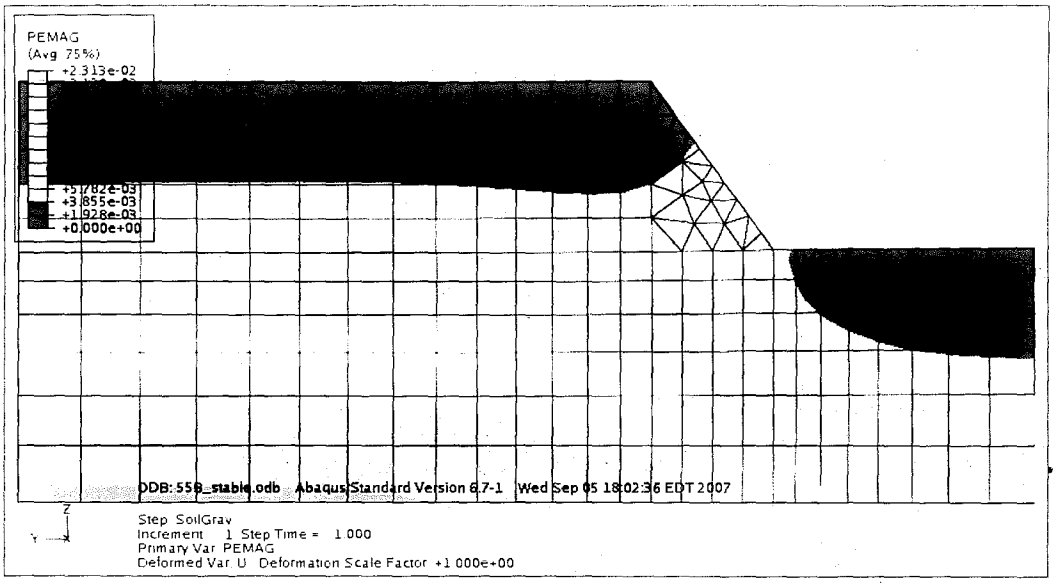

Figure 4.2.5. Plastic strain magnitudes in 55 degree stable slope, H=3.0 m.

The plastic deformation can also be presented only in terms of lateral strains. This is useful because much of the success or failure of the tube stack for slope stabilization is based on its restrictive ability of the lateral movement of the slope. Figures 4.2.6 and 4.2.7 illustrate that the distribution of lateral plastic strains on the face of the slope increases downward and peaks at the toe, as expected. One item to note is that in the 45 degree slope the lateral plastic strains increase gradually and are highest at the toe. In the 55 degree slope, the strains down the face of the slope are very small in comparison to the strains right at the toe.

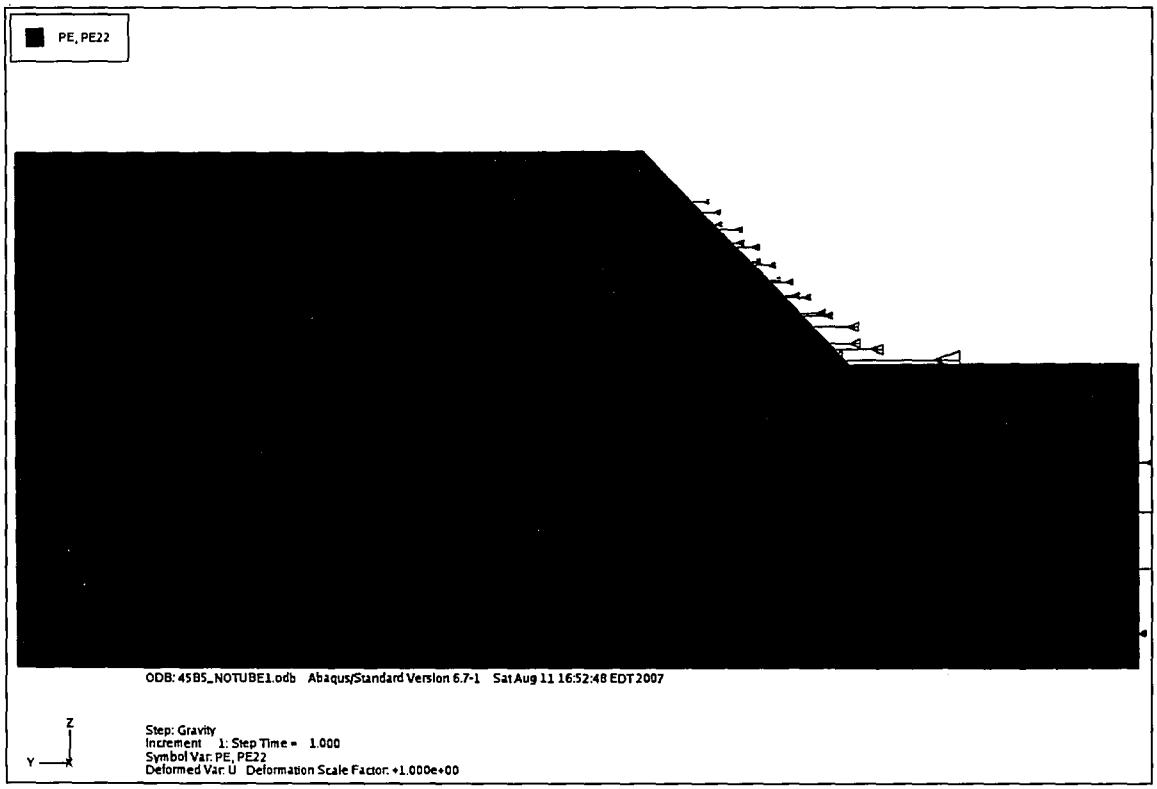

Figure 4.2.6. Lateral plastic strain along 45 degree slope face; H=3.2 m.

The plastic deformation can also be presented only in terms of lateral strains. This is useful because much of the success or failure of the tube stack for slope stabilization is based on its restrictive ability of the lateral movement of the slope. Figures 4.2.6 and 4.2.7 illustrate that the distribution of lateral plastic strains on the face of the slope increases downward and peaks at the toe, as expected. One item to note is that in the 45 degree slope the lateral plastic strains increase gradually and are highest at the toe. In the 55 degree slope, the strains down the face of the slope are very small in comparison to the strains right at the toe.

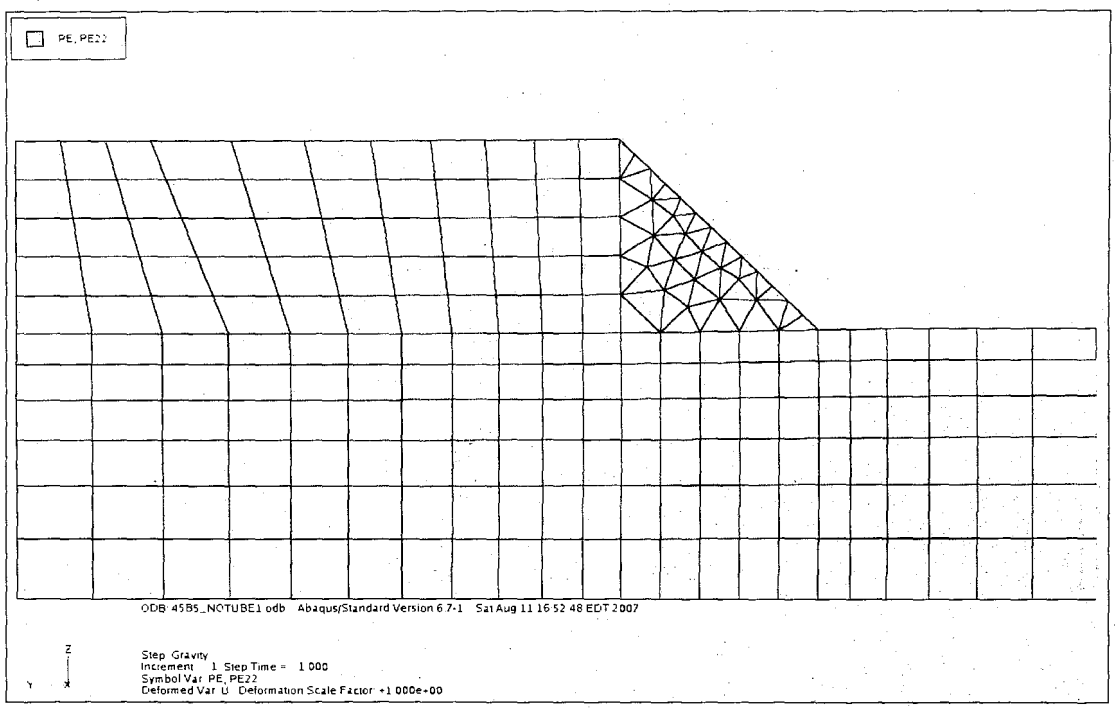

Figure 4.2.6. Lateral plastic strain along 45 degree slope face: H=3.2 m.

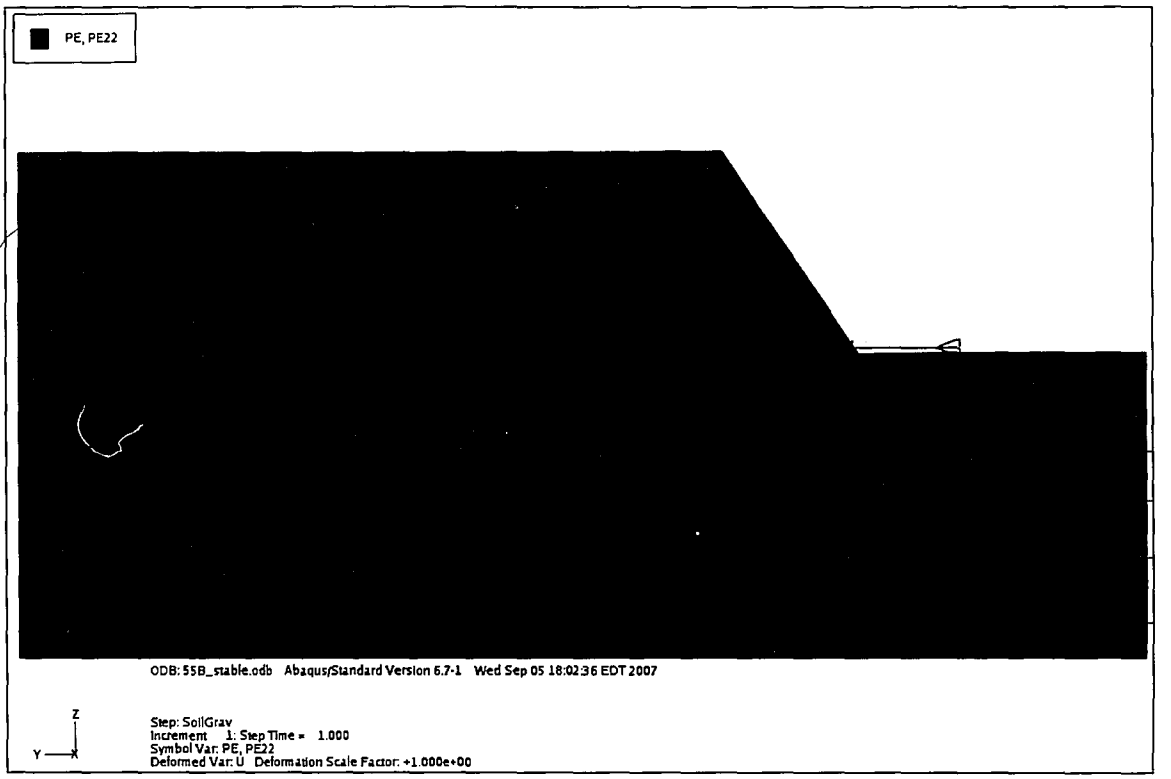

Figure 4.2.7. Lateral plastic strains along 55 degree slope face; H=3.0 m.

Another possible representation is in terms of deformations. Contours of lateral movement are shown in Figures 4.2.8 and 4.2.9. The two slopes behave the same, with the 55 degree slope deforming slightly less.

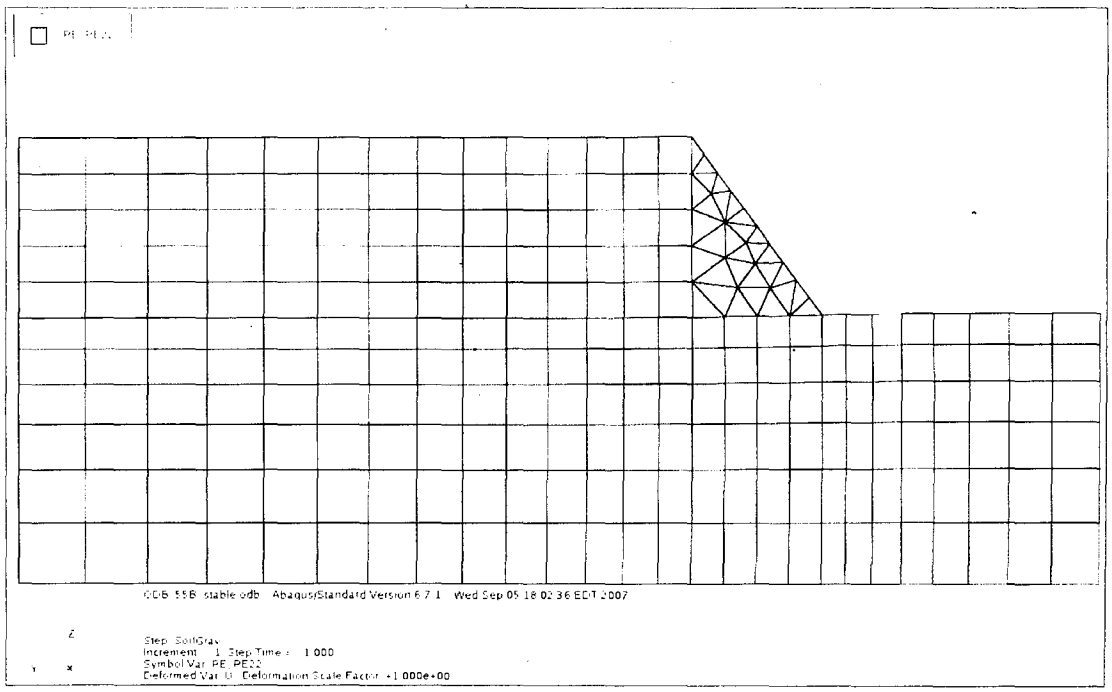

Figure 4.2.7. Lateral plastic strains along 55 degree slope face: H=3.0 m.

Another possible representation is in terms of deformations. Contours of lateral movement are shown in Figures 4.2.8 and 4.2.9. The two slopes behave the same, with the 55 degree slope deforming slightly less.

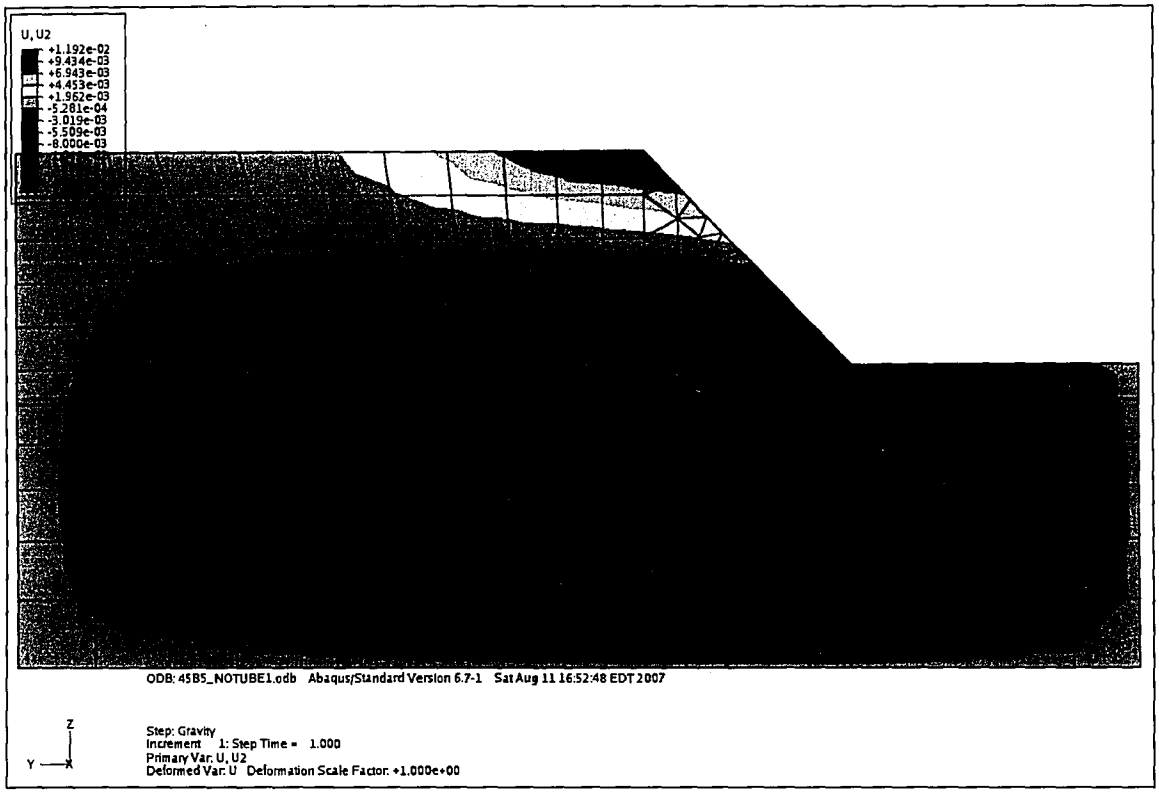

Figure 4.2.8. Lateral deformation of 45 degree slope; H=3.2 m.

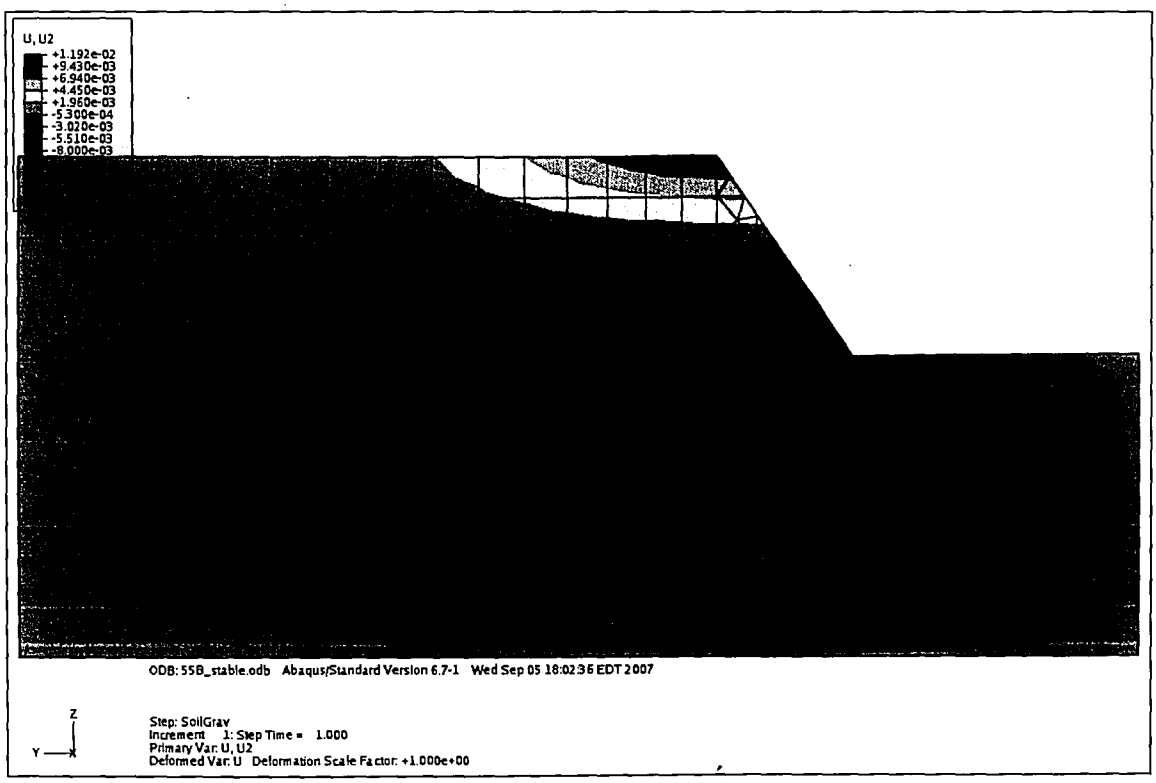

Figure 4.2.9. Lateral deformation of 55 degree slope; H=3.0 m.

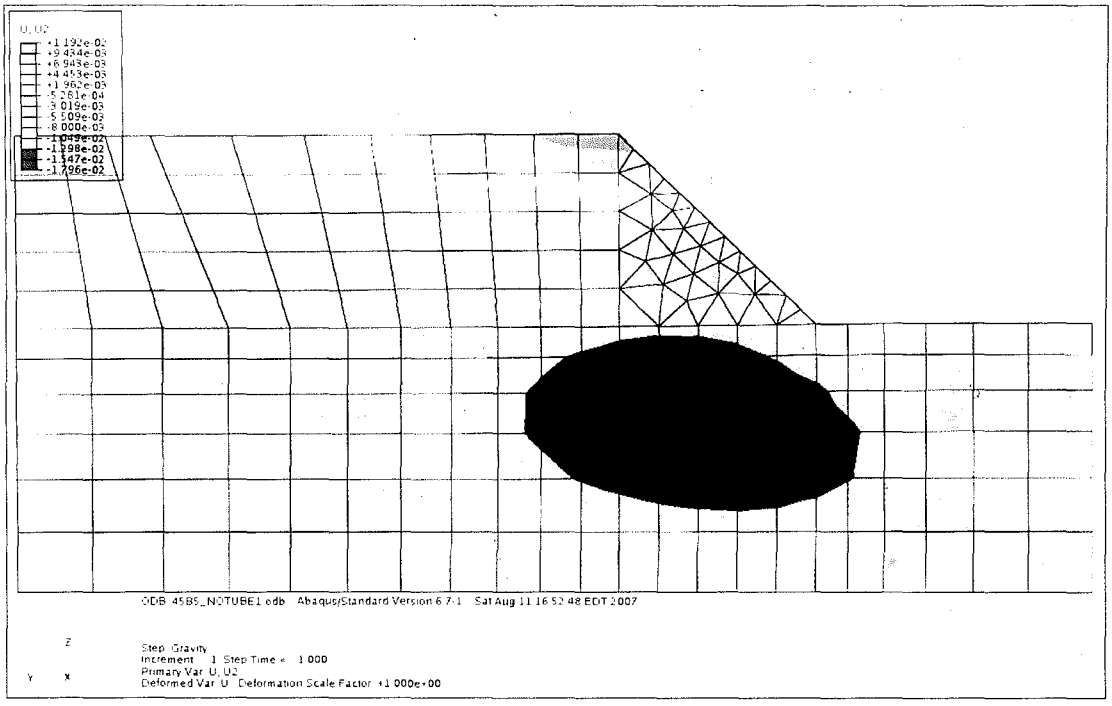

Figure 4.2.8. Lateral deformation of 45 degree slope: H=3.2 m.

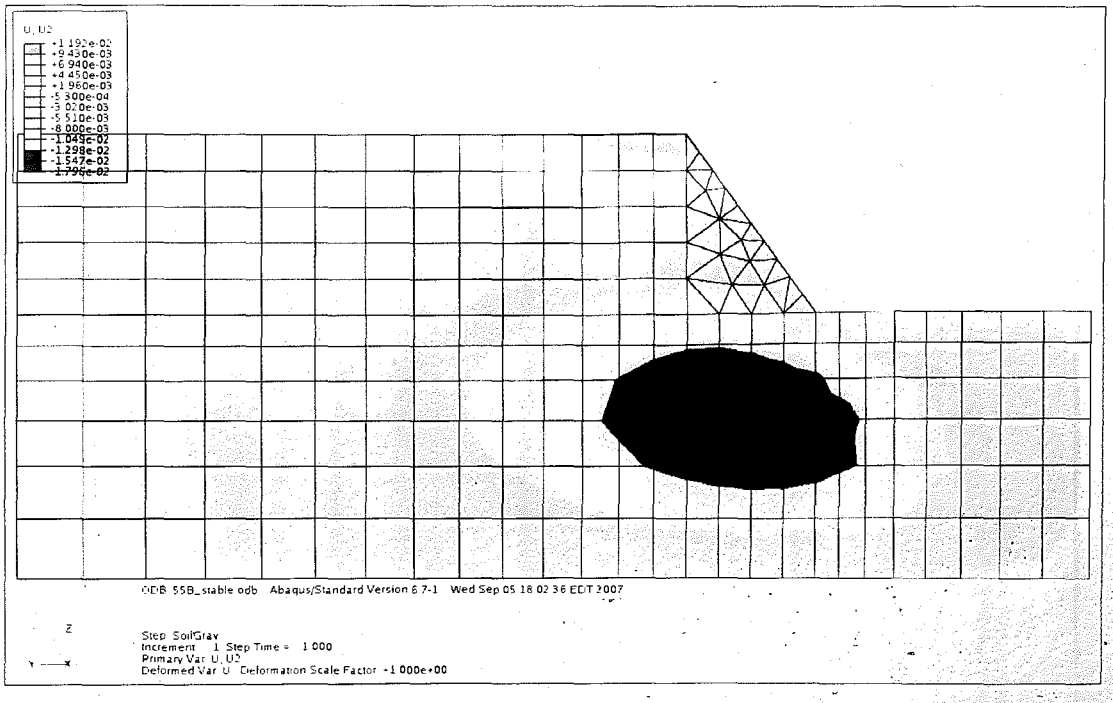

Figure 4.2.9. Lateral deformation of 55 degree slope: H=3.0 m.

Figures 4.2.8 and 4.2.9 show that the highest deformation occurs directly below the slope moving approximately 1.7 cm to the right for both slopes. The lateral movement at this location most likely influence the stability of the slope, but it does not coincide with the location of the maximum plastic stains and, as will be shown shortly, the maximum shear stresses. Therefore the movement at this location is of less concern. It is likely that the deformations here are mostly elastic. The soil at this location is subjected to a much higher hydrostatic pressure than the soil on the slope surface due to its depth. This will move its yield surface in the cap plasticity model and allow for higher elastic strains to occur before plastic yielding begins.

Figures 4.2.10 and 4.2.11 show the distribution of x-y shear stresses for the 45 and 55 degree slopes. As seen, the shear stress values within the embankment are similar in both magnitude and location only slightly higher in the 55 degree slope.

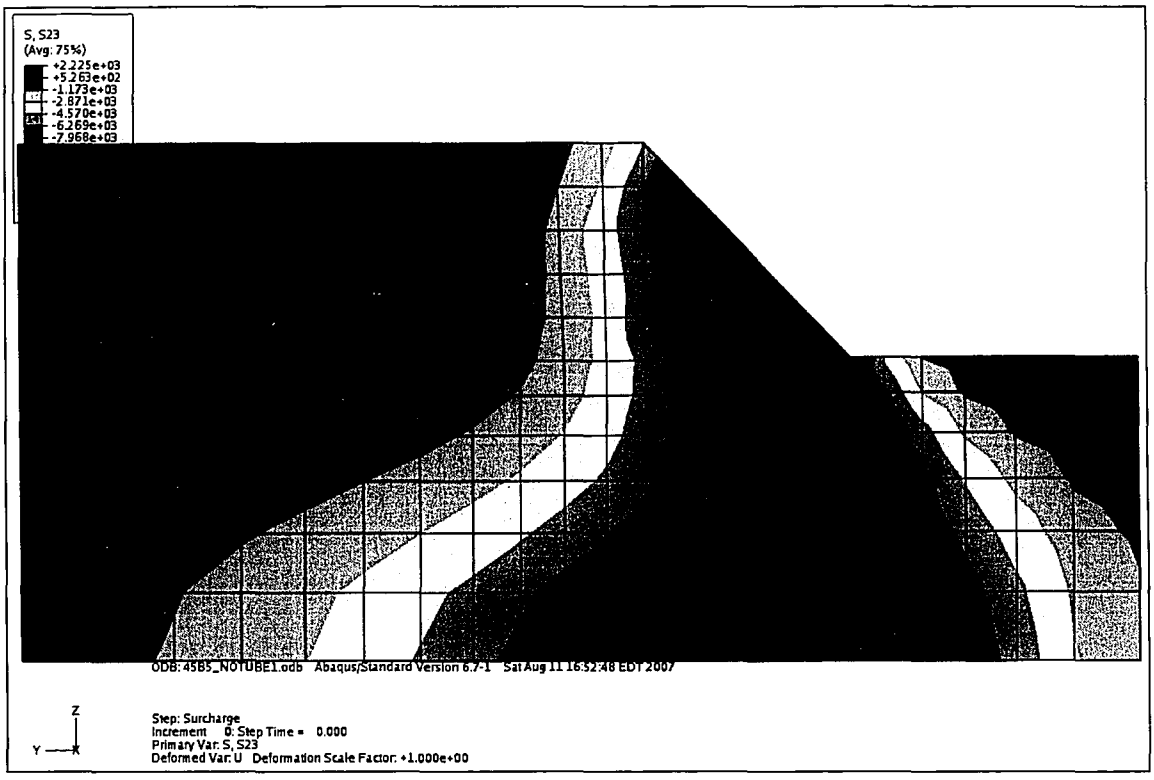

Figure 4.2.10. x-y shear stress distribution for 45 degree slope; H=3.2 m.

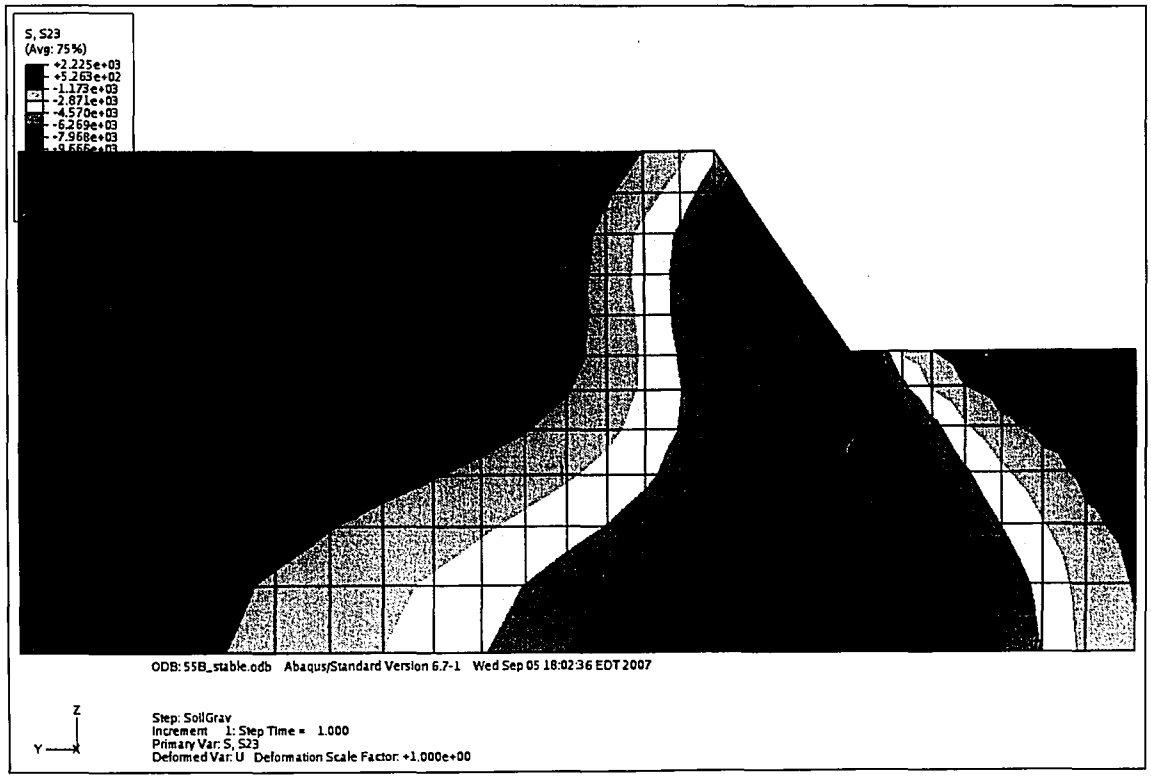

Figure 4.2.11. x-y shear stress for 55 degree stable slope; H=3.0 m.

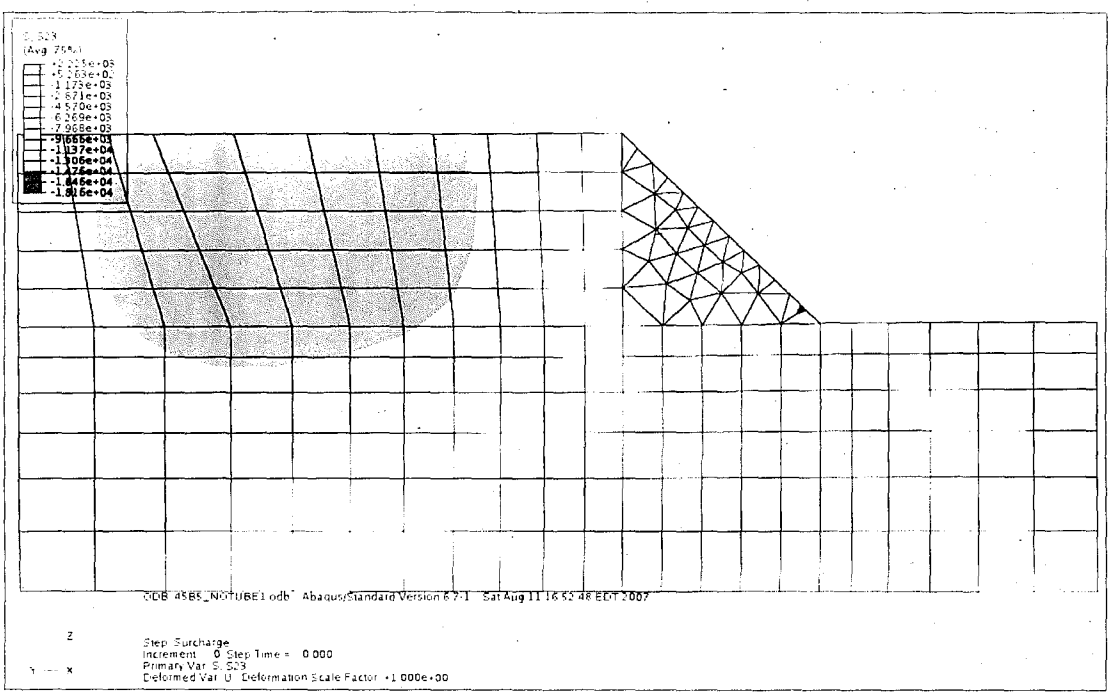

Figure 4.2.10. x-y shear stress distribution for 45 degree slope: H=3.2 m.

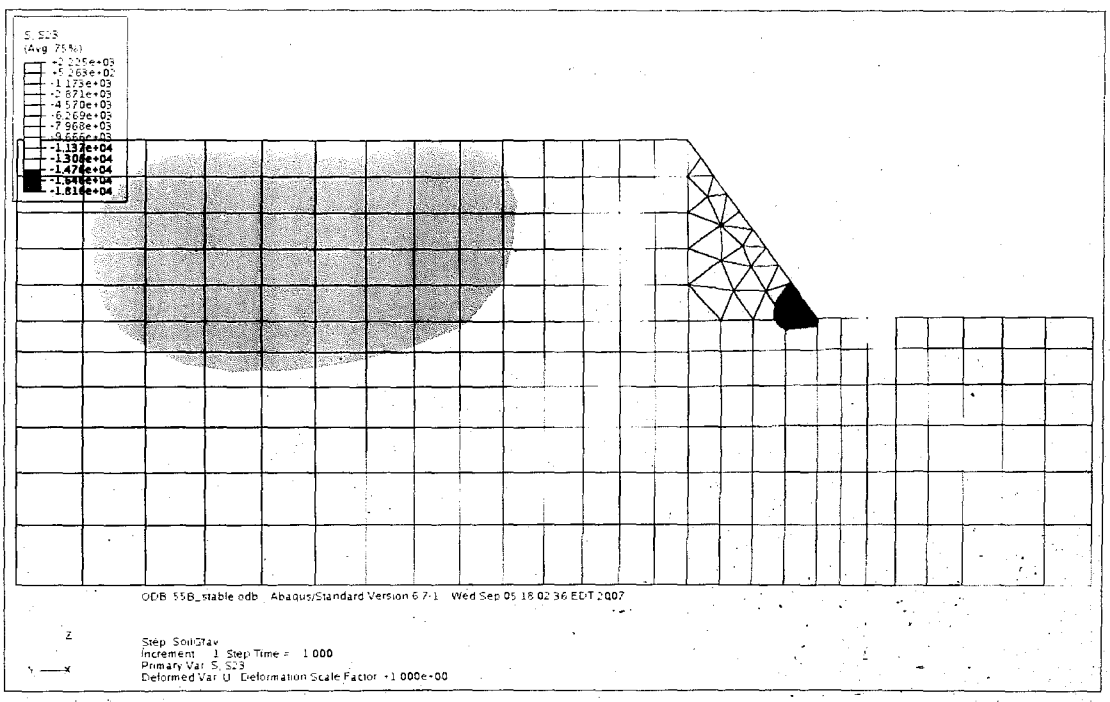

Figure 4.2.11. x-y shear stress for 55 degree stable slope: H=3.0 m.

Based on Figures 4.2.10 and 4.2.11 it is clear that the highest shear stresses are present at the toe of the slope. This is consistent with Figures 4.2.2 through 4.2.7 which show that the highest plastic strains also occur at the toe of the slope. According to plastic strains and shear stresses, the toe is a crucial point in the slope.

Based on the stable slope models, five regions of the embankment were selected to compare stress, strain, and deformation results between models, as shown in Figure 4.2.12. These locations are all in areas relevant to slope stability. Their corresponding stress and strain values are shown in Tables 4.2.1 and 4.2.2. These values will be compared to results from later models with the geotube structure in place.

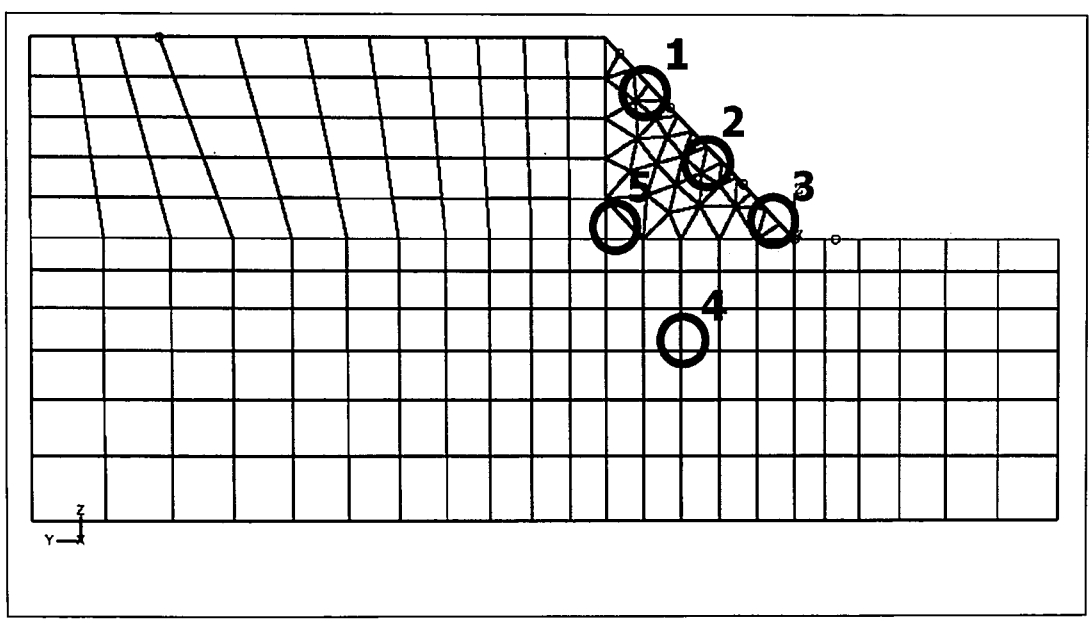

Figure 4.2.12. Selected critical locations for comparing results.

Table 4.2.1. Stress and strain results at selected locations for 45-degree stable slope model.

45° - Stable Slope – Gravity Load			
Location	Lateral Displacement (cm)	Plastic Strain Magnitude	x-y shear stress (Pa)
1	-0.39	0.0023	-9801
2	0.45	0.005	-12420
3	0.65	0.0066	-14326
4	1.79	0.0098	-9311
5	1.18	0.0064	-5937

Table 4.2.2. Stress and strain results at selected locations for 55-degree stable slope model.

55° - Stable Slope – Gravity Load			
Location	Lateral Displacement (cm)	Plastic Strain Magnitude	x-y shear stress (Pa)
1	-0.23	0.0042	-10585
2	0.57	0.0069	-12487
3	0.76	0.011	-16379
4	1.6	0.0091	-10271
5	1	0.0062	-8669

The finite element models constructed cannot simulate the formation of a slip circle as was shown in Figure 3.1.1. The assumption was made that the stack would directly restrain a soil slip circle from forming. Deep failure was not considered in any analysis or model and was assumed to not be a potential failure mode.

5 Preliminary Models

Before an effective design for a soil retaining wall composed of stacked geotubes could be developed, some preliminary models were needed. The purpose of these models was to first verify that the modelling techniques did in fact yield realistic results. Next, the procedure of sub-modelling and model assembly was explored and refined until models of different designs could be created and evaluated with ease.

5.1 Verification Model

A finite element model of a single tube was initially created and results were compared to available experimental data from literature. If the geometry from this initial model matched experimental data, the validity of the modelling techniques used and the results of subsequent models would be verified.

Liu [16] conducted a study where experimental results were used to verify a numeric model. The experiment consisted of a water-cement slurry filled tube of 1.04 m in circumference, which reached a height of 24.5 cm after deformation. A tube of same dimensions was modelled in ABAQUS using membrane elements with a mesh size of 3.7 cm. It was internally loaded with hydrostatic pressure considering the unit weight of the water-cement slurry to be twice that of water [16]. Table 5.1.1 summarizes the difference between the results of Liu's experiment and the finite element model. In this table "height" refers to the final tube height after being filled

or loaded with slurry and "base" refers to the length of the contact region for a cross-section view of a deformed tube. Figure 5.1.1 shows the final geometry of the finite element model compared to the final geometry of the tube in Liu's experiment [16]. Using a finer mesh can reduce the magnitude of the error shown in Table 5.1.1.

Table 5.1.1 Validation data for single slurry filled tube.

	FE Model	Liu [7] Data	Error
Height (m)	0.24	0.245	2.0%
Base (m)	0.22	0.25	12.0%

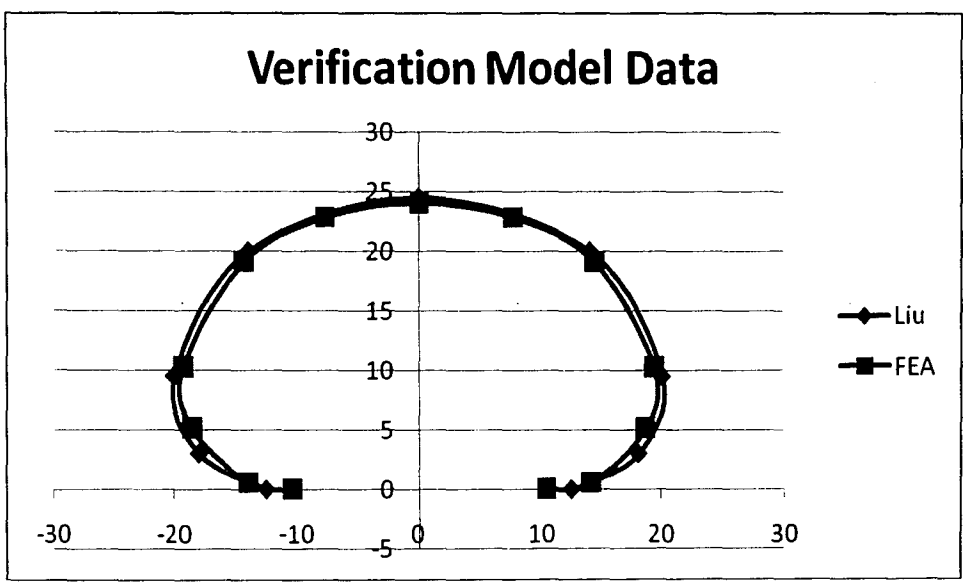

Figure 5.1.1. Verification model compared to Liu [16].

The most notable difference lies in the base contact area. However, the general shape of the deformed finite element model is very close to Liu's experimental data.

5.2 Sub Models

Different sub-models, each representing a different construction phase, were used in creating the completed model. The purpose of each sub-model is to determine initially geometry for one tube at a time.

5.2.1 Sub-model 1: Single membrane tube.

Liu [16] tested much smaller tube dimensions than would be used for an actual geotube structure. In the first sub-model, a single hollow membrane tube is defined as a uniform cylinder 2 m in diameter, 6 m long, with a wall thickness of 3 mm. This tube then was placed on an analytical rigid surface in the desired embankment shape near the toe of the slope. Aside from the scale-up dimensions, and the corresponding larger loads, the model is identical to the one that is used to model Liu's tube. First order rectangular membrane elements, approximately 0.12m x 0.12m, were used in the discretization of the tube. Reduced integration was used to shorten the computation time. The membrane elements were defined as an isotropic linear elastic material with Young's Modulus of 7.035 GPa, Poisson's ratio of 0.45, and a mass density of 75 kg/m^3, as given by Seay [18].

The model is oriented so that the origin of the system coordinates is at the toe of the slope. The x-axis runs parallel with the length of the tubes, the y-axis runs

horizontally perpendicular to the length of the tubes, and the z-axis runs vertically towards the top of the structure, depicted as the coordinates 1,2 and 3 in Figure 5.2.1.1. The model is a representative segment cut out of a much longer tube. The two ends of the tube segments are restrained in the x-direction.

The membrane tubes are also restrained along their vertical centrelines running along the vertical planes of symmetry in z direction. These centrelines are restrained from movement in the x and y directions. The x restraint will prevent wrinkling of the membrane elements from occurring. The y restraint will provide lateral stability for the tube when it is deforming. These restraints proved to be essential if a converging solution was to be found by ABAQUS for deformation of membrane tubes under internal hydrostatic loads. A contact interaction is defined between the tube and the rigid surface it is resting on. This effectively creates a restraint along the z-axis on the bottom of the tube.

The analysis of the single membrane tube is divided into four steps. First a uniform internal pressure of 12.36 kPa is applied. This is essential for the use of membrane elements here. This keeps the membrane in constant tension throughout the analysis and eliminates the possibility of wrinkling which would quickly lead to instabilities. Next a hydrostatic pressure is applied to the inside surface of the tube. The magnitude of the pressure is based on the unit weight of the soil-cement slurry, which Liu [16] used and is considered to be representative of the unit weight of a soil-water slurry that would be used in geotube construction. The hydrostatic

pressure has a maximum value of 41.20 kPa at the base of the tube and is set to zero at an elevation of 2.1 m. The 2.1 m elevation is above the top surface of the tube. This configuration simulates the pumping pressure when the tube is being pumped full of slurry [18]. Once the tube has deformed under the hydrostatic pressure, the initial uniform pressure is removed. Finally, gravity is applied to the tube resulting in an additional small amount of deformation. The initial and deformed shapes of the single tube can be seen in Figures 5.2.1.1 and 5.2.1.2. This resulting deformed shape is used as preliminary geometry for the bottom tube in stacking configuration.

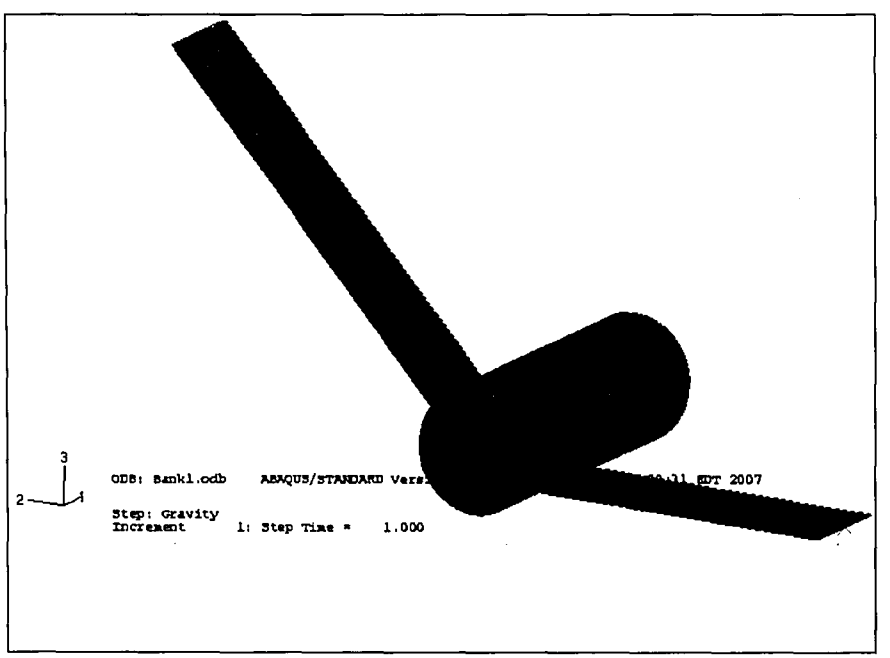

Figure 5.2.1.1. Sub-model 1: Initial shape. (The coordinates labelled as 1,2 and 3 correspond to model coordinates of x,y and z, respectively).

pressure has a maximum value of 41.20 kPa at the base of the tube and is set to zero at an elevation of 2.1 m. The 2.1 m elevation is above the top surface of the tube. This configuration simulates the pumping pressure when the tube is being pumped full of slurry [18]. Once the tube has deformed under the hydrostatic pressure, the initial uniform pressure is removed. Finally, gravity is applied to the tube resulting in an additional small amount of deformation. The initial and deformed shapes of the single tube can be seen in Figures 5.2.1.1 and 5.2.1.2. This resulting deformed shape is used as preliminary geometry for the bottom tube in stacking configuration.

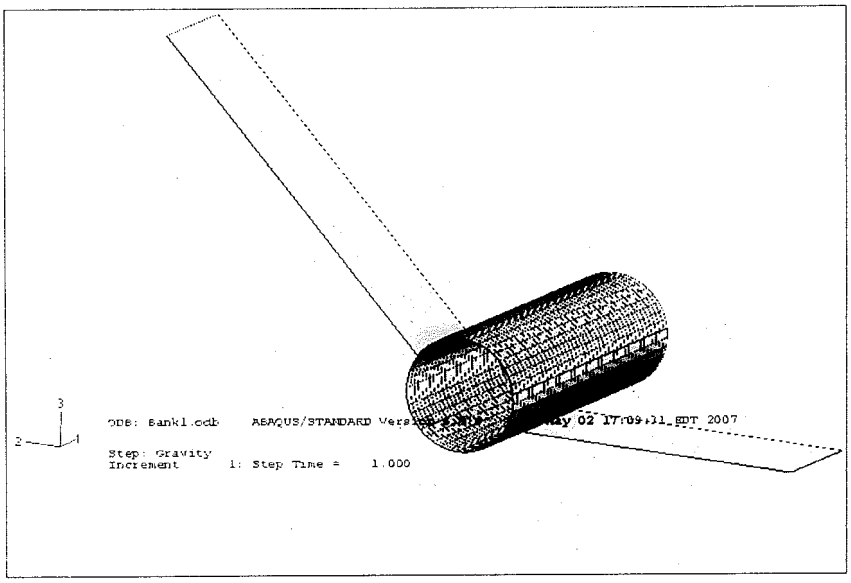

Figure 5.2.1.1. Sub-model 1: Initial shape. (The coordinates labelled as 1,2 and 3 correspond to model coordinates of x,y and z, respectively).

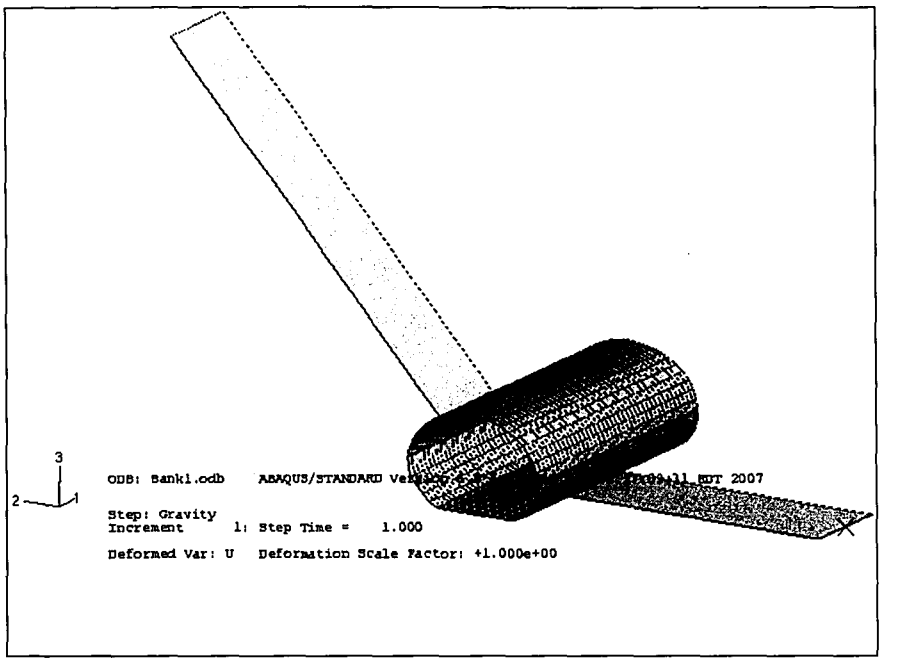

Figure 5.2.1.2. Sub-model 1: Deformed shape.

5.2.2 Sub-model 2: Solid bottom tube and membrane middle tube.

Using the deformed geometry obtained from the membrane model, a tube identical in shape and size is defined. This time, however, the tube is a solid mass of material. A skin is defined on the outer surface of the tube to represent the geotextile. The skin is assigned the same membrane elements used in the membrane models and simulates the geotextile surrounding the soil in the tube. The soil filling the tube is discretized into 0.12 m sized rectangular elements. A first order three dimensional stress element is used with reduced integration.

The solid tube is placed on the same analytical rigid surface that was used in sub-model 1. Its ends are restrained in the x-direction (axially). A coefficient of friction of 0.5 is defined between the tube and the soil slope surface [5].

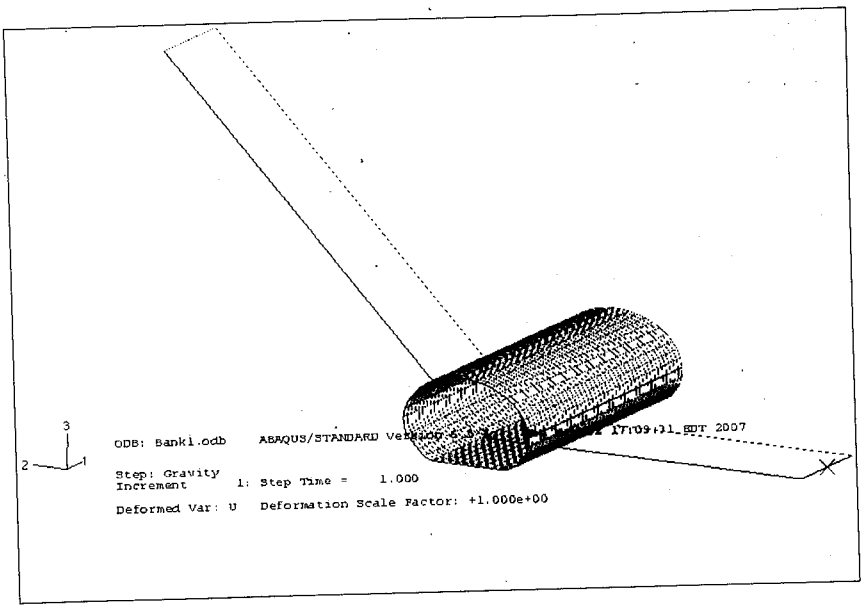

Figure 5.2.1.2. Sub-model 1: Deformed shape.

5.2.2 Sub-model 2: Solid bottom tube and membrane middle tube.

Using the deformed geometry obtained from the membrane model, a tube identical in shape and size is defined. This time, however, the tube is a solid mass of material. A skin is defined on the outer surface of the tube to represent the geotextile. The skin is assigned the same membrane elements used in the membrane models and simulates the geotextile surrounding the soil in the tube. The soil filling the tube is discretized into 0.12 m sized rectangular elements. A first order three dimensional stress element is used with reduced integration.

The solid tube is placed on the same analytical rigid surface that was used in sub-model 1. Its ends are restrained in the x-direction (axially). A coefficient of friction of 0.5 is defined between the tube and the soil slope surface [5].

The membrane tube in the middle is also restrained in the x and y directions along its vertical centrelines, similar to sub-model 1. The membrane tube is also initially restrained in the z-direction along its bottom centreline. It is positioned out of contact with the rest of the model in such a way that when deformed 0.1 m downward, it will barely come into contact with the slope and the top of the bottom tube. A coefficient of friction of 0.3 is defined between the tubes to capture the behaviour of the tubes sliding relative to each other [3].

The membrane tube is then loaded internally with a uniform pressure of 12.36 kPa as before. The tube is then entirely allowed to deform downwards to initiate contact with the bottom tube and the slope. This movement is defined in the model on only the top half of the tube. In doing this, the bottom half of the tube is free to deform when contact occurs. It acts like an air filled cushion providing a "soft contact". Otherwise, if the movement was defined on the bottom half of the tube as well, it would not stop at contact with the other surfaces, leading to large stress and strain concentrations developing at the contact points and could prevent a solution. Once this contact is established, gravity is applied to keep the tube in place. Next, the hydrostatic pressure is applied in the same manner as that of the bottom tube followed by the release of the initial uniform pressure. The deformed shape of the middle tube membrane obtained as shown in Figure 5.2.2.1. This established geometry is used as the initial shape when defining the solid tubes in the next phase of the completed stacked model.

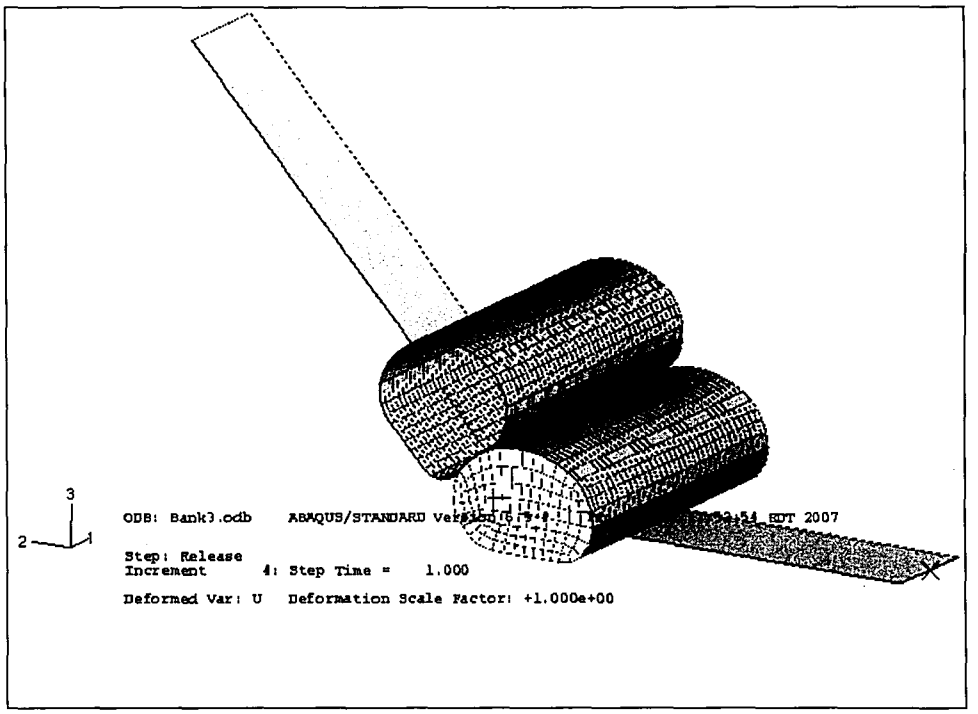

Figure 5.2.2.1. Sub-model 2: Deformed shape.

5.2.3 Sub-Model 3: Solid bottom two tubes with membrane top tube

The loading and restraint schemes of sub-model 3 are identical to sub-model 2. Sub-model 3 contains a solid middle tube stacked on the bottom tube. A membrane tube is loaded to determine the shape of the top tube. The deformed stage of sub-model 3 is shown in Figure 5.2.3.1

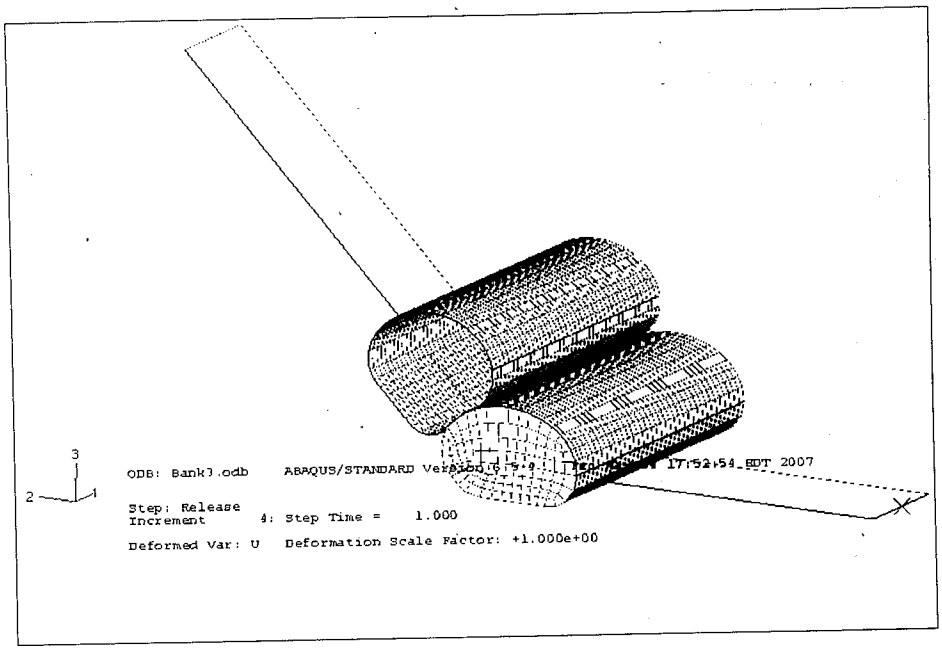

Figure 5.2.2.1. Sub-model 2: Deformed shape.

5.2.3 Sub-Model 3: Solid bottom two tubes with membrane top tube

The loading and restraint schemes of sub-model 3 are identical to sub-model 2. Sub-model 3 contains a solid middle tube stacked on the bottom tube. A membrane tube is loaded to determine the shape of the top tube. The deformed stage of sub-model 3 is shown in Figure 5.2.3.1

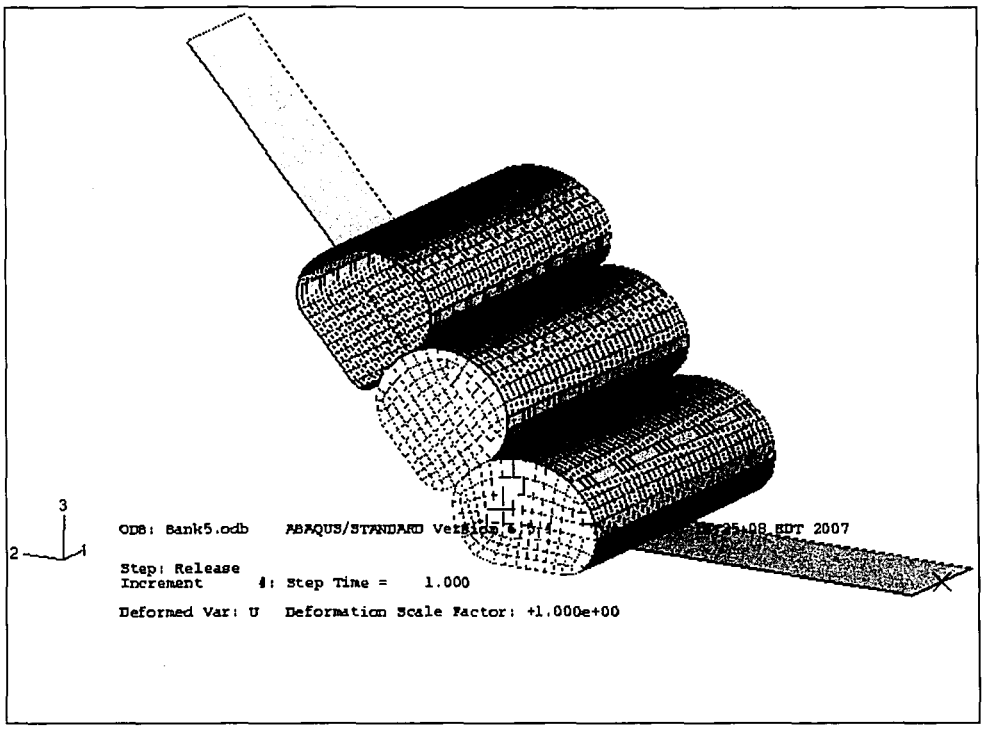

Figure 5.2.3.1. Sub-model 3: Deformed Shape.

5.2.4 Complete Stack: All solid tubes on soil slope and foundation.

The final assembled model includes the three solid tubes resting on the embankment. (Figure 3.2.1). At this point, however, only the tubes' initial geometry has been obtained. They are not acting in any way as a soil retention structure and up until now, and the bottom tube has been restrained laterally in the interest of temporarily stabilizing the structure. The tubes are placed on an unstable embankment, as determined from the earlier slope models, and any artificial restraints must be removed. The embankment is modelled the same way it was for the slope models. A section of the completed model is shown in Figure 6.1.1.1.

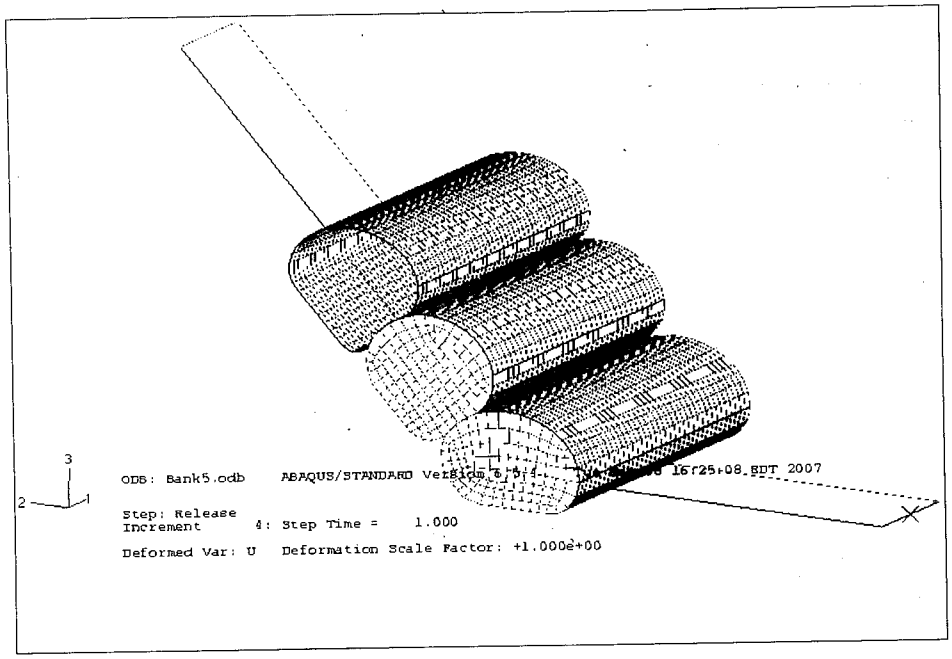

Figure 5.2.3.1. Sub-model 3: Deformed Shape.

5.2.4 Complete Stack: All solid tubes on soil slope and foundation.

The final assembled model includes the three solid tubes resting on the embankment. (Figure 3.2.1). At this point, however, only the tubes' initial geometry has been obtained. They are not acting in any way as a soil retention structure and up until now, and the bottom tube has been restrained laterally in the interest of temporarily stabilizing the structure. The tubes are placed on an unstable embankment, as determined from the earlier slope models, and any artificial restraints must be removed. The embankment is modelled the same way it was for the slope models. A section of the completed model is shown in Figure 6.1.1.1.

As the stack of solid tubes was placed on the modelled embankment and loaded with gravity, it was clear that the structure was failing by means of sliding. This had been observed earlier. This specific failure mode was confirmed by running models with and without lateral restraints on the bottom tube. The ABAQUS solver could obtain a converging solution when gravity was applied with the restraints for sliding. The solver was unable to complete the analysis, indicating a divergence from a solution when the same model was run without restraining the bottom tube.

6 Retaining wall designs

The following models are all different design attempts aimed at achieving two things: a stable structure and a structure that improves slope stability. The stability of the structure relies on the bottom tube remaining stationary. For improving slope stability, the goal of the structure is to reduce stresses and strains in the embankment.

The primary goal of the designs was to eliminate lateral movement of the stack. After this was achieved, modifications could be explored that improved the structure's performance in improving the slope stability. It had been previously observed that the structure was prone to movement by means of sliding down the embankment slope. The issue had been temporarily avoided by imposing an artificial lateral constraint on the bottom tube. This constraint was removed and consequently the bottom tube needed to be restrained with an innovative design

alteration. The primary criteria for such an alteration was to keep the construction process easy and straightforward but still maintain the functionality of the structure.

6.1 Design 1

Design 1 did not satisfy the ease of construction stipulation, but it did allow for some insight as to how well a stabilized structure would work. It was simply recognized that the bottom tube had to be restrained somehow so a flat rigid vertical plane was placed in front of the bottom tube.

6.1.1 Design 1 Development

The idea of constructing a rigid completely unmoving wall in front of the bottom tube is unrealistic, but it was used as a model constraint because it achieved the same effect that a more realistic modification would be required to achieve. As the structure was loaded with gravity, the bottom tube would deform along this plane, but still remain in place. A section of design 1 is shown in Figure 6.1.1.1.

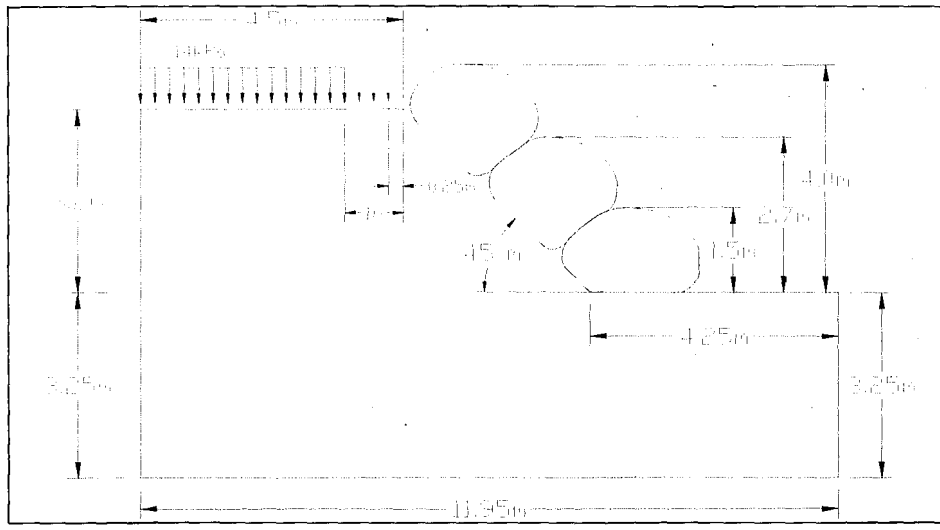

Figure 6.1.1.1. Section of design 1.

This model provided the first look at how the tube stack would affect stresses and strains in the unstable slope. The stack performed well by directly restraining lateral movement of the slope's surface. Models of 45 degree and 55 degree slopes with applied surcharge loads were created and analyzed. The surcharge loads were intended to simulate a two-lane road structure at the top of the embankment. A magnitude of 14 kPa was selected for road surcharge load. 14 kPa is equal to about 300 psf which is slightly above a traffic surcharge load for retaining wall design as defined by AASHTO Standard Specifications for Highway Bridges [2]. The surcharge in the models of design 1 began at the leftmost edge of the embankment and approached to the top edge of the slope by variable distances of 1 meter or 0.25 meter.

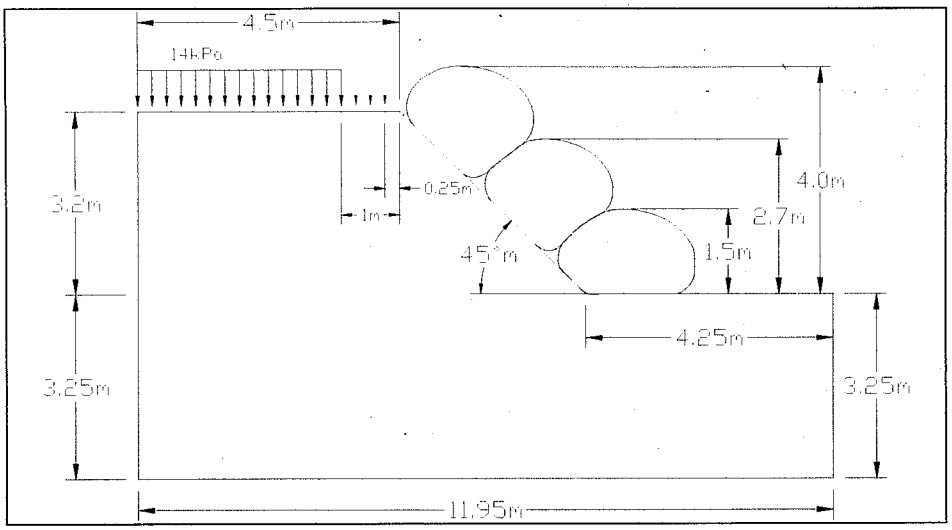

Figure 6.1.1.1. Section of design 1.

This model provided the first look at how the tube stack would affect stresses and strains in the unstable slope. The stack performed well by directly restraining lateral movement of the slope's surface. Models of 45 degree and 55 degree slopes with applied surcharge loads were created and analyzed. The surcharge loads were intended to simulate a two-lane road structure at the top of the embankment. A magnitude of 14 kPa was selected for road surcharge load. 14 kPa is equal to about 300 psf which is slightly above a traffic surcharge load for retaining wall design as defined by AASHTO Standard Specifications for Highway Bridges [2]. The surcharge in the models of design 1 began at the leftmost edge of the embankment and approached to the top edge of the slope by variable distances of 1 meter or 0.25 meter.

6.1.2 Results From Design 1 Models

The success and effectiveness of this structure is based on its ability to reduce strains and displacements of an unstable slope subject to surcharge and gravity loads. The embankments modelled in design 1 differ in geometry from the stable slope models. Additionally, the internal angle of friction, φ, of 18.3 degrees was used in design 1. This is considerably lower than any of the other models. It is for this reason that stress and strain values will only be compared to slopes without tubes (modelled specifically for design 1) that have the same geometry and friction angle.

Figure 6.1.2.1 shows the maximum principal plastic strain vectors for the unstable 55-degree slope without the tubes. The location of the highest magnitude principle strains is seen near the slope toe. This is similar to the response of the earlier stable slope models with the higher friction angle and different embankment geometry.

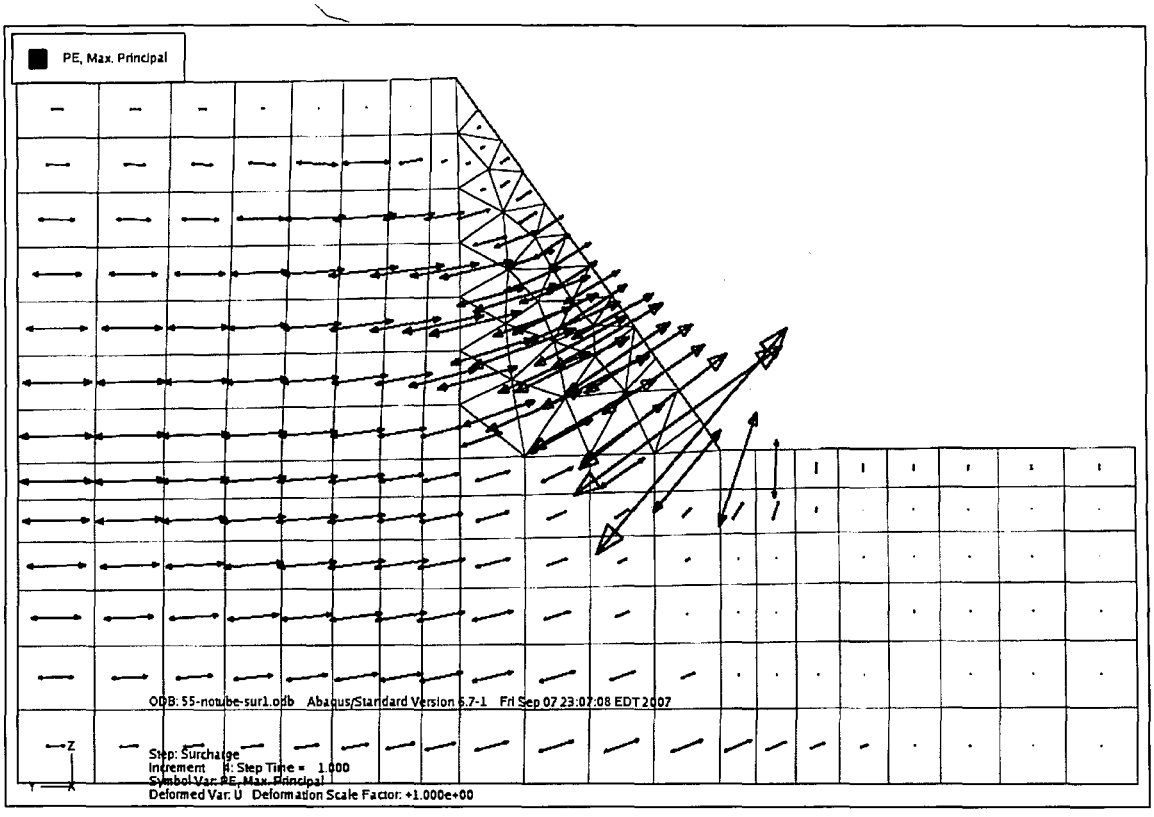

Figure 6.1.2.1. Maximum principle plastic strain vectors; 55-degree slope w/o tubes.

The lateral component of displacement is illustrated in Figure 6.1.2.2. The zone right above the toe is of the highest magnitude. The slope deforms horizontally to the right by 5.5 cm at this location. This behaviour differs from the stable slope models. In the stable slope models the maximum displacement was occurring a few meters beneath the slope. In these models of design 1, though, the bottom tube is in an ideal place to directly restrain the region experiencing the largest lateral deformation.

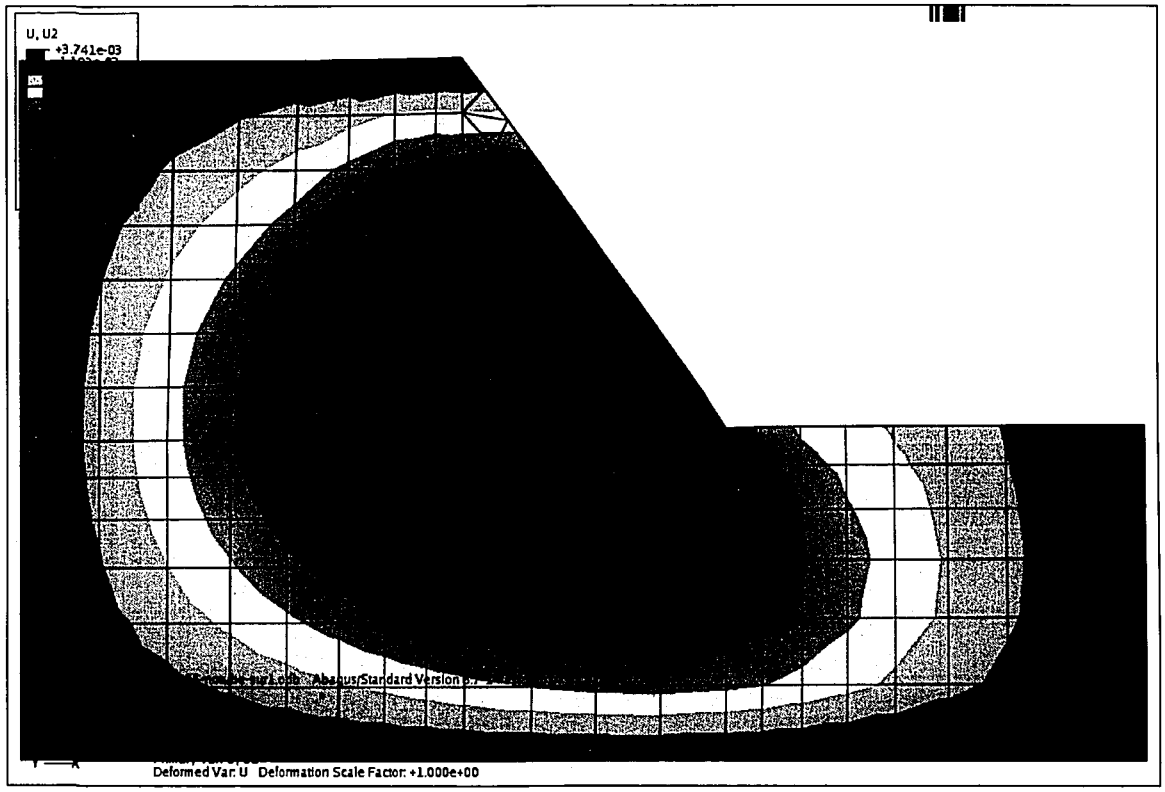

Figure 6.1.2.2. Lateral displacement in 55-degree slope without tubes for design 1.

Figure 6.1.2.3 shows the lateral displacements for the same slope and surcharge load, with geotubes in place.

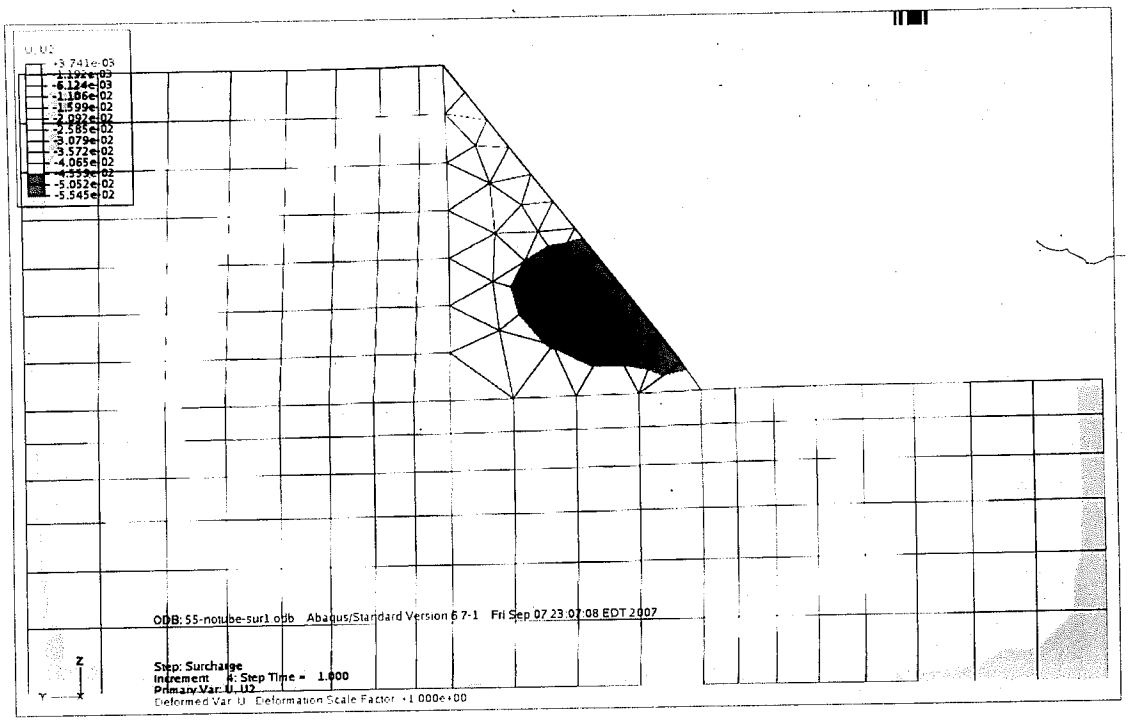

Figure 6.1.2.2. Lateral displacement in 55-degree slope without tubes for design 1.

Figure 6.1.2.3 shows the lateral displacements for the same slope and surcharge load, with geotubes in place.

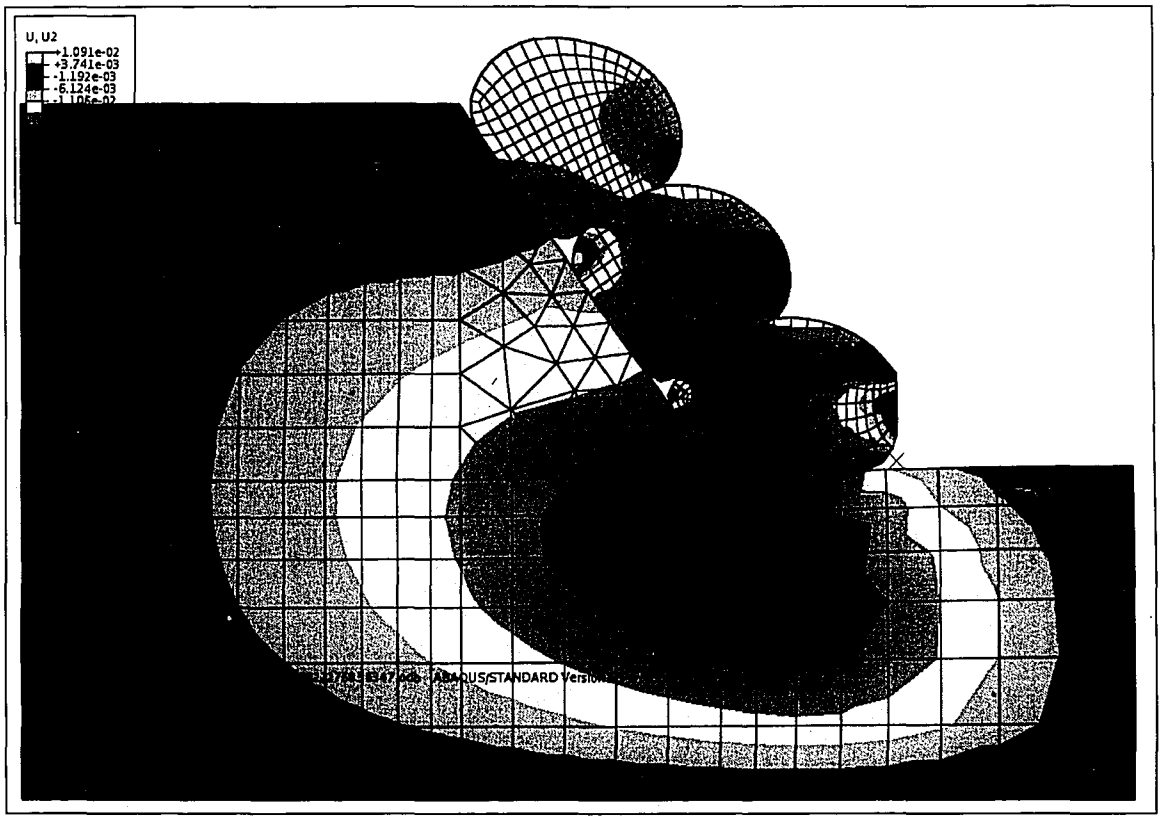

Figure 6.1.2.3. Lateral displacements in 55 degree slope with tubes for design 1.

Figures 6.1.2.2 and 6.1.2.3 demonstrate that the magnitude of lateral displacement is considerably reduced due to the implementation of the geotube stack.

In Figures 6.1.2.4 and 6.1.2.5, the values of lateral displacement at the nodes along the face of the slope for each model are plotted against their vertical height. The dashed lines represent the results of the models with tubes. The reductions in strains are clearly visible where each tube is resting against the slope. These curves demonstrate that the slope surface deform significantly less when the tubes are in place.

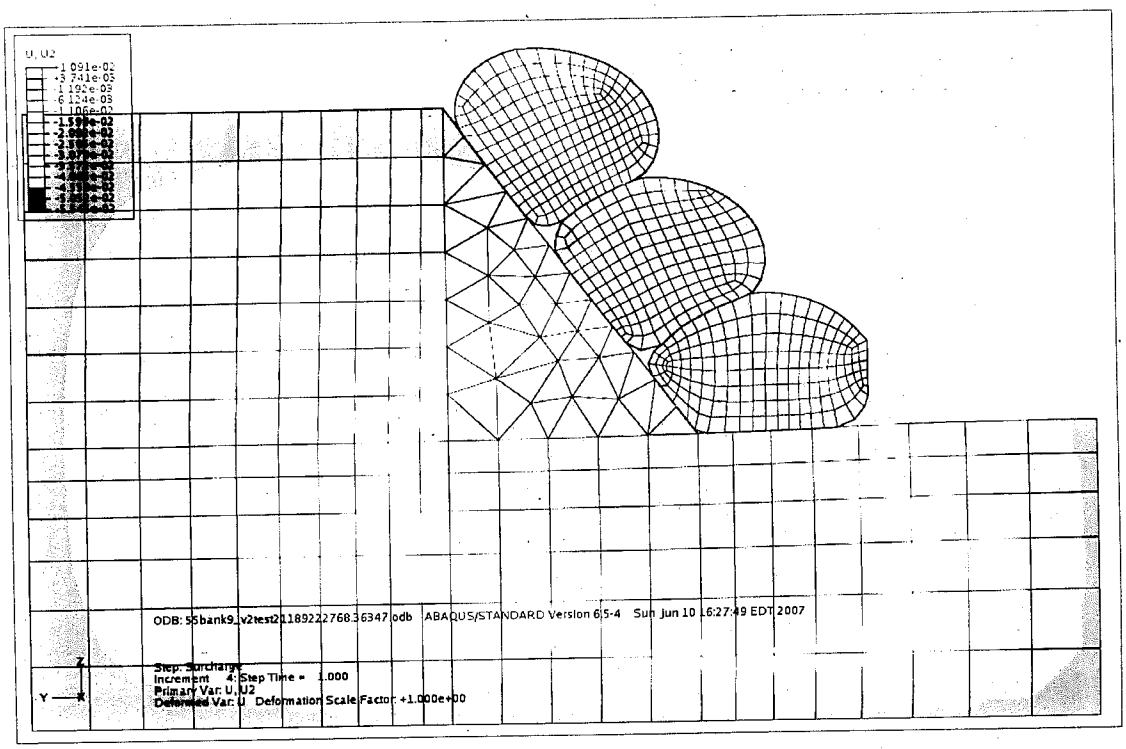

Figure 6.1.2.3. Lateral displacements in 55 degree slope with tubes for design 1.

Figures 6.1.2.2 and 6.1.2.3 demonstrate that the magnitude of lateral displacement is considerably reduced due to the implementation of the geotube stack.

In Figures 6.1.2.4 and 6.1.2.5, the values of lateral displacement at the nodes along the face of the slope for each model are plotted against their vertical height. The dashed lines represent the results of the models with tubes. The reductions in strains are clearly visible where each tube is resting against the slope. These curves demonstrate that the slope surface deform significantly less when the tubes are in place.

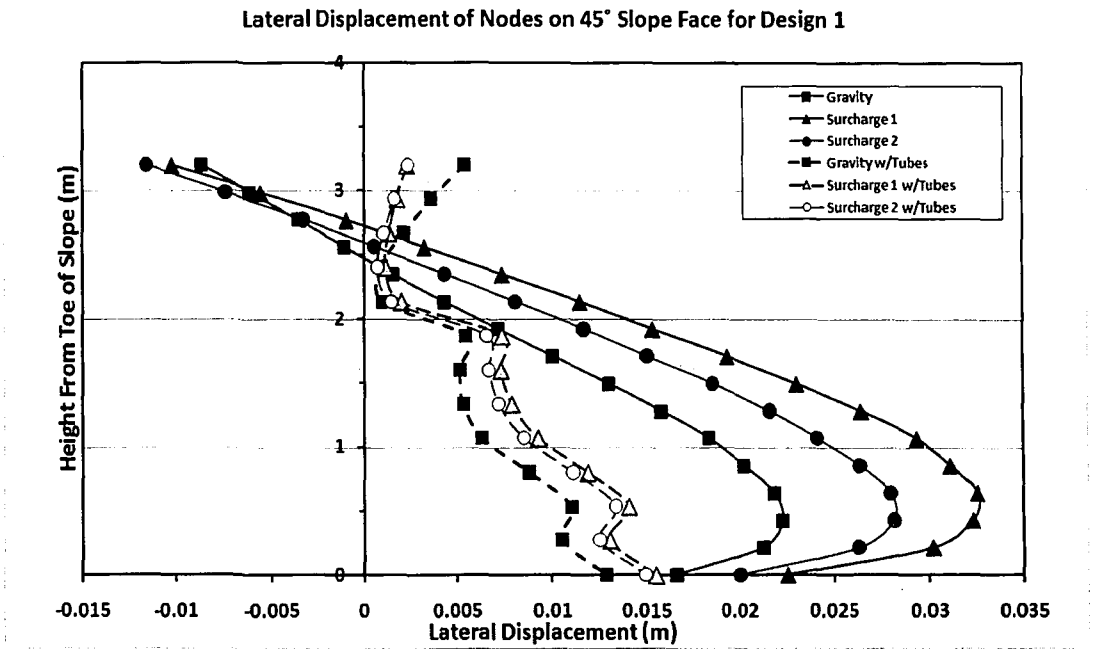

Figure 6.1.2.4. Lateral displacement of nodes on 45 degree slope face for design 1.

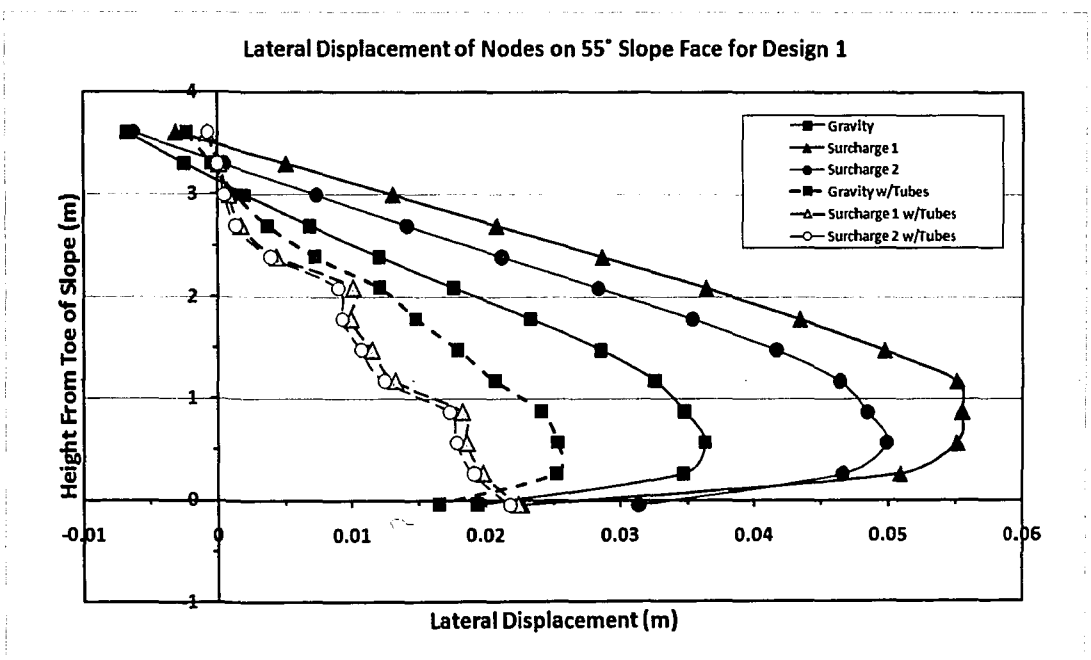

Figure 6.1.2.5. Lateral displacement of nodes on 55 degree slope face for design 1.

Figure 6.1.2.6 is similar to Figures 6.1.2.4 and 6.1.2.5, but it contains the solutions obtained for the two different angle slope loaded with gravity only. This figure serves to show that the tubes on the 55-degree slope have more of an influence than the tubes on the 45 degree slope. They are approximately twice as effective on the steeper slope at reducing lateral movement. This may be attributed to the fact that when the tubes are stacked steeper, they are carrying more of their own weight and less is being transferred to the slope underneath. If the slope carries more weight, particularly on the upper half, it has more pressure causing it to bulge out near the bottom.

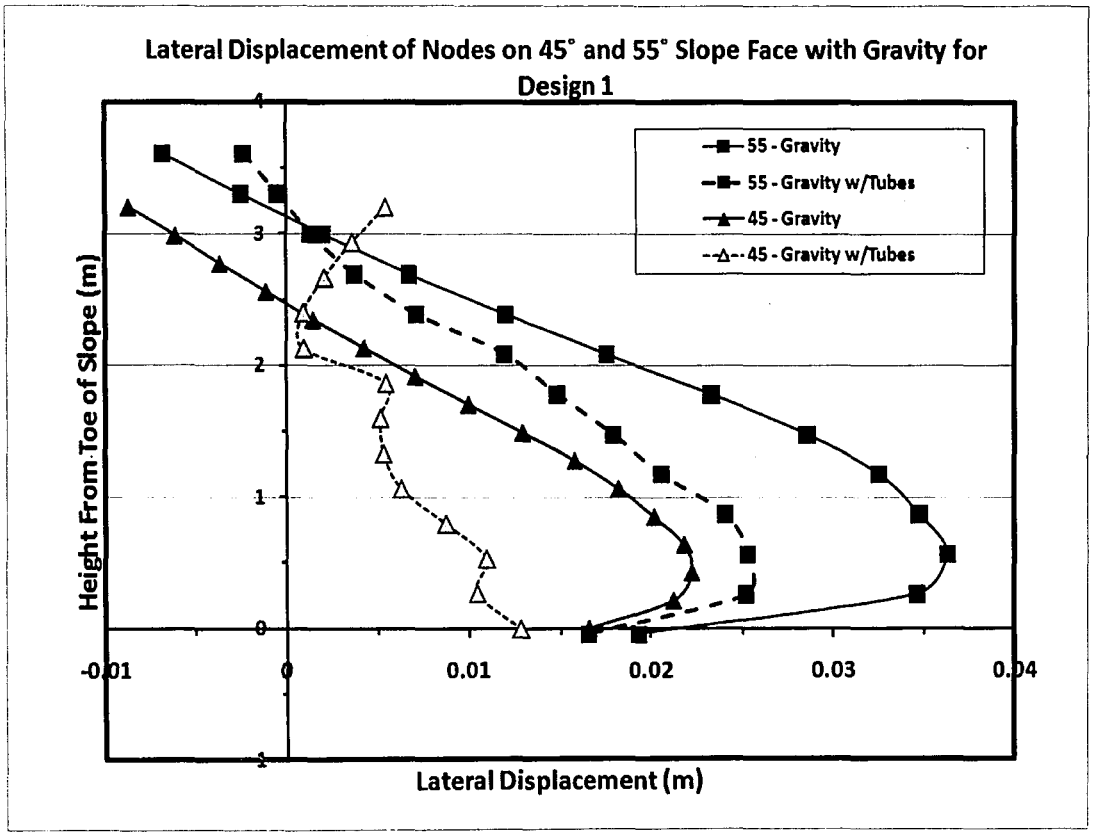

Figure 6.1.2.6. 45 and 55-degree slope lateral displacement comparison with and without tubes.

Tables 6.1.2.1 and 6.1.2.2 compare stress and strain values between models under gravity load with and without tubes for design 1. As was mentioned earlier, the slope models without the tubes in this comparison are not the same as the stable slope models. Models of embankments without the tubes were created specifically for design 1 because of the different geometry and friction angle. One of these models was shown in Figure 6.1.2.2. The comparative stress and strain values, however, are from the selected locations identified in Figure 4.2.12. A third column in the table, under the lateral displacement and plastic strain sections show the percent increase or reduction in these parameters caused by the tubes. This value is calculated by equation 3, as following:

$$\%\text{Reduction} = \frac{(\Delta_{w/tubes} - \Delta_{w/o,tubes})}{\Delta_{w/tubes}} \qquad (3)$$

For the shear stress values, the third column also included which lists the percent increase or reduction in the shear stress magnitude. This is calculated by equation 4:

$$\%\text{Reduction} = \frac{(|\Delta_{w/o,tubes}| - |\Delta_{w/tubes}|)}{\Delta_{w/o,tubes}} \qquad (4)$$

Table 6.1.2.1. Stress and strain results comparison at selected locations for 45-degree design 1 model under gravity load.

Design 1 - 45° - Gravity Load									
	Lateral Displacement (cm)			Plastic Strain Magnitude			x-y shear stress (Pa)		
Location	w/o tubes	w/ tubes	% +/-	w/o tubes	w/ tubes	% +/-	w/o tubes	w/ tubes	% Δ mag.
1	0.63	0.06	-90.5	0.004	0.003	-28.9	-8428	1782	-79
2	1.86	0.55	-70.4	0.004	0.005	22.7	-8441	-3817	-55
3	2.275	1.084	-52.4	0.014	0.004	-69.3	-10323	-1127	-89
4	2.61	1.36	-47.9	0.011	0.017	54.5	-9043	-4325	-52
5	2.356	0.691	-70.7	0.01	0.013	30	-5445	1829	-66

Table 6.1.2.2. Stress and strain results comparison at selected locations for 55-degree design 1 model under gravity load.

Design 1 - 55° - Gravity Load									
	Lateral Displacement (cm)			Plastic Strain Magnitude			x-y shear stress (kPa)		
Location	w/o tubes	w/ tubes	% +/-	w/o tubes	w/ tubes	% +/-	w/o tubes	w/ tubes	% Δ mag.
1	1.322	0.31	-76.6	0.004	0.011	175	-7469	-835	-89
2	3.17	1.18	-62.8	0.014	0.009	-35.7	-7094	-9267	30.6
3	3.53	1.574	-55.4	0.026	0.006	-78.8	-11457	3867	-66
4	2.861	1.719	-39.9	0.011	0.019	72.7	-12453	-3321	-73
5	2.81	1.212	-56.9	0.013	0.014	7.69	-9332	1347	-86

The most notable aspect of Tables 6.1.2.1 and 6.1.2.2 is that lateral displacements are reduced significantly in all locations examined, as negative sign under % change indicates a reduction in that particular value. Plastic strain and shear stress magnitudes are improved in some places, but are worse in others. The areas that are worse can be attributed to the fact that the slope, while deforming less, is also supporting the weight of the tubes.

One aspect of this model that can be improved on is the length that the top of the embankment extends behind the slope. In this model, the surcharge proximity varies from the edge the slope but in both cases extents to the left boundary of the modelled space at the top of the slope. Because of this aspect, the left edge of the embankment may act as an unrealistic boundary, which influence the behaviour around the slope and the tubes. Future models will extend the left boundary farther enough so that there is a zone of unloaded embankment top – that is no surcharge.

Another item of the model that will be changed is the angle of friction. The soil modelled here has an angle of friction, φ, equal to 18.3 degrees. This is quite low. Future models will have and angle of friction, φ, equal to 35 degrees.

In overall analysis, it is evident that the geotube stack does, in fact, reduce the displacements in each slope configuration considered here. However, the problem of the rigid wall remains. A more realistic restraining method for the bottom tube is of importance.

6.2 Design 2

Design 2 utilized a geo-textile blanket, presumably the same material that was used in the tubes themselves, that was attached to the bottom tube and ran along the slope surface underneath the middle and top tube. The idea was that the weight of the top two tubes pressing down on the blanket underneath would generate enough friction to prevent the bottom tube, which was attached to the blanket, from moving once the rigid wall from design 1 was removed. An anchor at the top of the blanket was also considered to add to its restraining capability.

6.2.1 Design 2 Development

Design 2, which incorporated a blanket of geotextile on the slope surface was challenging to model using finite elements. Membrane elements are by nature

relatively unstable due to the fact that they have zero bending stiffness. To avoid wrinkling and excessive non-linear deformations the membrane must be in tension. In design 2, a membrane blanket was sandwiched in between the slope and the tubes. These interactions are relatively complex. Two deformable solid surfaces, the tubes and the soil are interacting with each other via the membrane. For the interactions to yield accurate results, the structure must be static and unmoving. If the tubes slide at all, the membrane will wrinkle and experience non-uniform stresses and strains. To avoid this, the interactions must already be established and functioning correctly before the tubes are loaded with gravity. The catch is that the tubes' weights are exactly what provides the friction necessary for the interactions to work. Effectively a loop is created where stability and correct interaction behaviour depend on each other and neither can exist unless the other already does. In theory, the mechanism of the blanket stabilizing the structure is possible, but attempting to model this with finite elements introduces too many opportunities for instabilities to develop, particularly in the membrane elements composing the blanket.

6.2.2 Results from Design 2 Model

A model of design 2 depending on artificial constraints was developed with a converging solution. The constraints required to achieve this were to prevent the blanket under the tubes from separating from the slope and to anchor it at the top. Since the bottom tube was attached to the blanket it was prevented from sliding. When the same model was run that allowed the blanket to separate from the slope

but still retained the anchor at the top, the ABAQUS solver could not reach a solution.

There are two likely reasons for this. The first lies in the aforementioned difficulties modelling membrane elements and the crucial interactions that are imposed on them here. The second reason could be that on the line along the bottom tube where the blanket is attached, excessive stress concentrations quickly lead to divergence from a solution when applying the stiffness equations of the model. In reality the blanket would be stitched to the tube. Stitches in the geotextile are essentially the weak links of the structure. A stitch connecting the blanket to the bottom tube would tear if too large of a force applies to it. It may be possible to develop a method of stitching the blanket to the tube that minimize the risk of tear, hence distribute stress more evenly, but this was not attempted in any of the models nor was it the goal of this research.

6.3 Design 3

Design 3 uses a principle similar to that of design 1. It uses an outside component to stabilize the bottom tube. In the interest of replacing the rigid wall with something more realistic, stakes were used instead. In construction, these stakes could be transported and installed by driving them into the ground directly in front of the bottom tube. They could be any shape or material as long as they could resist the bending and shear imposed by tube sliding into them.

6.3.1 Design 3 Development

Attempts with 3, 4 and 5 evenly spaced stakes were made for the 45-degree slope configuration. All models proved to be successful, but the one with four stakes spaced two meters apart was chosen for all subsequent models.

The stakes were modelled as discrete rigid tubes. These are non-deformable components of the model completely restrained in every direction. They are meshed with rigid elements. This approach was chosen to initially avoid the process of determining a minimum material strength and section for each stake. A design for the stakes was not under consideration.

Due to the success of the stakes as a restraining method for the bottom tube, work could proceed and more information could be gathered on the reliability of the structure and performance under a variety of loading conditions. The surcharge of 14 kPa was applied to the 45 and 55-degree slope configurations. The proximity of the surcharge to the edge of the slope was varied as 0 m, 0.5 m and 1 m. The width of the surcharge area was 7.6 meters (approximately two traffic lanes). Design 3 results are compared with results from the stable slope models. Data from twenty-one variations on models of design 3 will be used.

All models use two load steps. The first step applies gravity to the entire model. The second step applies the surcharge load. Figure 6.3.1.1 is a sketch showing the configuration of a section of design 3 and the surcharge load types applied.

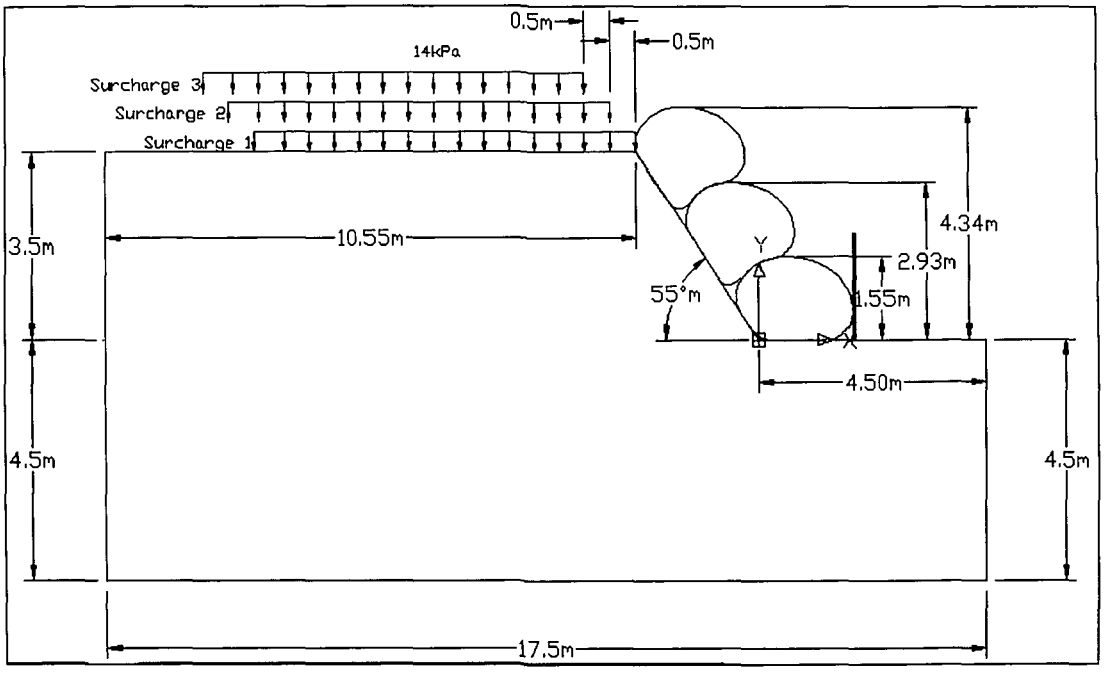

Figure 6.3.1.1. Section of design 3.

A comparison of Figures 6.3.1.1 and 6.1.1.1 will show that the soil block modelled as the foundation and embankment used in design 3 has larger dimensions than the one used in design 1. The surcharge proximities are different as well. Also, the internal friction angle, φ, was increased to 35 degrees.

6.3.2 Results From Design 3 Models

In analysis it was found that though plastic strain and shear stress were reduced in some locations, lateral deformations increased by the application of tubes in more

locations. Tables 6.3.2.1, 6.3.2.2-a, and 6.3.2.2-b are comparisons of stress and strain values at the predetermined select locations (see Figure 4.2.12) between design 3 models with tubes in place and models without tubes. The results shown in these tables are from embankments under a gravity load. Note that for the 55-degree models, there are two models without tubes: the stable 3.0m high model and the unstable 3.5m high model. These comparisons are presented separately in two tables for the 55-degree slope.

Table 6.3.2.1. Stress and Strain results at standard locations for 45 degree slope in design 3.

Design 3 - 45° - Gravity Load									
	Lateral Displacement (cm)			Plastic Strain Magnitude			x-y shear stress (Pa)		
Location	stable	w/ tubes	% +/-	stable	w/ tubes	% +/-	stable	w/ tubes	% Δ mag.
1	-0.39	-0.17	-56.9	0.002	0.004	87	-9801	-4186	-57
2	0.45	0.18	-60	0.005	0.006	22	-12420	-8593	-31
3	0.65	0.79	21.5	0.007	0.003	-53	-14326	-3496	-76
4	1.796	1.197	-33.4	0.01	0.013	32.7	-9311	-4416	-53
5	1.19	0.513	-56.9	0.006	0.009	45.3	-5937	1836	-69

Table 6.3.2.2-a. Stress and strain results at standard locations for 55-degree slope in design 3; H=3.0 m.

Design 3 - 55° - Gravity Load; H=3.0 m (stable)									
	Lateral Displacement (cm)			Plastic Strain Magnitude			x-y shear stress (Pa)		
Location	w/o tubes	w/ tubes	% +/-	w/o tubes	w/ tubes	% +/-	w/o tubes	w/ tubes	% Δ mag.
1	-0.1	-0.32	239	0.003	0.005	42.4	-9869	-2249	-77
2	0.97	0.554	-42.9	0.008	0.009	6.02	-12809	-6963	-46
3	1.173	1.25	6.55	0.013	0.003	-81.1	-16143	-5612	-65
4	1.91	1.3	-31.9	0.011	0.014	27.3	-10563	-4102	-61
5	1.45	0.92	-36.6	0.008	0.01	35.1	-9740	-910	-91

Table 6.3.2.2-b. Stress and strain results at standard locations for 55 degree slope in design 3; H=3.5 m

Design 3 - 55° - Gravity Load; H=3.5 m (unstable)									
	Lateral Displacement (cm)			Plastic Strain Magnitude			x-y shear stress (Pa)		
Location	stable	w/ tubes	% +/-	stable	w/ tubes	% +/-	stable	w/ tubes	% Δ mag.
1	-0.23	-0.32	40	0.004	0.005	11.9	-10585	-2249	-79
2	0.57	0.554	-2.81	0.007	0.009	27.5	-12487	-6963	-44
3	0.76	1.25	64.5	0.011	0.003	-77.3	-16379	-5612	-66
4	1.6	1.3	-18.8	0.009	0.014	53.8	-10271	-4102	-60
5	1	0.92	-8	0.006	0.01	67.7	-8669	-910	-90

These tables show that the lateral deformations are increased by the tubes in more locations than before, including the toe section (location 3). Plastic strain magnitudes are decreased overall and shear stresses are decreased significantly everywhere.

Figures 6.3.2.1 and 6.3.2.2 show lateral deformation of nodes on the slope surface plotted against their vertical location. These charts show results from all models including all surcharges applied and the slope angles. As noted before, the tubes reduce the deformations, but in many, the deformations are higher, particular to interest the toe area.

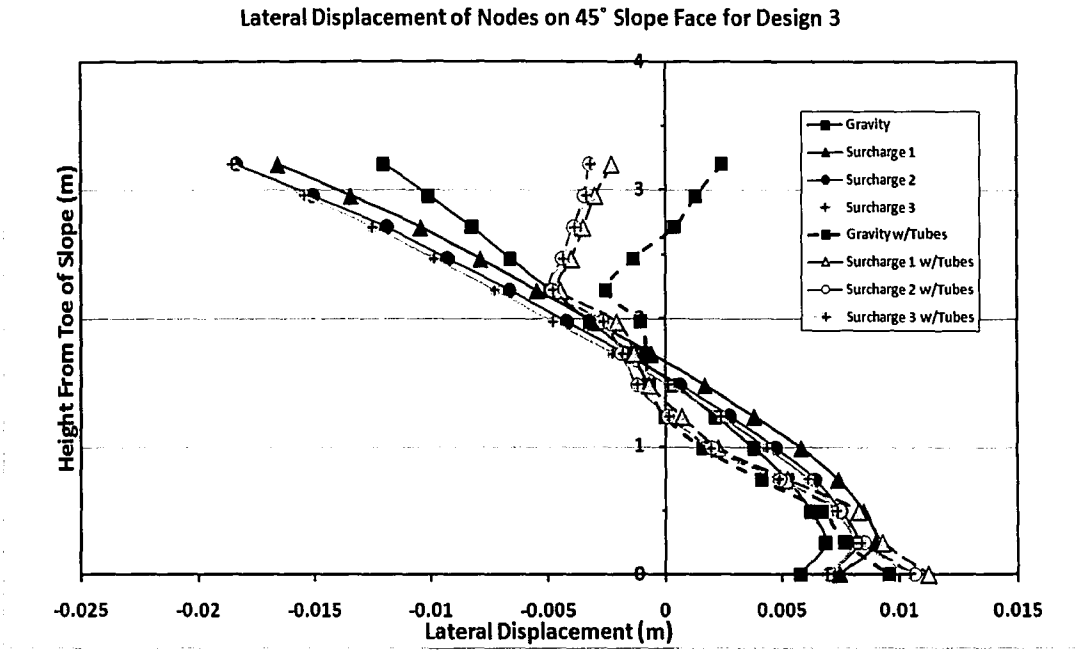

Figure 6.3.2.1. Lateral displacements for 45 degree slopes.

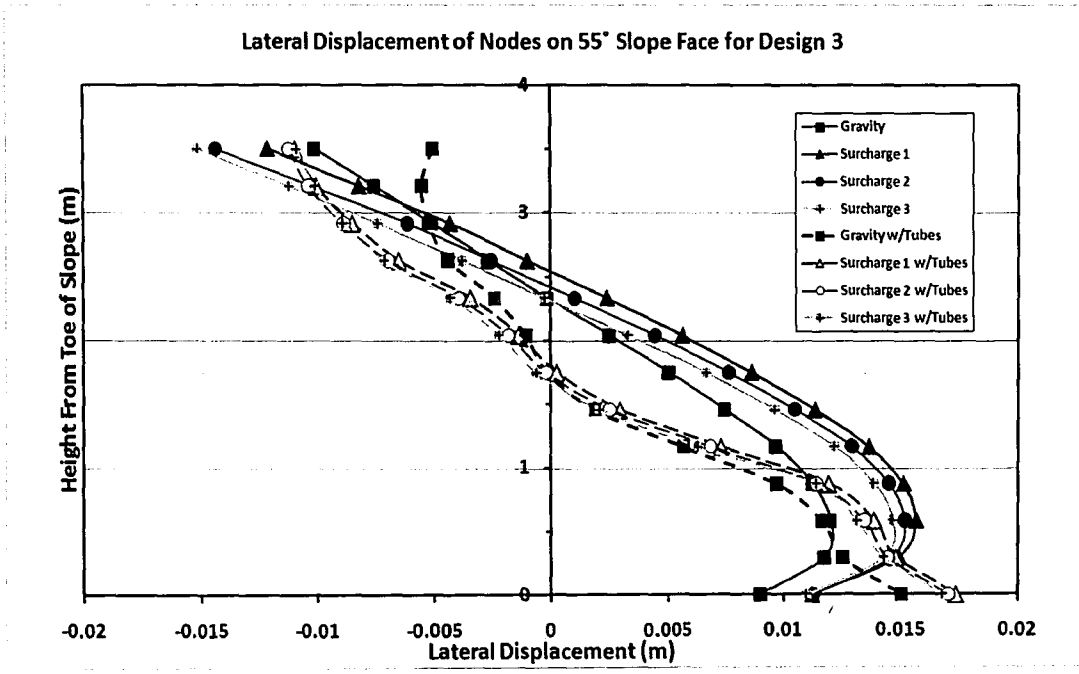

Figure 6.3.2.2. Lateral displacements for 55 degree slopes.

Figures 6.3.2.3 shows lateral displacements of nodes on the slope surface for 45 and 55-degree slopes under surcharge. The purpose of this chart is to illustrate the difference in influence that the structure has for the two slope angles. In the 45degree slope the tubes have more of an influence near the top. The displacement is much higher with the tubes in place than in the 55-degree slope. In both slopes the tubes increase movement at the toe, but in the 55-degree slope this increase is slightly higher.

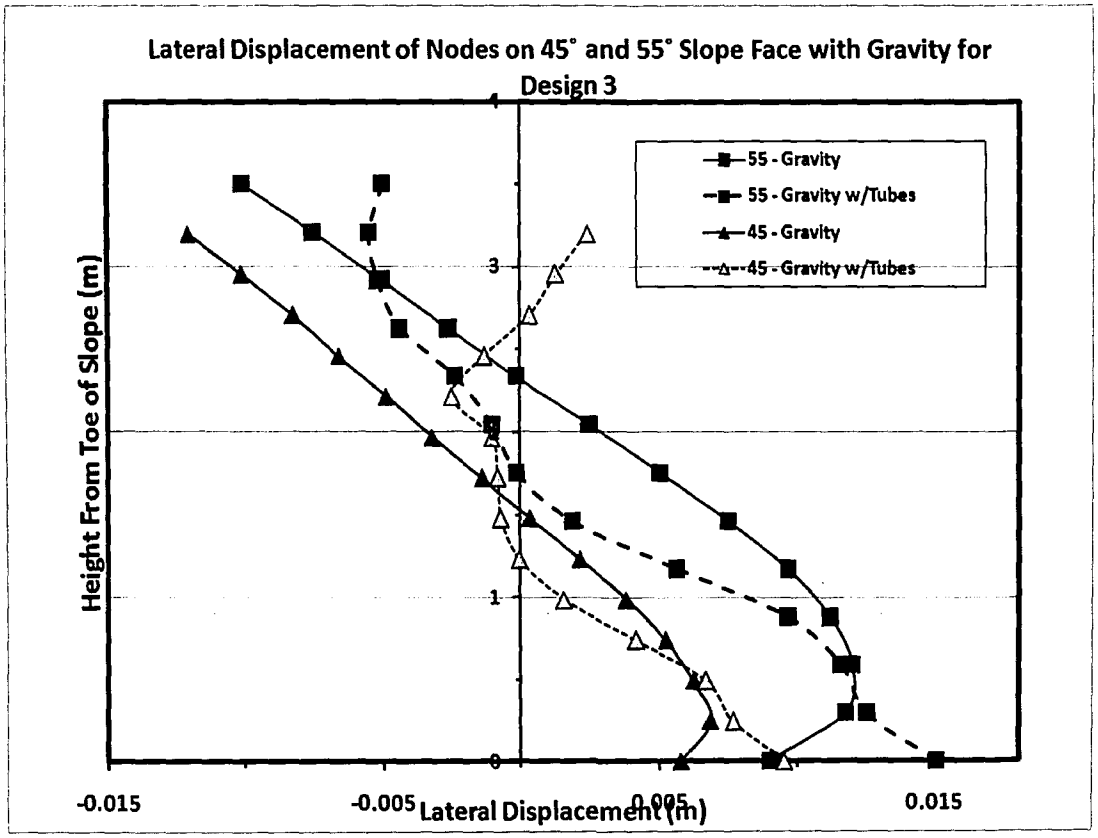

Figure 6.3.2.3. 45 and 55 degree slope lateral displacement comparison with and without tubes.

These models of geo-tube applied embankments did behave quite differently than the embankments without tubes modelled for design 1 due to the different geometry and

friction angle used. An exception is the maximum principle plastic strain vectors. Shown in Figure 6.3.2.4, are the maximum principle plastic strain vectors for the 55 degree embankment used in design 3 with gravity applied. Note that this embankment has a height of 3.5 which is 0.5 meters higher than the 55 degree stable slope that was shown earlier in the stable slope models' results. Figure 6.3.2.4 is intended to be representative of the behaviour of all of the slopes without tubes modelled for design 3. In all of these models with different slope angles and surcharge proximities the stress and strain magnitudes varied, but the overall deformation trends were the same.

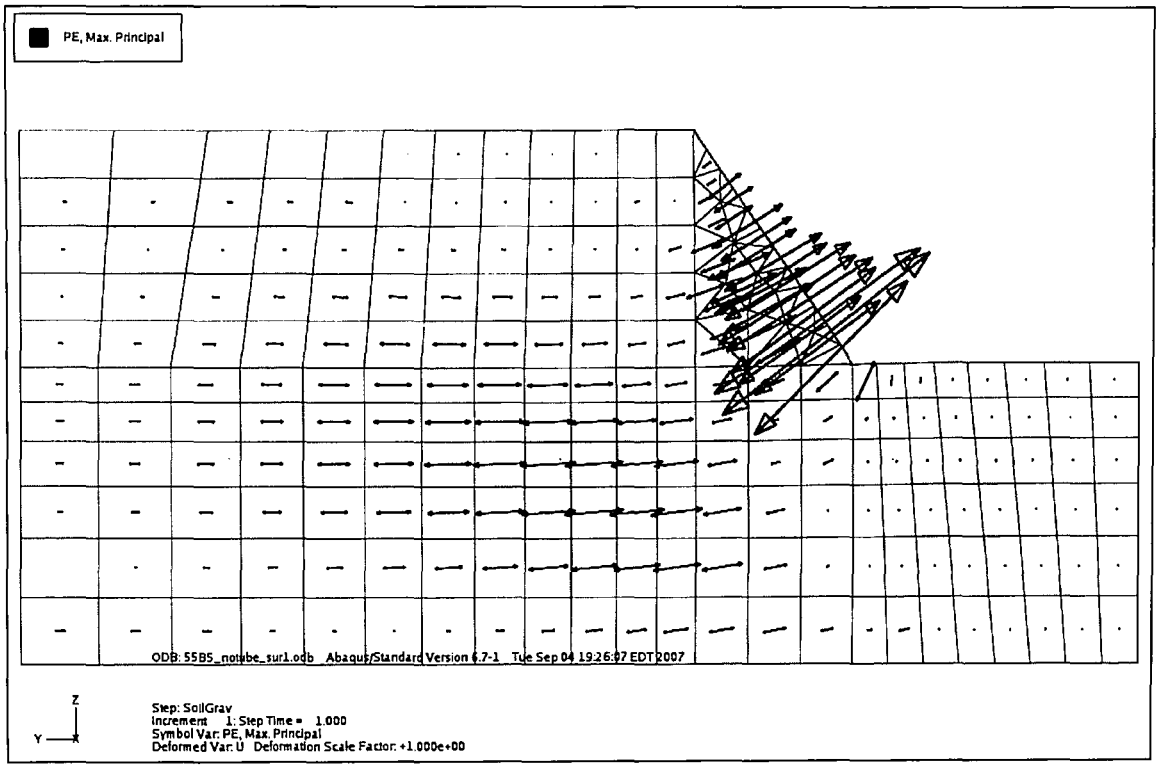

Figure 6.3.2.4. Maximum principle plastic strain vectors for the 55 degree embankment used in design 3.

The vectors in Figure 6.3.2.4 are very similar to those from the embankments modelled for design 1 as well as the 3.0-meter high stable embankment. Shown next is a comparison of results between this slope with and without tubes. The comparison will show exactly how the tubes influence the embankment distribution of deformations. The magnitudes and distributions in the following figures vary slightly between the two slope angles, but general behaviour shown for the 55-degree slope angle is representative of what would be seen in the 45-degree slope as well as for all of the surcharge variations. Figures 6.3.2.5 and 6.3.2.6 show the lateral deformation contours for the two cases, without and with geo-tubes.

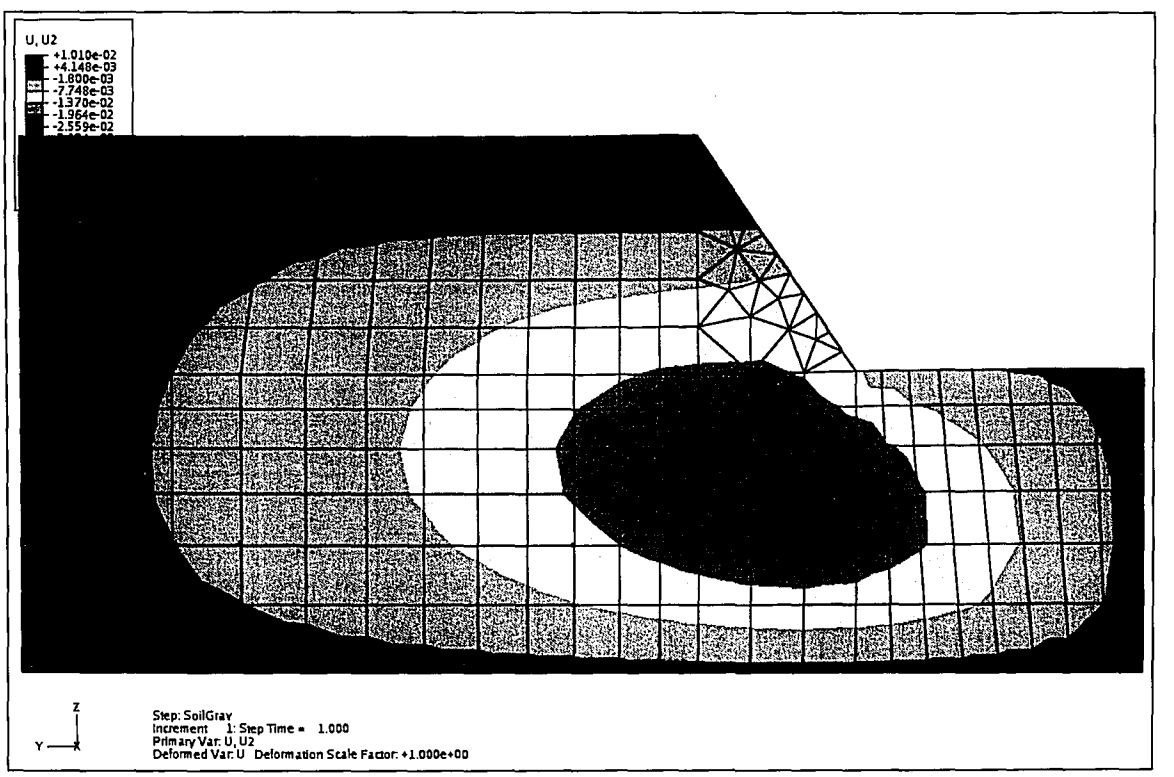

Figure 6.3.2.5. Lateral deformation of 55 degree slope under gravity without tubes.

The vectors in Figure 6.3.2.4 are very similar to those from the embankments modelled for design I as well as the 3.0-meter high stable embankment. Shown next is a comparison of results between this slope with and without tubes. The comparison will show exactly how the tubes influence the embankment distribution of deformations. The magnitudes and distributions in the following figures vary slightly between the two slope angles, but general behaviour shown for the 55-degree slope angle is representative of what would be seen in the 45-degree slope as well as for all of the surcharge variations. Figures 6.3.2.5 and 6.3.2.6 show the lateral deformation contours for the two cases, without and with geo-tubes.

Figure 6.3.2.5. Lateral deformation of 55 degree slope under gravity without tubes.

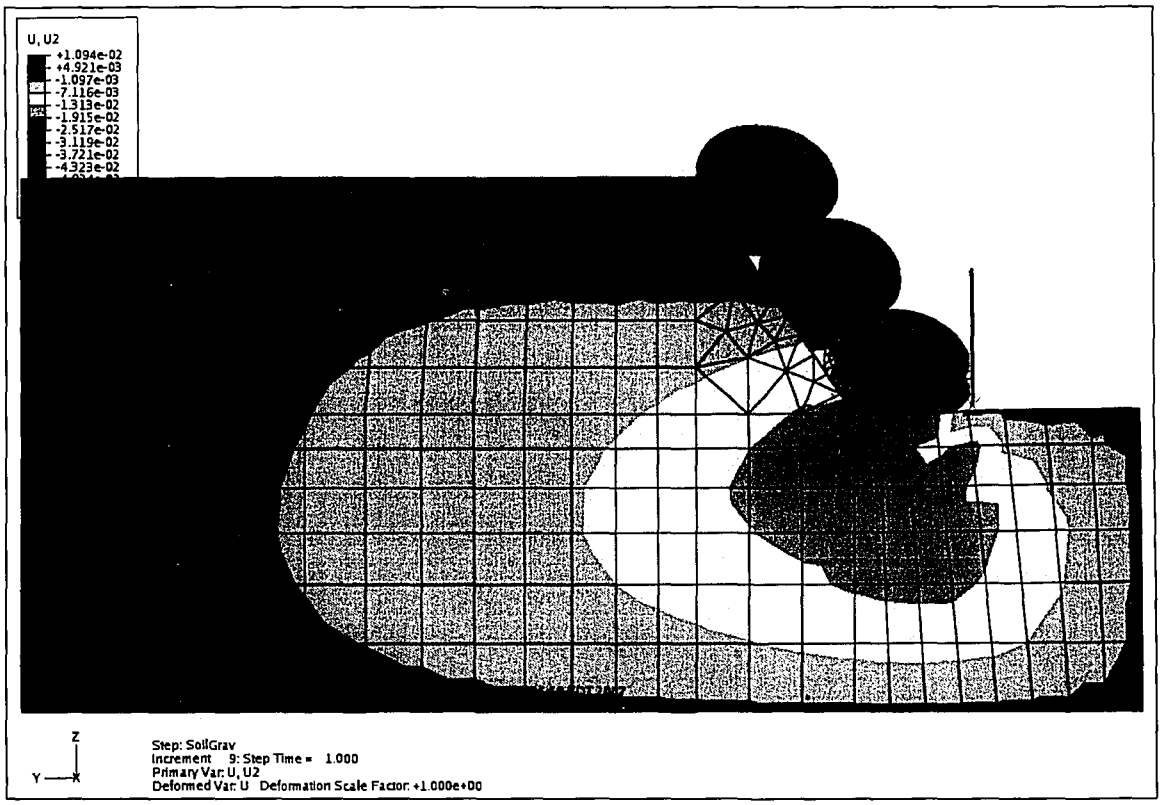

Figure 6.3.2.6. Lateral deformation of 55 degree slope under gravity with tubes.

When comparing these two figures, one can observe that the lateral deformation along most of the slope is similar between the two resulting distributions. The exception is at the toe where it is higher with the tubes, contrary to what the role of this structure was originally intended to be. The mechanism at work here seems to be that the top and middle tubes are so massive that they weigh down on the upper half of the slope excessively causing the bottom half to squeeze out. The stakes appear to be much less effective at bracing the bottom tube in place than the rigid wall was. One method of confirming the theory of the upper tubes squeezing out the bottom half of the slope is to examine scaled lateral deformation plots. Figures 6.3.2.7 and 6.3.2.8 are lateral displacements scaled up one hundred times.

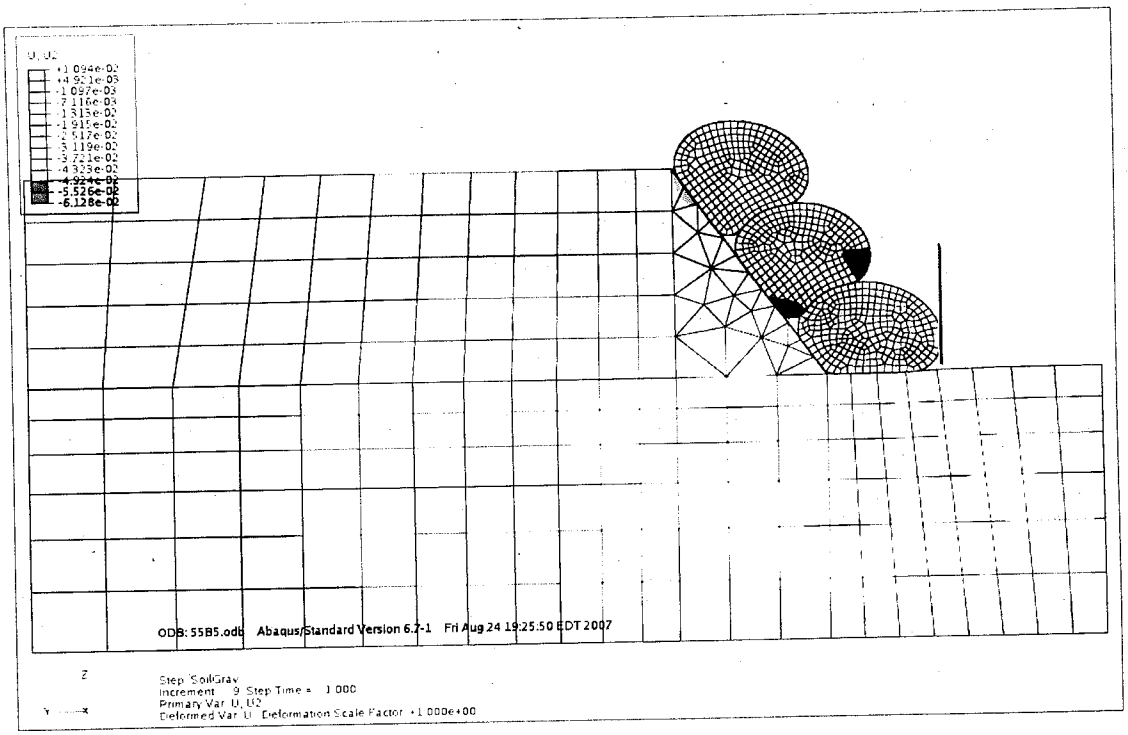

Figure 6.3.2.6. Lateral deformation of 55 degree slope under gravity with tubes.

When comparing these two figures, one can observe that the lateral deformation along most of the slope is similar between the two resulting distributions. The exception is at the toe where it is higher with the tubes, contrary to what the role of this structure was originally intended to be. The mechanism at work here seems to be that the top and middle tubes are so massive that they weigh down on the upper half of the slope excessively causing the bottom half to squeeze out. The stakes appear to be much less effective at bracing the bottom tube in place than the rigid wall was. One method of confirming the theory of the upper tubes squeezing out the bottom half of the slope is to examine scaled lateral deformation plots. Figures 6.3.2.7 and 6.3.2.8 are lateral displacements scaled up one hundred times.

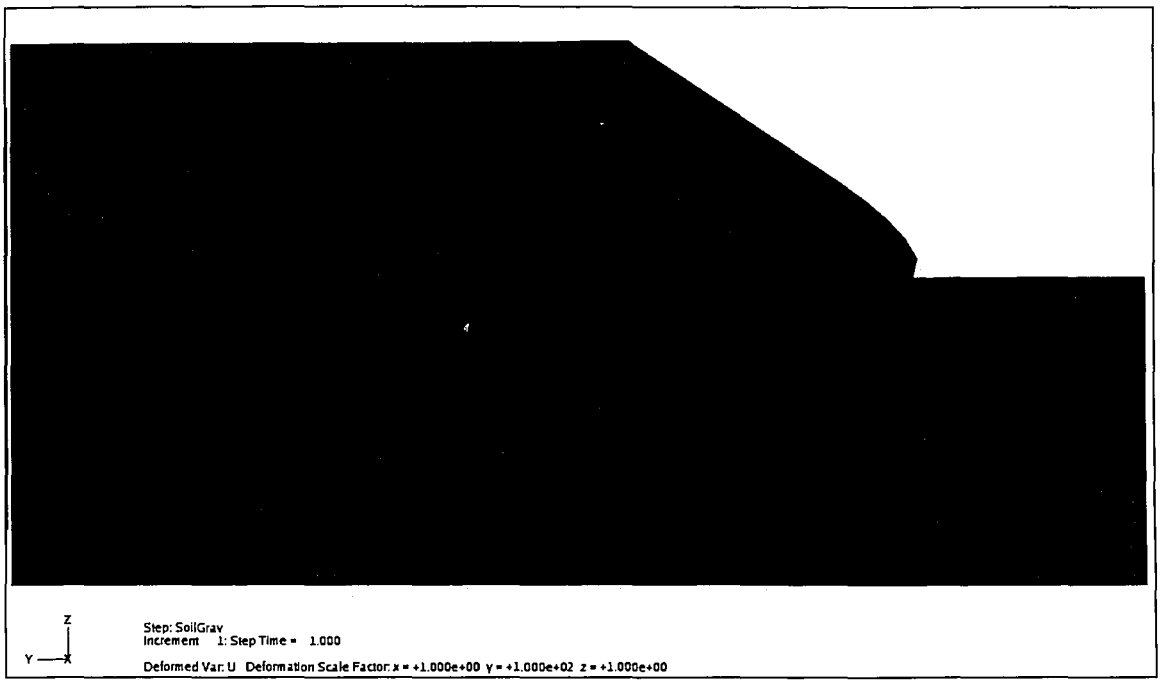

Figure 6.3.2.7. Lateral displacement scaled up 100 times for 55-degree slope under gravity without tubes.

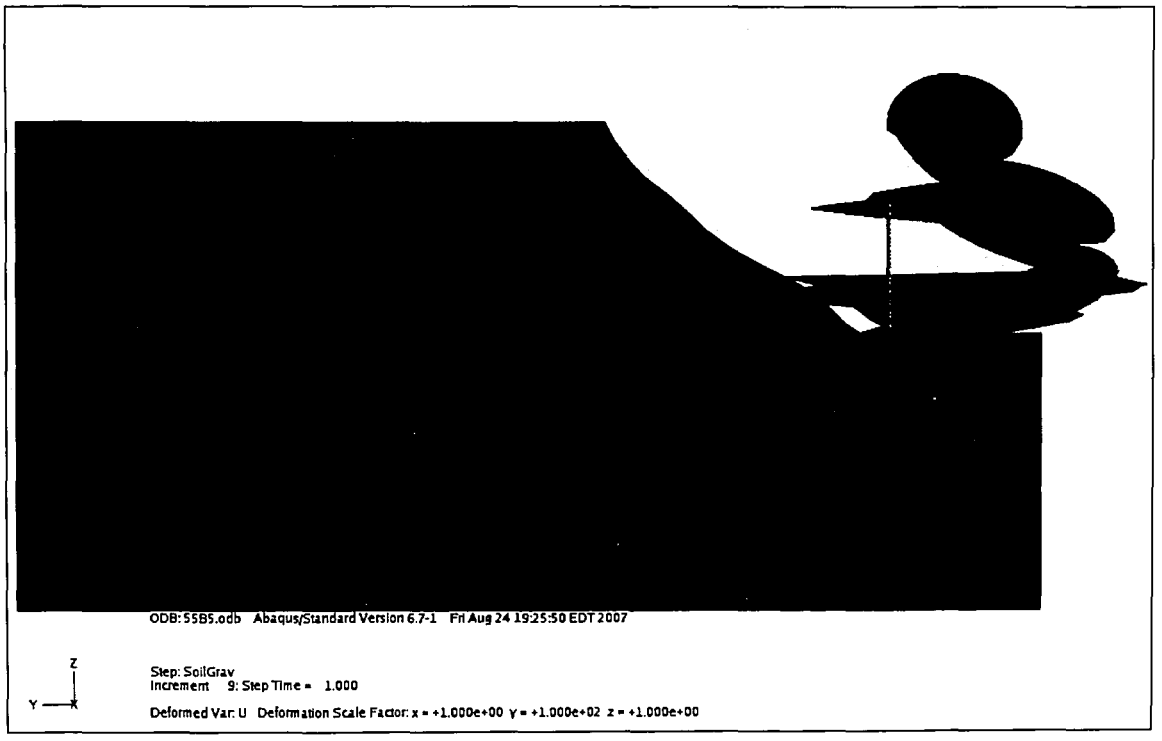

Figure 6.3.2.8. Lateral displacement scaled up 100 times for 55-degree slope under gravity with tubes.

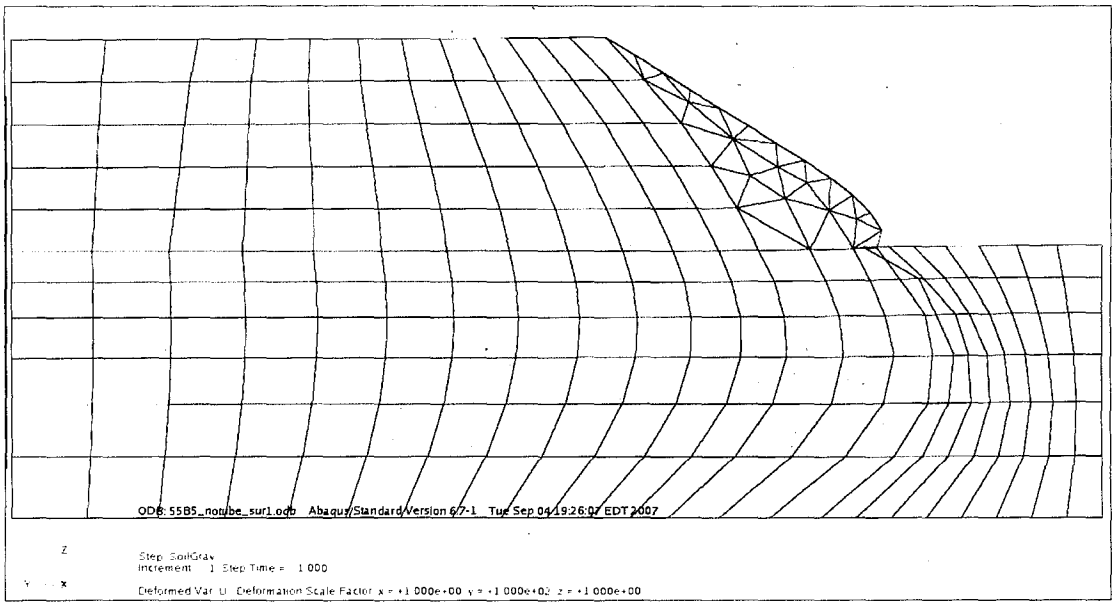

Figure 6.3.2.7. Lateral displacement scaled up 100 times for 55-degree slope under gravity without tubes.

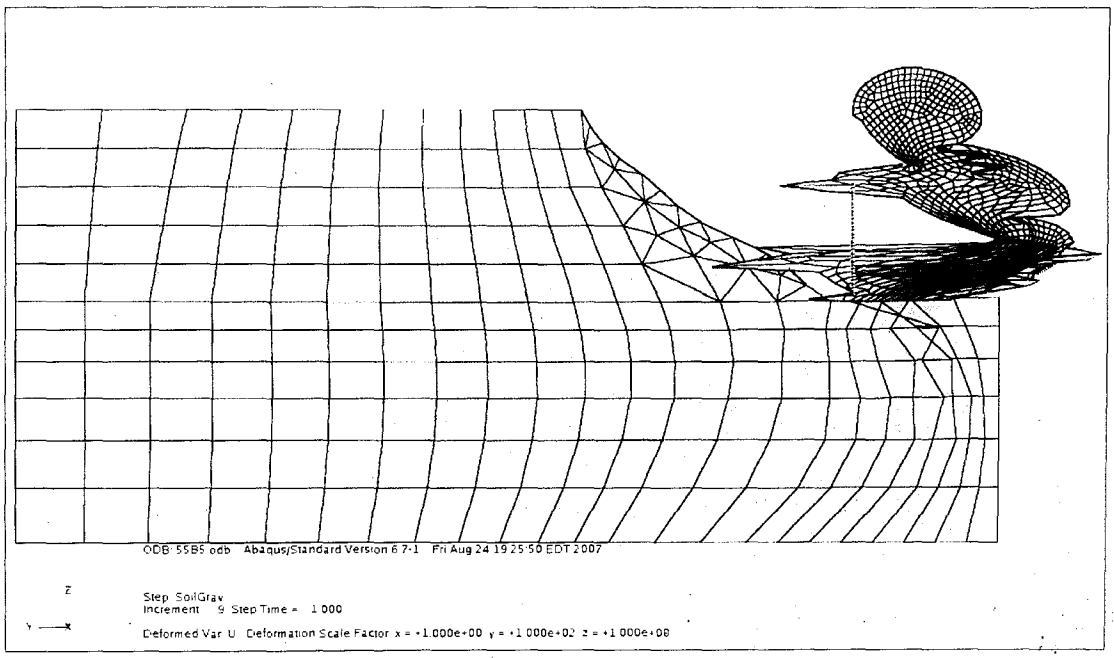

Figure 6.3.2.8. Lateral displacement scaled up 100 times for 55-degree slope under gravity with tubes.

In Figure 6.3.2.7, without the tubes, the slope deforms to the right bulging out from the embankment just above the toe. The slope surface's shape in Figure 6.3.2.8 is different. It appears to be depressed near the top and squeezed out near the bottom. It also is evident that the tubes are sliding to the right more than the slope surface is. This means that the stack is actually sliding down the slope.

The weight of the upper two tubes is detrimental to the stability of the whole system. The stability of the stack relies on the bottom tube remaining stationary. The bottom tube is responsible for stabilizing the slope as well as stabilizing the entire tube structure. The top tubes cause lateral movement of the bottom tube by squeezing out the soil behind it and by pushing directly on it.

While greater movement of the slope surface is observed with the tubes in place, the amount of plastic strain occurring in this movement is smaller. Plastic strain magnitude contours for design 3 are shown in Figures 6.3.2.9 and 6.3.2.10.

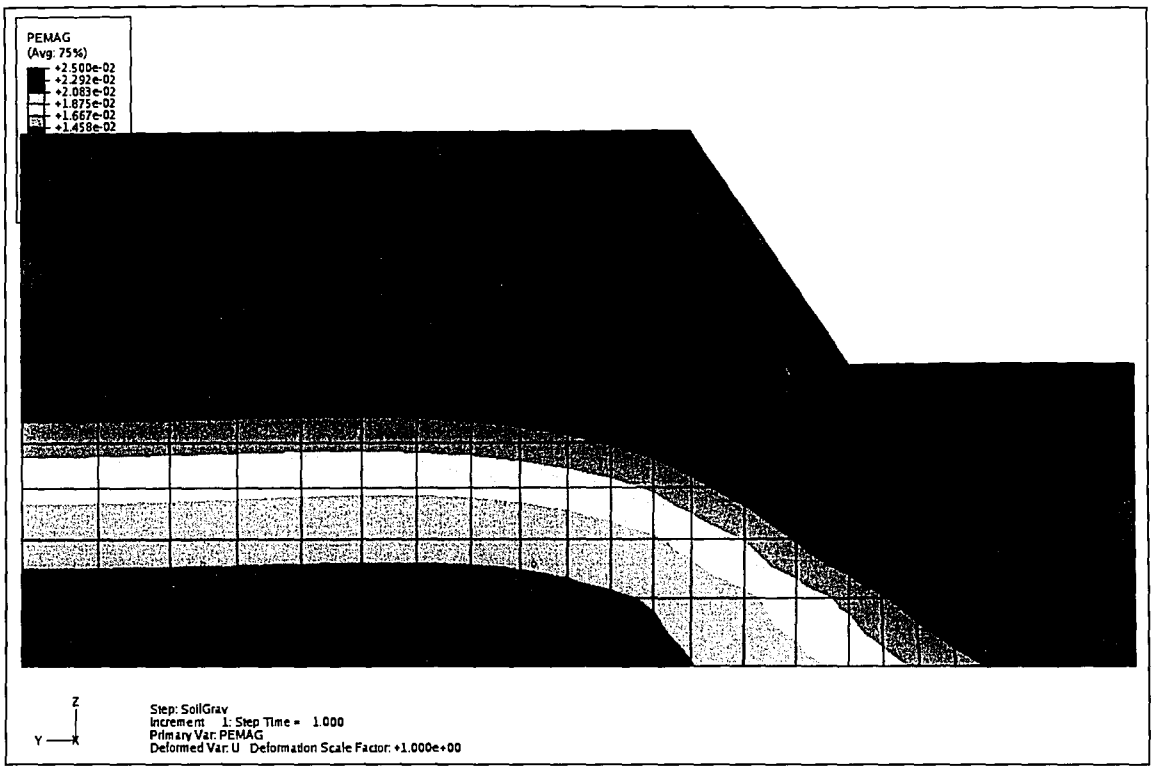

Figure 6.3.2.9. Plastic strain magnitude contours for 55-degree slope without tubes.

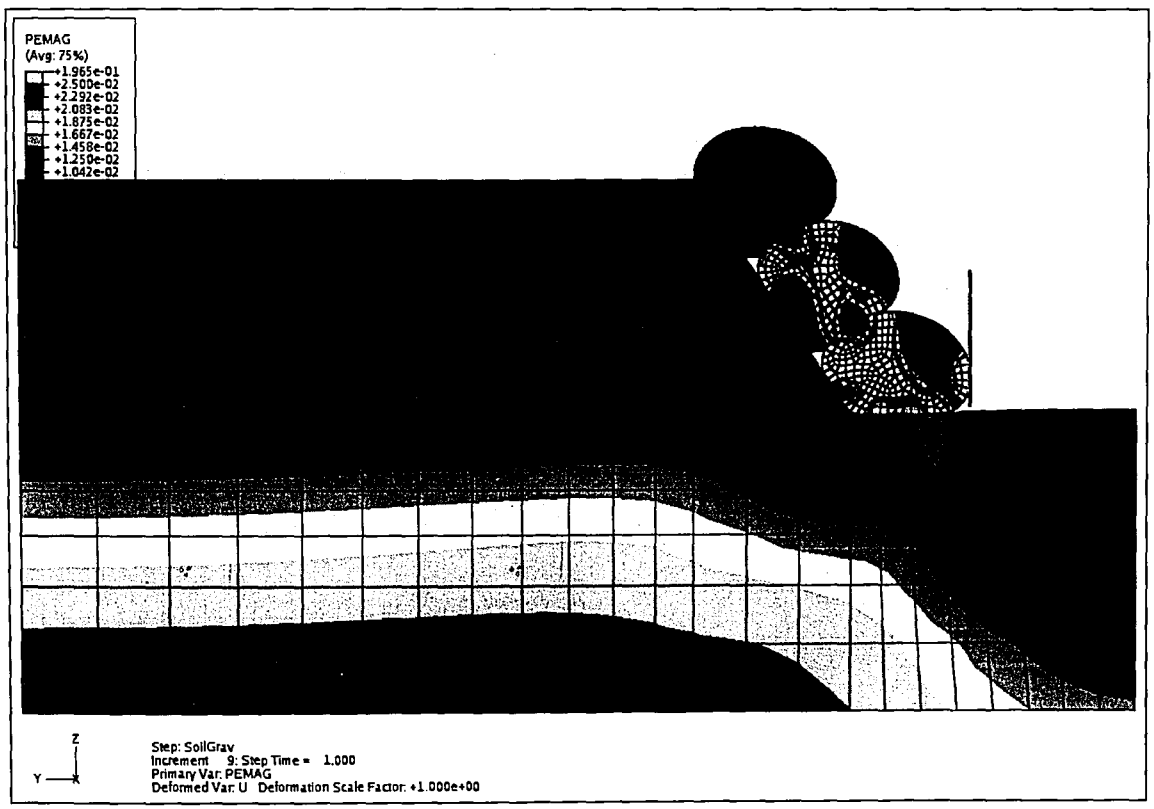

Figure 6.3.2.10. Plastic strain magnitude for 55-degree slope with tubes.

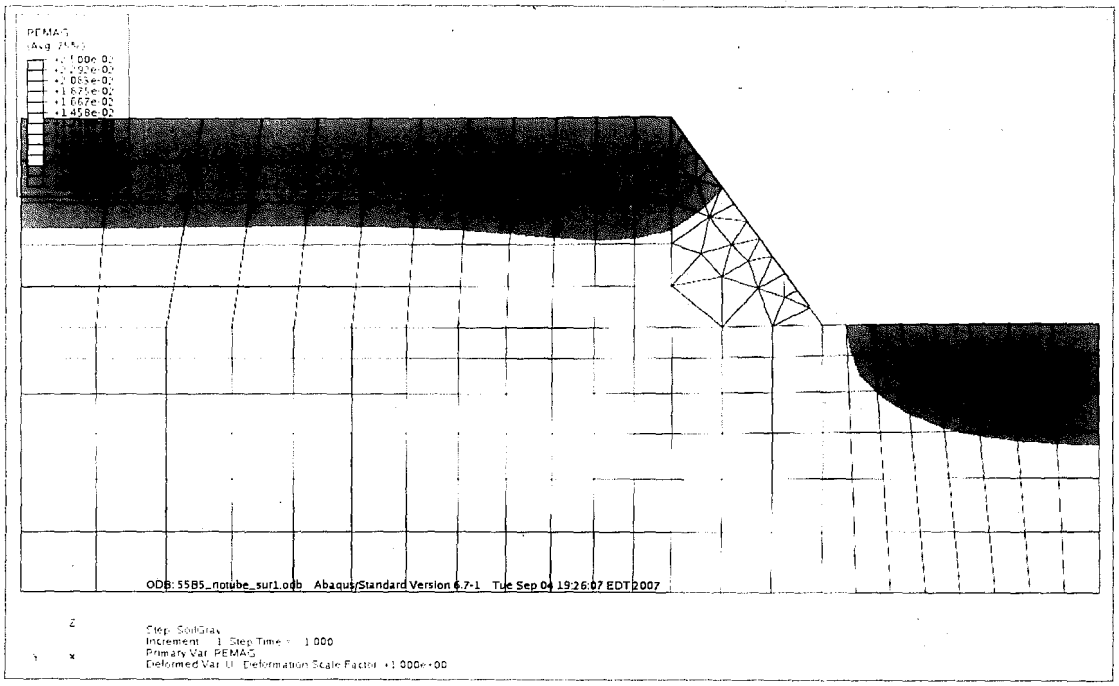

Figure 6.3.2.9. Plastic strain magnitude contours for 55-degree slope without tubes.

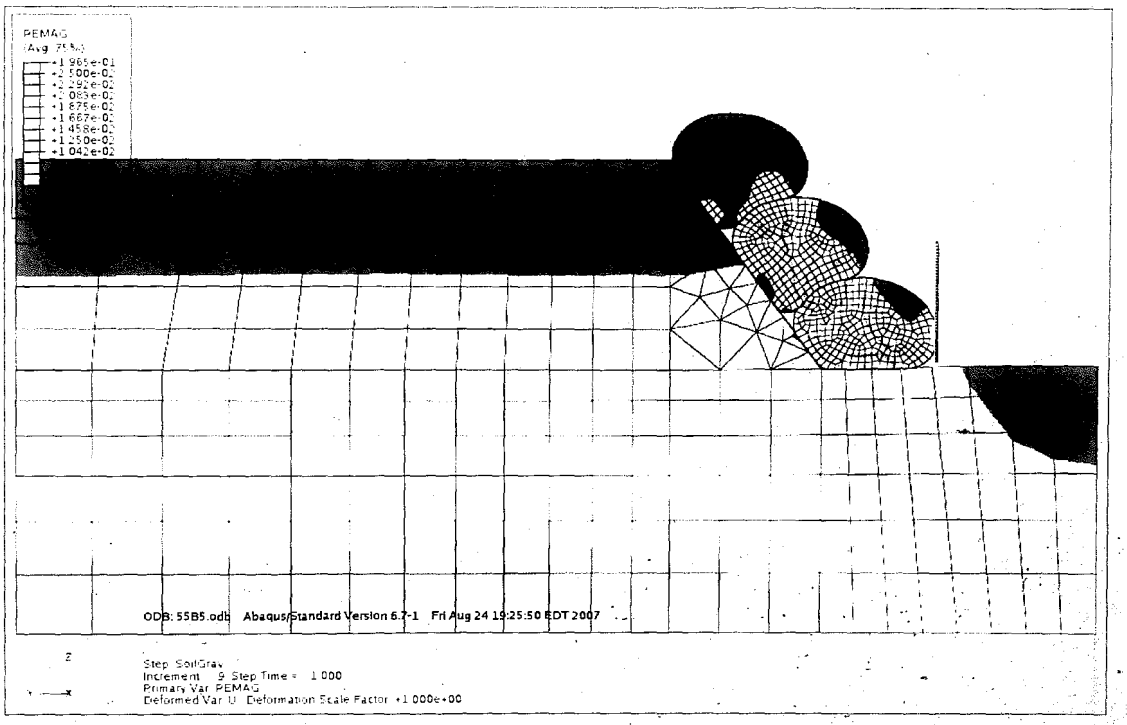

Figure 6.3.2.10. Plastic strain magnitude for 55-degree slope with tubes.

The difference in plastic strains is not large, but the tubes provide an improvement nonetheless. As is shown in Figures 6.3.2.9 and 6.3.2.10 the plastic strain contours generally are horizontal bands varying with soil depth. The only exception to this is a small region centralized around the toe of the slope. This is the same location as the bulge in lateral displacement seen in Figure 6.3.2.7. When the tubes are in place, the plastic strain in this region is effectively reduced. The plastic strain is slightly higher in areas of the slope further up.

There is a new region under the right side of the bottom tube that clearly has higher plastic strains. The increase here is caused by all of the tubes' weight pressing down on the bottom tube as discussed before, however this is not causing an instability of the slope. It may be the source of a bearing capacity failure, but investigating such aspects were out of the scope of this study.

If the slope is deforming more with the tubes but experiencing with lower plastic strain, this may mean that the slope is experiencing higher elastic strain. This notion is counter intuitive, but can be explained again by the tubes weight. This weight is causing the soil underneath to be subjected to higher hydrostatic pressure. This strengthens the soil elements and moves their yield surface in the Cap Plasticity model. A comparison of hydrostatic pressures on the elements in the embankment is shown in Figures 6.3.2.11 and 6.3.2.12. It is clear that the pressures are indeed higher in the model with the tubes as was expected.

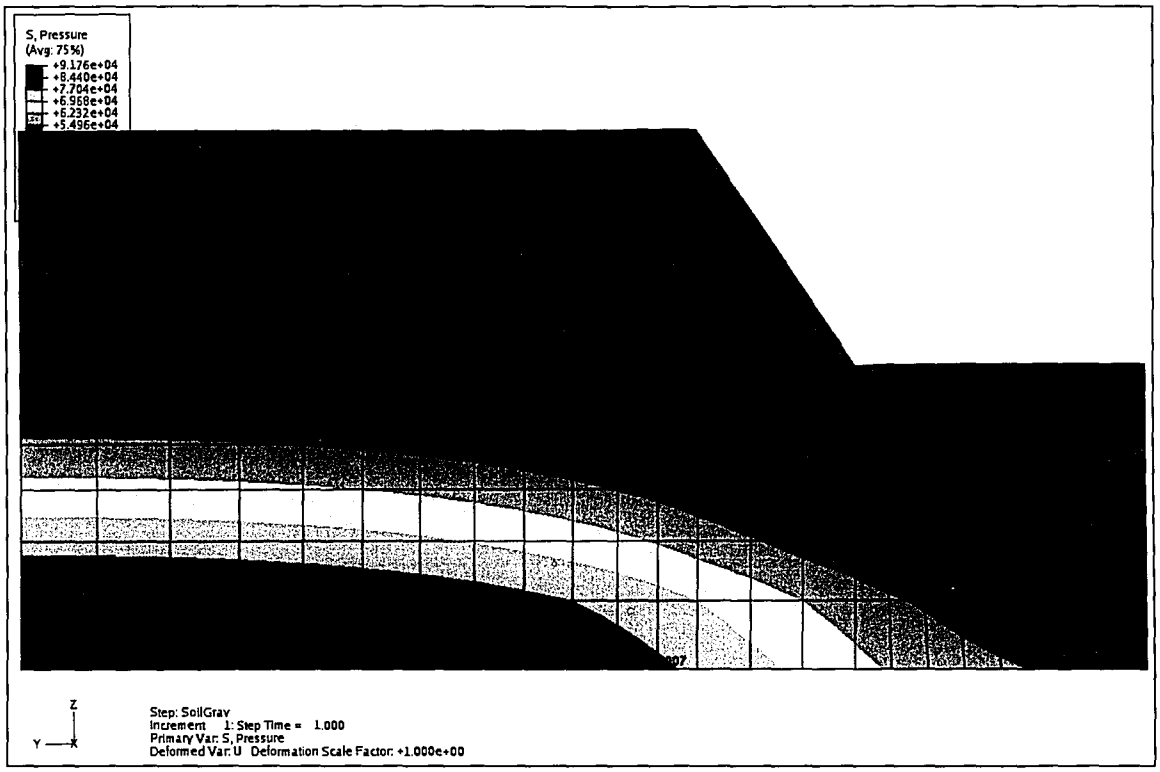

Figure 6.3.2.11. Hydrostatic pressure distribution for 55-degree slope without tubes.

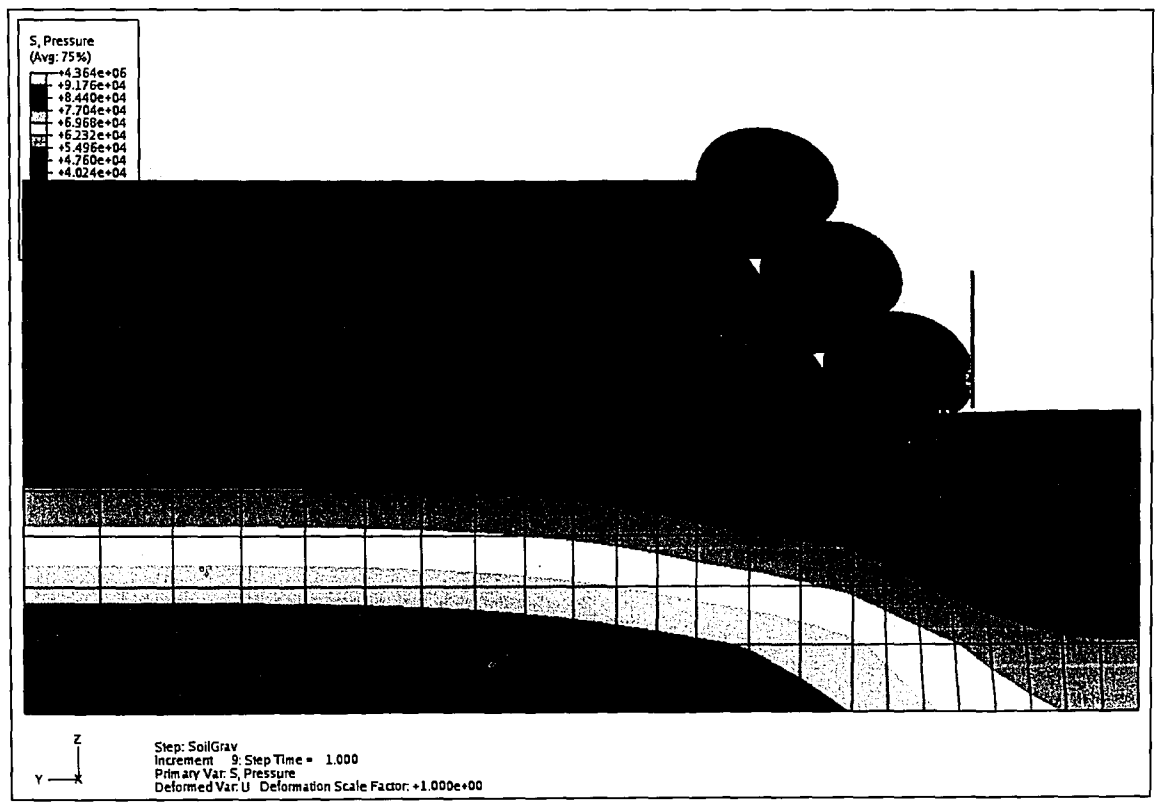

Figure 6.3.2.12. Hydrostatic pressure distribution for 55-degree slope with tubes.

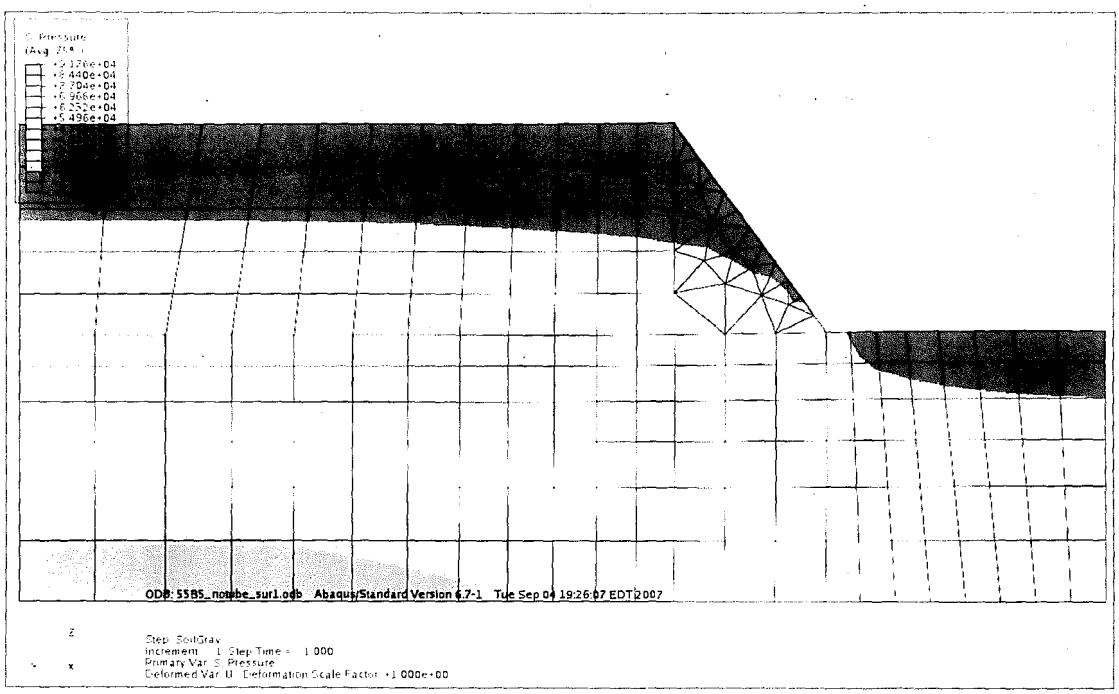

Figure 6.3.2.11. Hydrostatic pressure distribution for 55-degree slope without tubes.

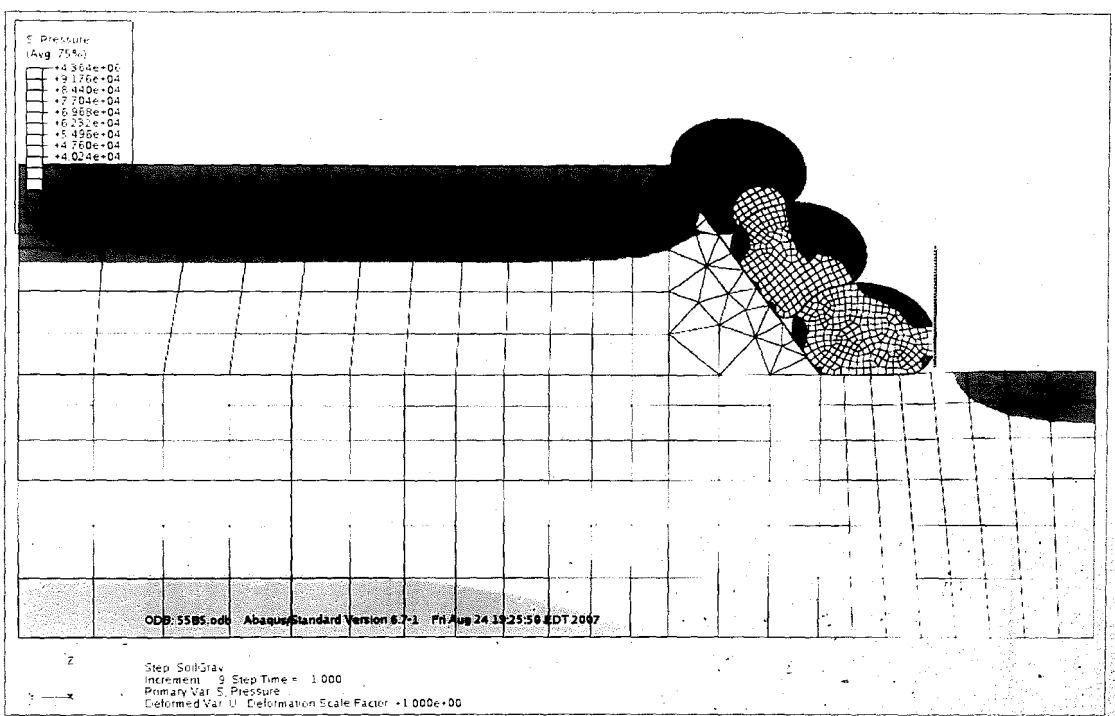

Figure 6.3.2.12. Hydrostatic pressure distribution for 55-degree slope with tubes.

One last variable to examine is the x-y shear stress. This is also slightly improved with the tubes in place (Figures 6.3.2.13 and 6.3.2.14).

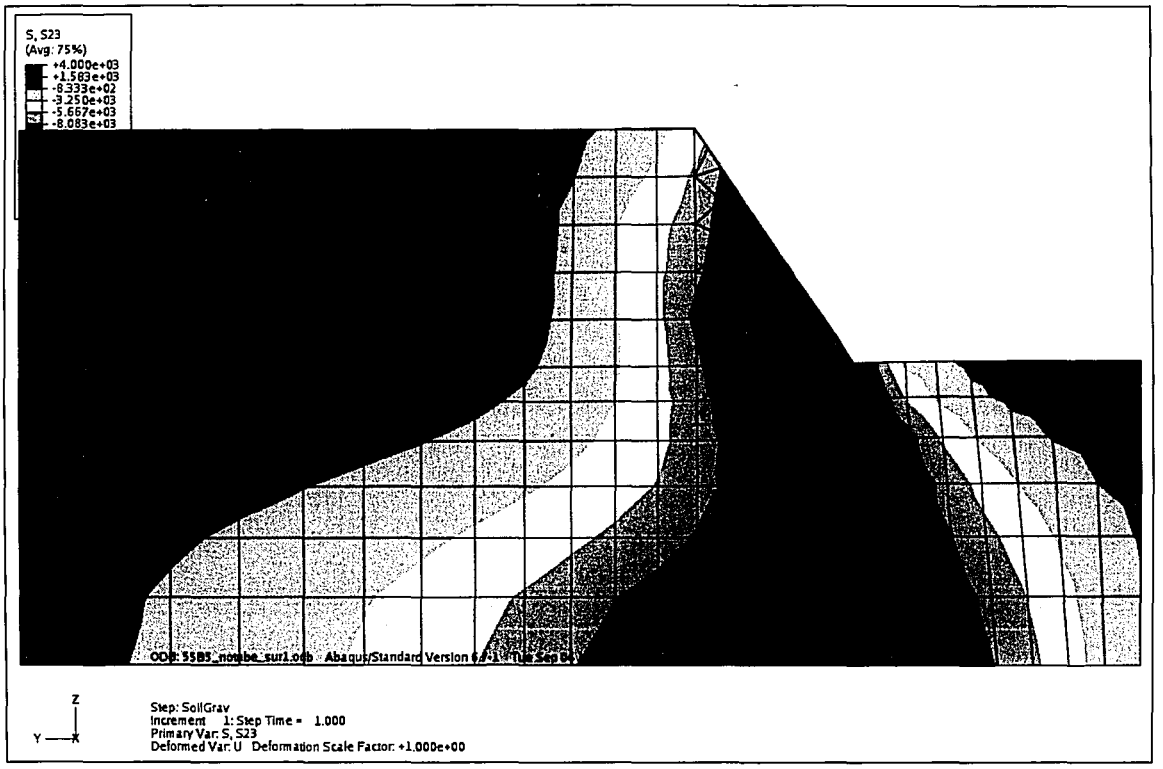

Figure 6.3.2.13. x-y shear stress in 55 degree slope without tubes.

One last variable to examine is the x-y shear stress. This is also slightly improved with the tubes in place (Figures 6.3.2.13 and 6.3.2.14).

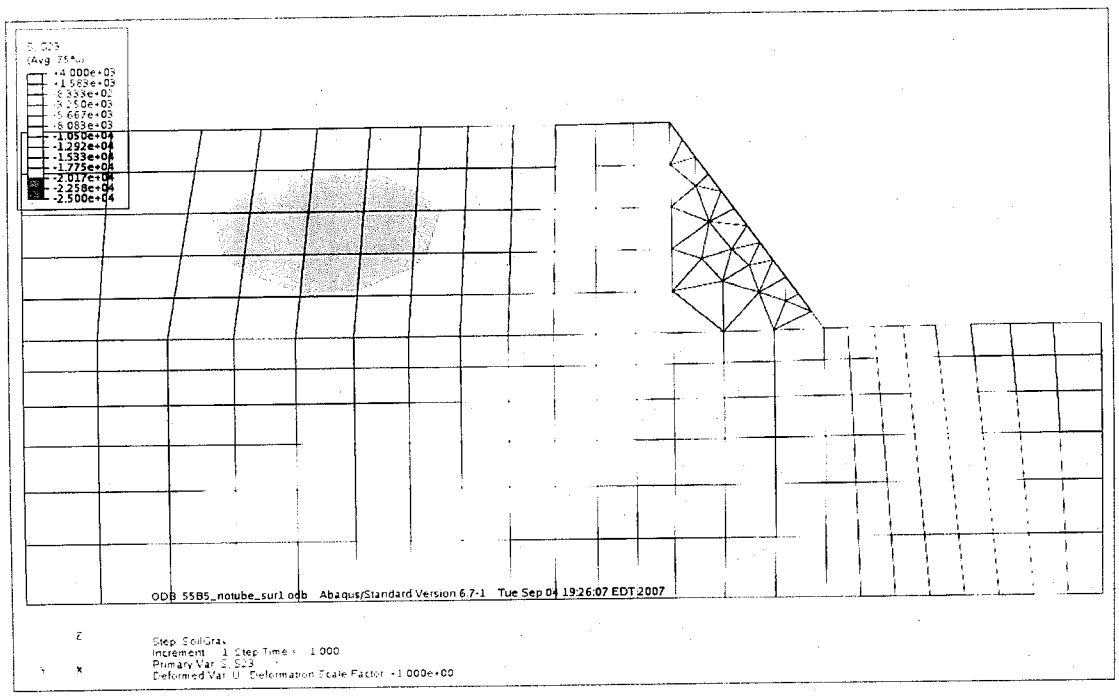

Figure 6.3.2.13. x-y shear stress in 55 degree slope without tubes.

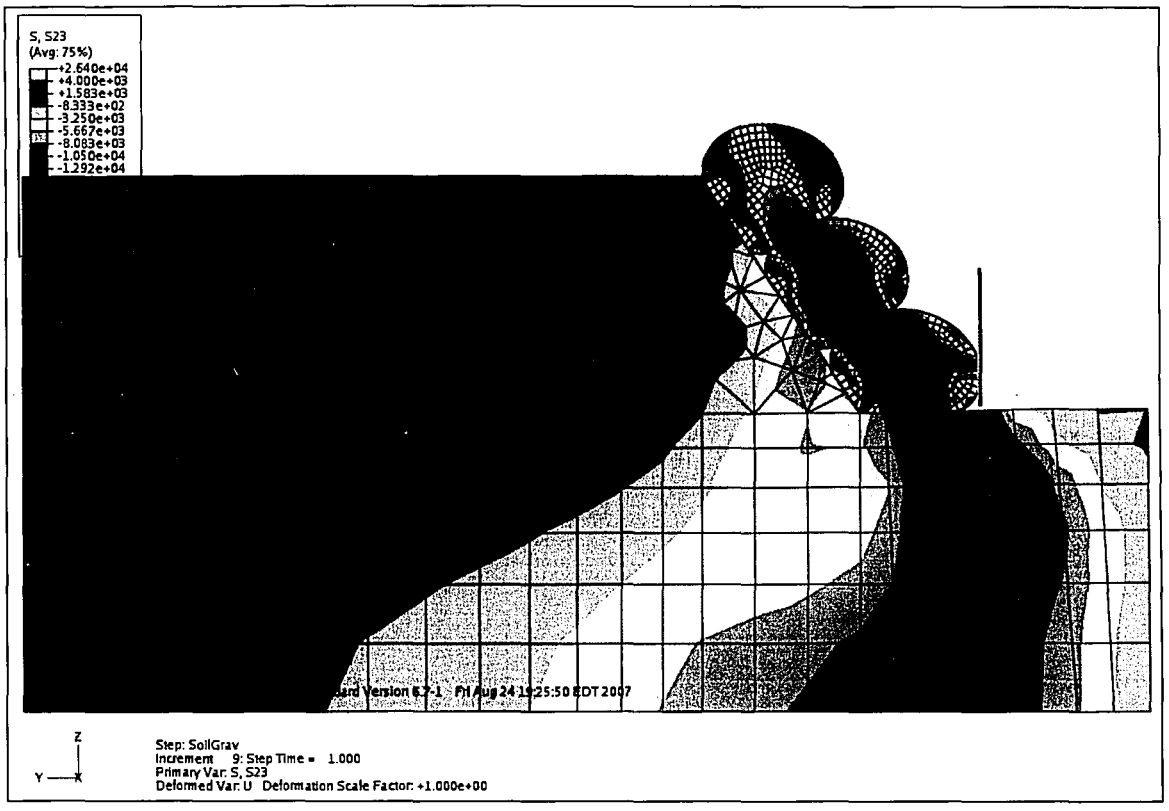

Figure 6.3.2.14. x-y shear stress for 55 degree slope with tubes.

In comparing figures 6.3.2.13 and 6.3.2.14 it can be seen that when the tube stack is in place some areas of the embankment experience a reduction in shear stress, but other areas experience an increase. One of the areas that was not improved is the small region directly under the top tube. This area is not crucial to the stability of the whole slope, so this increase is of little concern. There also is an increase below the bottom tube in the same region where plastic strains were seen to have increased. This area, again, is not considered to be crucial area for slope stability.

The crucial area is behind the slope surface near the toe. In the model without the tubes, the shear stress at this location is approximately 17 kPa. In the model with the

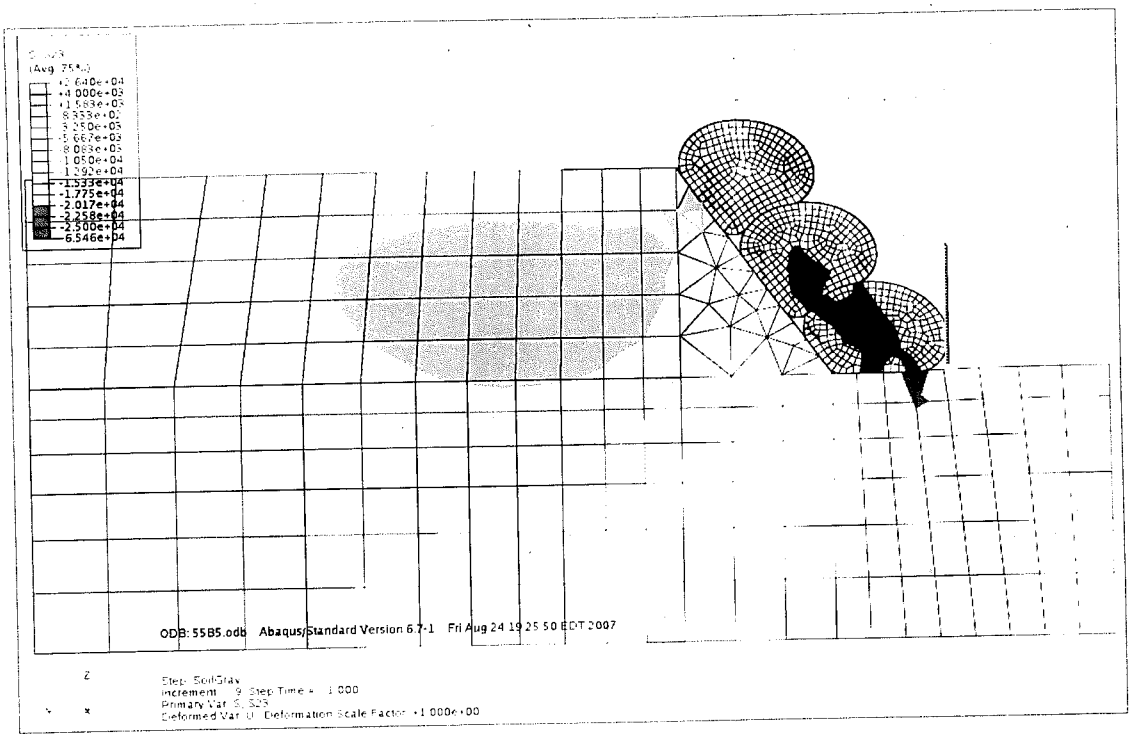

Figure 6.3.2.14. x-y shear stress for 55 degree slope with tubes.

In comparing figures 6.3.2.13 and 6.3.2.14 it can be seen that when the tube stack is in place some areas of the embankment experience a reduction in shear stress, but other areas experience an increase. One of the areas that was not improved is the small region directly under the top tube. This area is not crucial to the stability of the whole slope, so this increase is of little concern. There also is an increase below the bottom tube in the same region where plastic strains were seen to have increased. This area, again, is not considered to be crucial area for slope stability.

The crucial area is behind the slope surface near the toe. In the model without the tubes, the shear stress at this location is approximately 17 kPa. In the model with the

tubes the shear stress at the same location is approximately 6 kPa, which is a significant improvement.

According to the results from the finite element models of design 3, the tube structure causes more lateral deformation of the slope, but slightly reduces plastic strain and x-y shear stresses around the toe. A criteria selected earlier for success in improving slope stability was using the tube stack to limit lateral deformation. It had been assumed though, that higher later deformations would also indicate higher plastic strains and shear stress values. Because this was not the case, it is not entirely clear from the model whether or not the tubes improved slope stability. Hence, since the lateral deformations increased with the tubes in place, design 3 can be considered to be ineffective in improving slope stability.

6.4 Design 4

After examining the results from the design 3 models, the behaviour of the different slopes and the effects of the tube stack were much better understood. The results indicated that the weights of the top and middle tubes were causing the slope to deform more than it would deform under its own self-weight. The first thing that comes to mind to solve this problem is to reduce the weight of the top two tubes. This is a natural step in the design evolution because it had become clear that there was no reason the top two tubes should be the same size as the bottom tube since bottom tube is the most important stability feature. The bottom tube holds up the

entire structure and holds the toe in place at the same time. The top tube stabilizes a small section of the slope near the top that may be of little concern to overall slope stability.

6.4.1 Design 4 Development

One model was created with tube size decreasing up the slope to observe the effects of this design improvement. The bottom tube's initial diameter would be increased to 2.84m, the middle tube would be decreased to 1.89m, and the top tube would be decreased to 1.26m. These initial geometry changes also affected the loads applied to them. Table 6.4.1.1 summarizes all of the geometry and loads applied for the new tube sizes. In the new configuration z_h is the height of the hydrostatic pressure distribution. Figure 6.4.1.1 shows a typical section of design 4.

Table 6.4.1.1. Adjustments for tubes and loads in Design 4.

	Diamter (m)	P_h (kPa)	z_h (m)	P_{in} (kPa)
Top Tube	2.84	59.9	2.98	17.55
Middle Tube	1.89	39.9	1.98	11.68
Bottom Tube	1.26	26.5	1.32	77.84

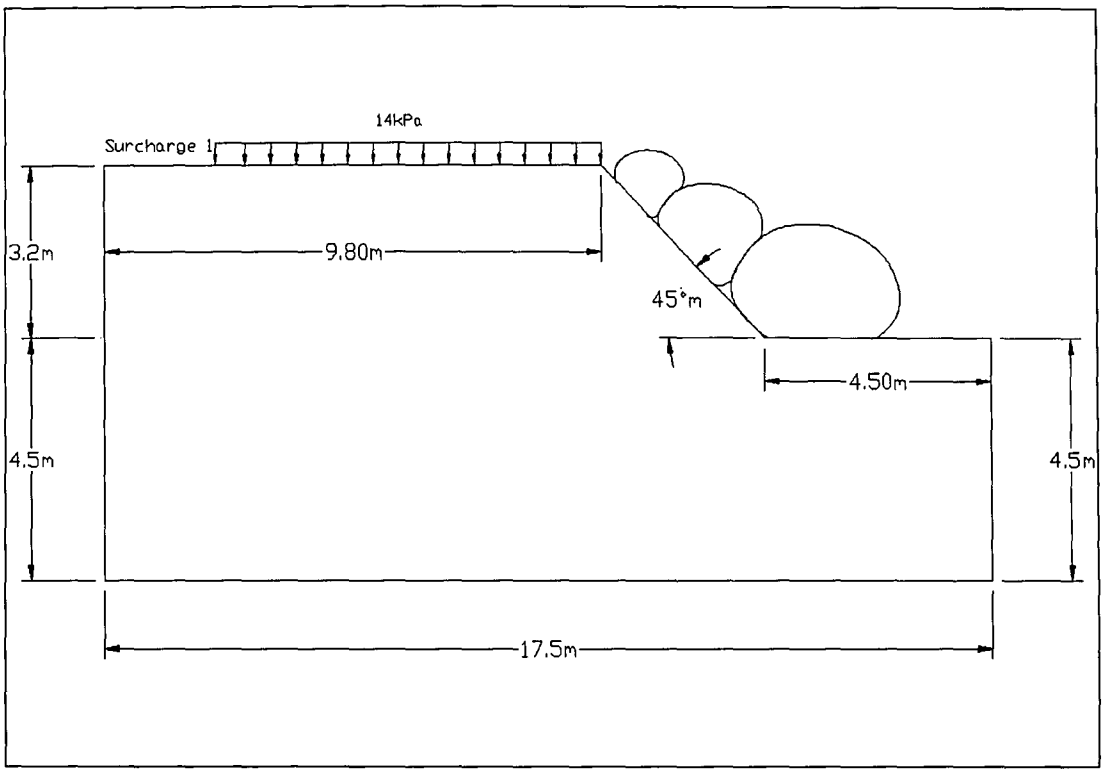

Figure 6.4.1.1. Section of design 4.

6.4.2 Results for Design 4 Model

The bottom tube in design 4 was sufficiently heavy to prevent the structure from failing due to sliding without external restrain. However, because the tube was so much heavier, the vertical deformation of the stack and the slope was higher. It was not until the results for this design that it became clear the extent of coupling between the vertical and horizontal movements in the model. When the slope subsides vertically, it tips backwards causing the area near the toe to move to the right and the area near the top to move to the left, similar to a flexible wall. This behaviour was seen in the scaled displacements in Figure 4.2.1. In the case of design 4, though, the vertical movement was so large that although the top of the slope did

tip, but the net movement of all points on the surface was all towards the right. Figure 6.4.2.1 illustrates this by showing the lateral displacements of nodes on the surface of the slope. Stress and strain values for design 4 are seen in Table 6.4.2.1.

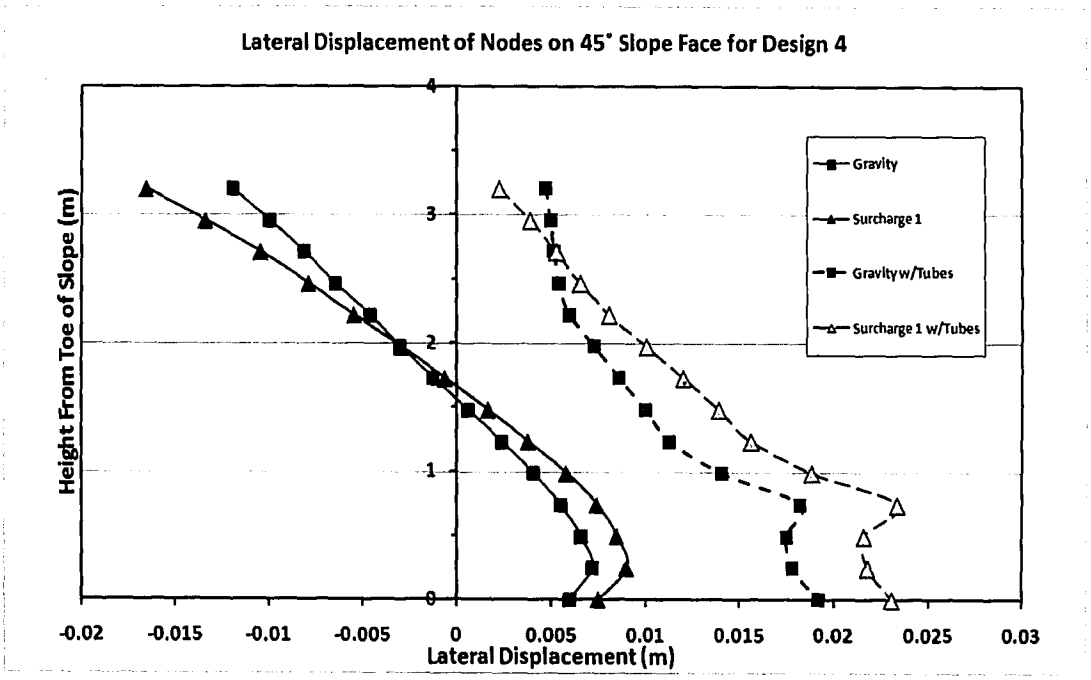

Figure 6.4.2.1. Lateral displacements for design 4.

Table 6.4.2.1. Stress and strain results at standard locations for 45 degree slope in design 4.

Design 4 - 45° - Gravity Load									
	Lateral Displacement (cm)			Plastic Strain Magnitude			x-y shear stress (Pa)		
Location	stable	w/ tubes	% +/-	stable	w/ tubes	% +/-	stable	w/ tubes	% Δ mag.
1	-0.39	0.603	-253	0.002	0.003	39.1	-9801	-3925	-60
2	0.45	1.23	173	0.005	0.005	2	-12420	-3579	-71
3	0.71	1.785	151	0.007	0.003	-50	-14326	-4917	-66
4	1.796	1.93	7.46	0.01	0.017	73.5	-9311	-5306	-43
5	1.19	1.43	20.2	0.006	0.011	71.9	-5937	-4.6	-100

All results for design 4 can be compared to the 45-degree stable slope already modelled in Table 6.4.2.1. Immediately from this table it is seen that the tubes in general increased the lateral movement of the slope dramatically, but reduced the shear stresses. The following figures will help to illustrate this. First, the lateral displacement contours are shown in Figures 6.4.2.2 and 6.4.2.3. The results shown are for models loaded only with gravity.

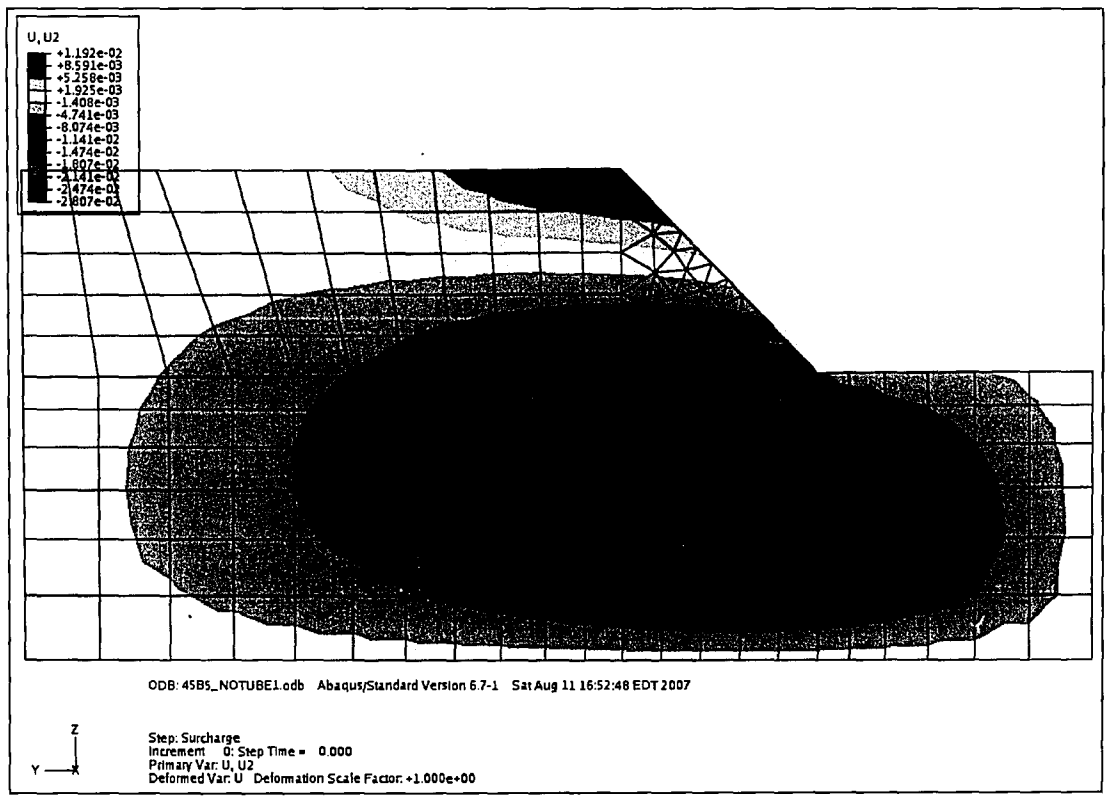

Figure 6.4.2.2. Lateral displacement contours for 45 degree stable slope without tubes.

All results for design 4 can be compared to the 45-degree stable slope already modelled in Table 6.4.2.1. Immediately from this table it is seen that the tubes in general increased the lateral movement of the slope dramatically, but reduced the shear stresses. The following figures will help to illustrate this. First, the lateral displacement contours are shown in Figures 6.4.2.2 and 6.4.2.3. The results shown are for models loaded only with gravity.

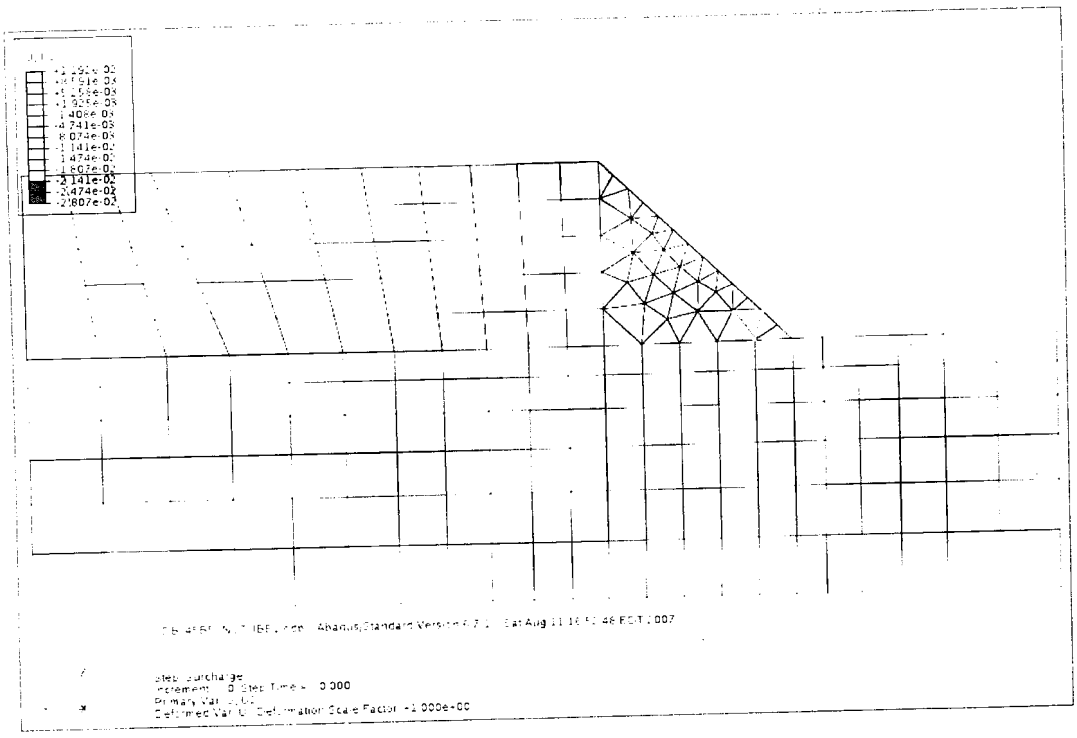

Figure 6.4.2.2. Lateral displacement contours for 45 degree stable slope without tubes.

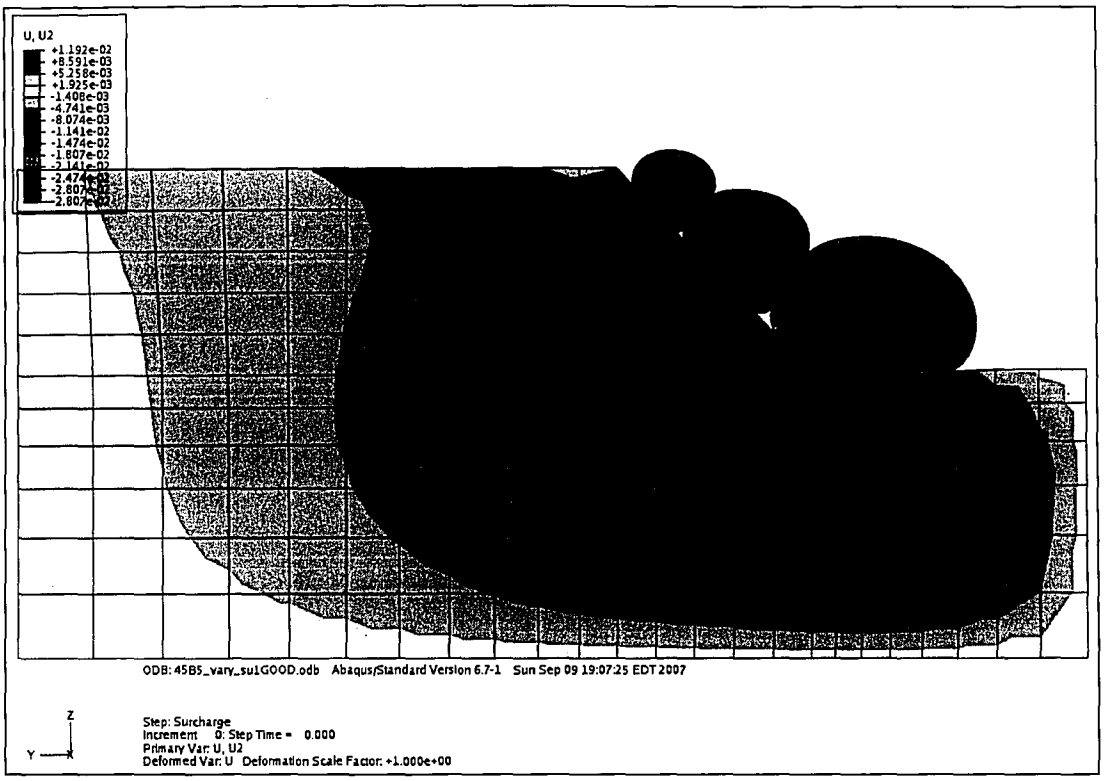

Figure 6.4.2.3. Lateral displacement contours for design 4.

Figure 6.4.2.2 has a similar distribution of lateral displacements that is seen in Figure 6.3.2.5 for the 55-degree slope in design 3. The region of maximum displacements in the embankment under the slope moves to the same location, under the toe when tubes are put in place. This was also seen in Figure 6.3.2.6 for design 3. One item of note in Figure 6.4.2.3 is that the maximum lateral displacements in the whole model are at the front of the bottom tube within the tube itself. This indicates that, while the tube is large enough to keep the structure stable, it is not effective at minimizing movement of the system as a whole. Essentially it allows the stack and slope to move as one unit without compromising structural stability.

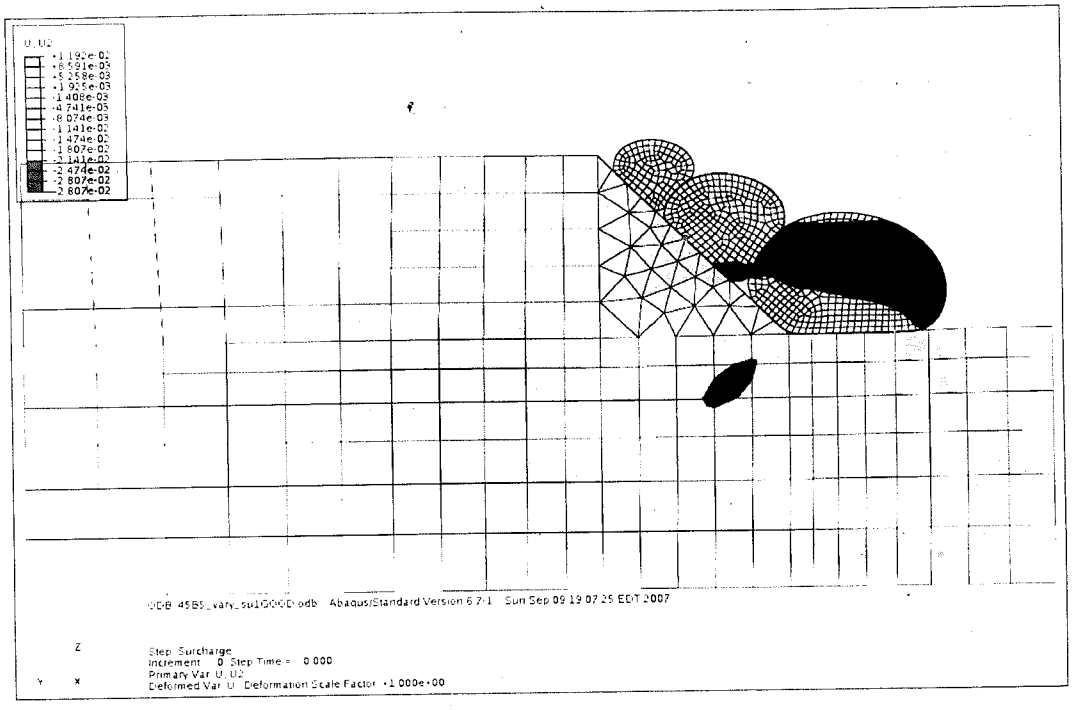

Figure 6.4.2.3. Lateral displacement contours for design 4.

Figure 6.4.2.2 has a similar distribution of lateral displacements that is seen in Figure 6.3.2.5 for the 55-degree slope in design 3. The region of maximum displacements in the embankment under the slope moves to the same location, under the toe when tubes are put in place. This was also seen in Figure 6.3.2.6 for design 3. One item of note in Figure 6.4.2.3 is that the maximum lateral displacements in the whole model are at the front of the bottom tube within the tube itself. This indicates that, while the tube is large enough to keep the structure stable, it is not effective at minimizing movement of the system as a whole. Essentially it allows the stack and slope to move as one unit without compromising structural stability.

Figures 6.4.2.4 and 6.4.2.5 compare plastic strain magnitude distributions for models of design 4, with and without tubes loaded with gravity.

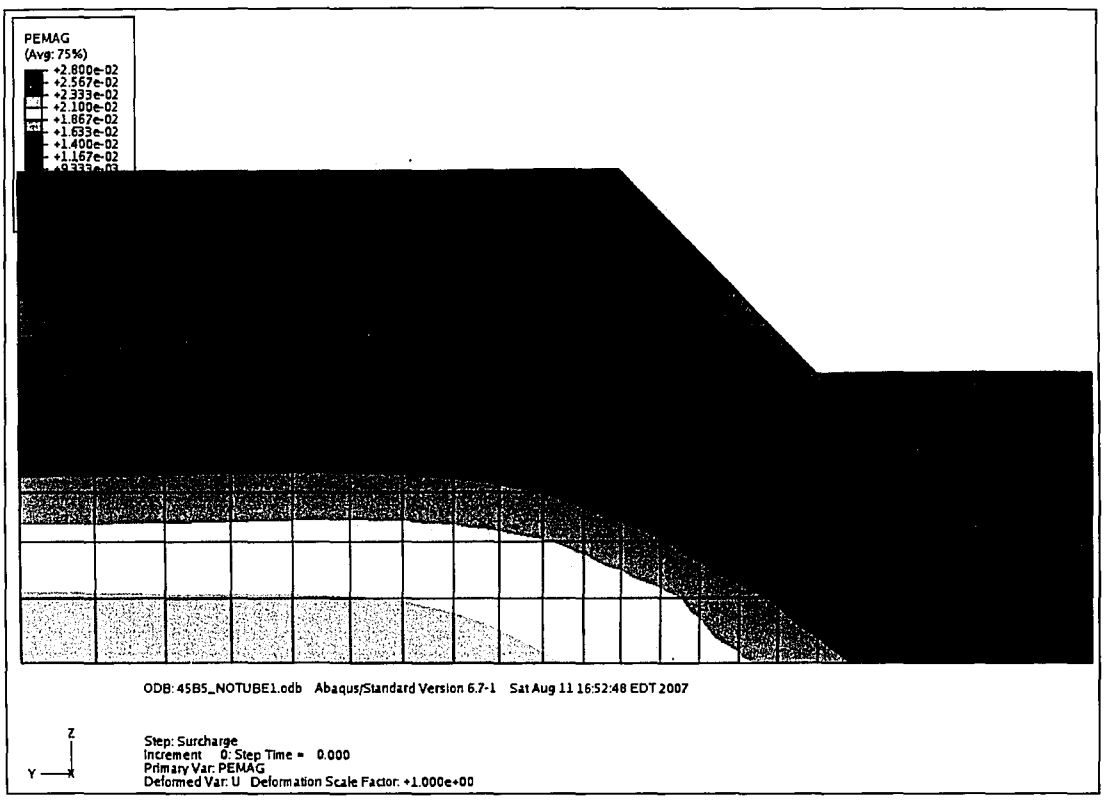

Figure 6.4.2.4. Plastic strain magnitudes for 45 degree stable slope without tubes.

Figures 6.4.2.4 and 6.4.2.5 compare plastic strain magnitude distributions for models of design 4, with and without tubes loaded with gravity.

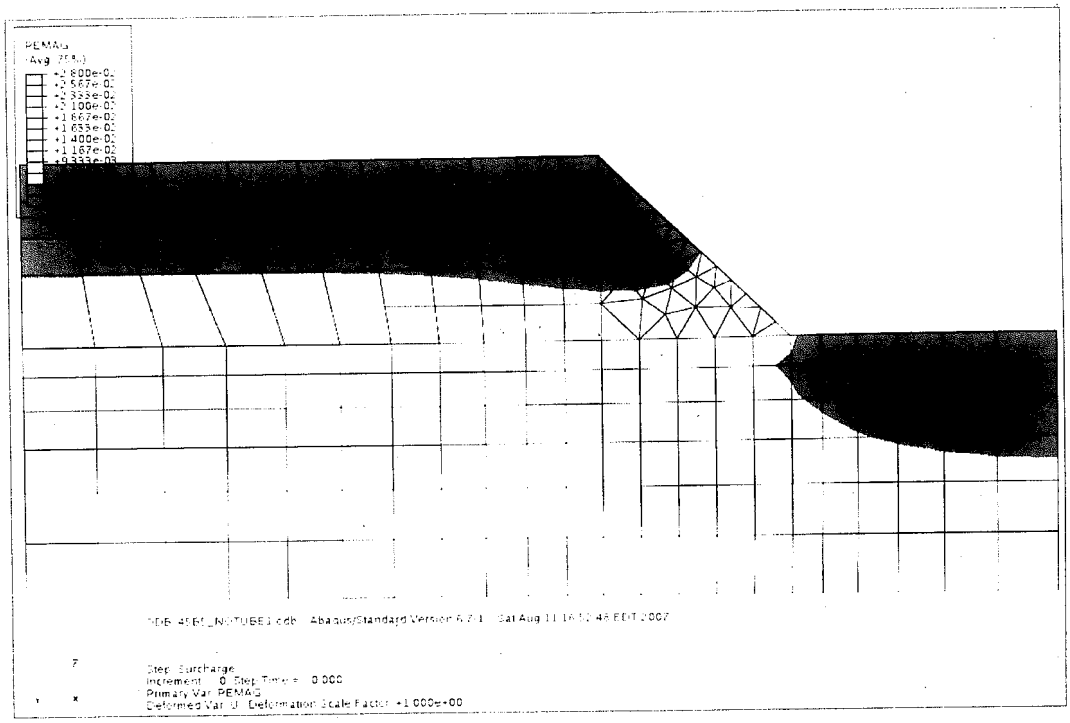

Figure 6.4.2.4. Plastic strain magnitudes for 45 degree stable slope without tubes.

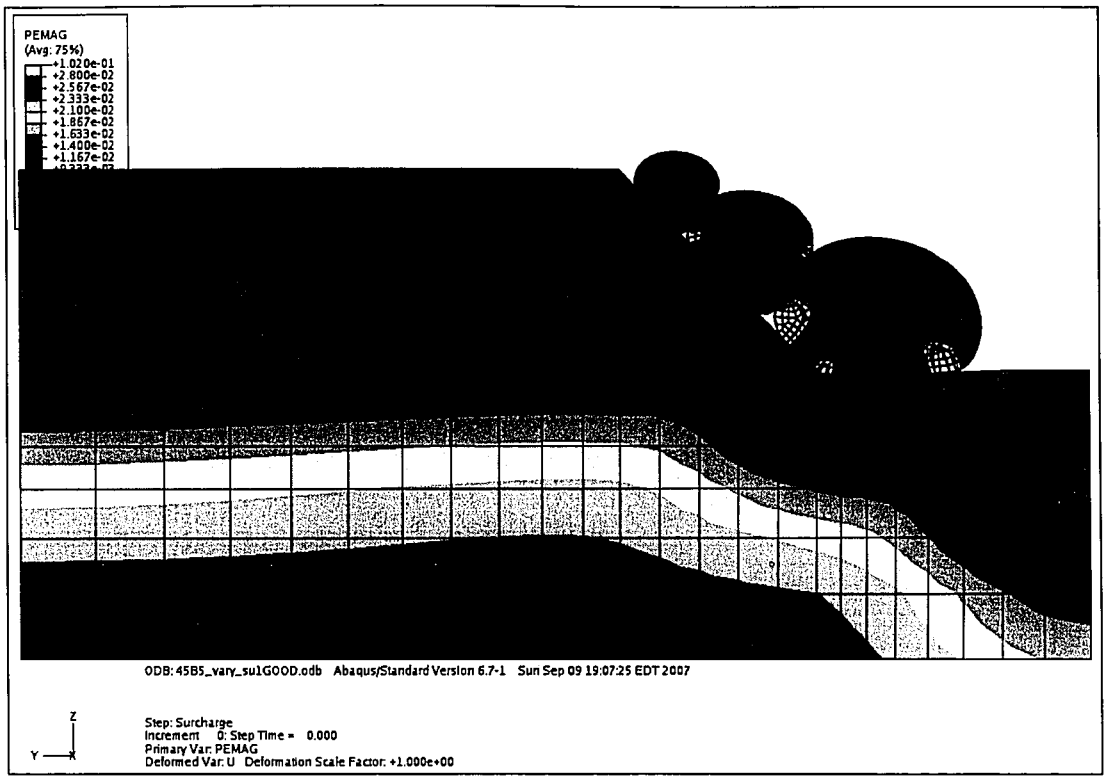

Figure 6.4.2.5. Plastic strain magnitudes for design 4 under gravity load.

According to Figures 6.4.2.4 and 6.4.2.5, the plastic strain magnitudes are slightly increased when the tubes are put in place. This indicates that tubes result in further instability.

The following are figures showing x-y shear stresses for design 4.

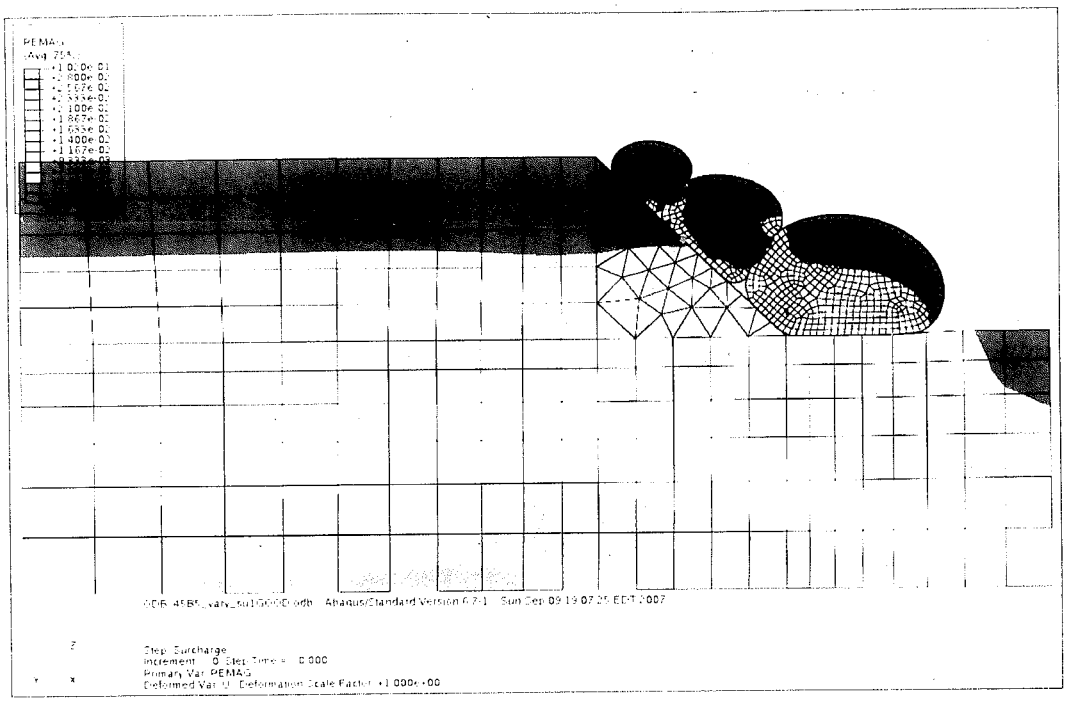

Figure 6.4.2.5. Plastic strain magnitudes for design 4 under gravity load.

According to Figures 6.4.2.4 and 6.4.2.5, the plastic strain magnitudes are slightly increased when the tubes are put in place. This indicates that tubes result in further instability.

The following are figures showing x-y shear stresses for design 4.

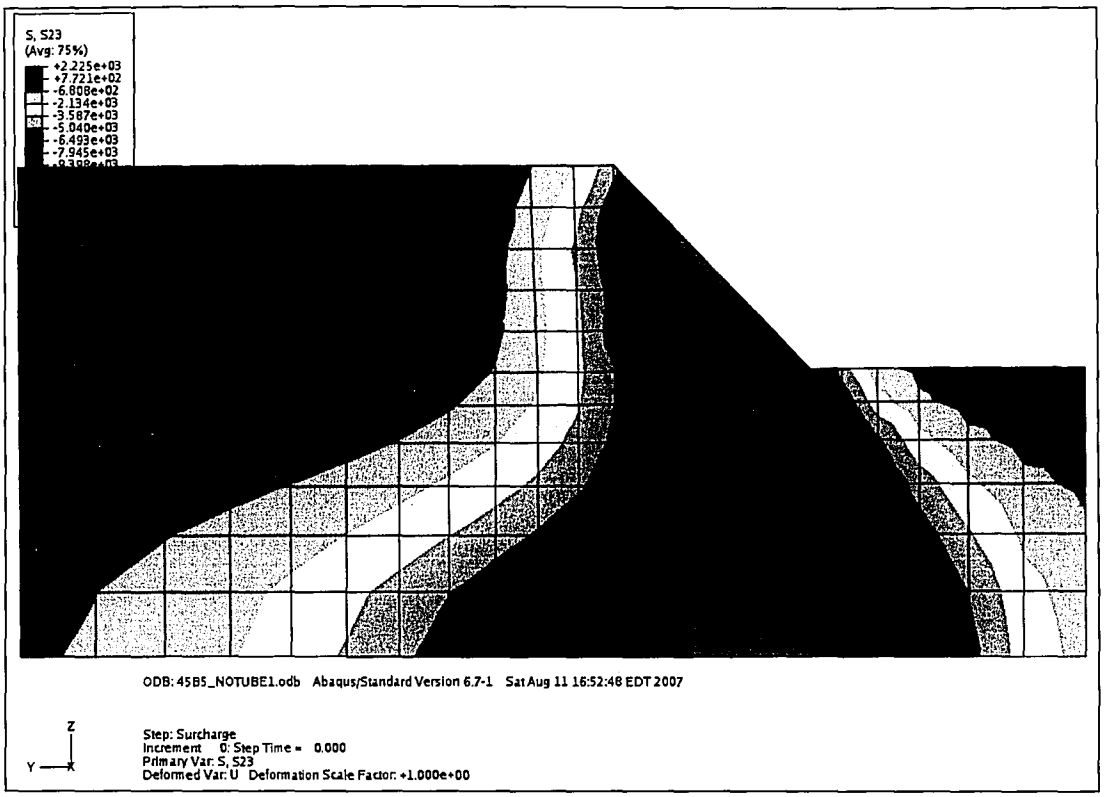

Figure 6.4.2.6. x-y shear stress contours for stable 45 degree slope.

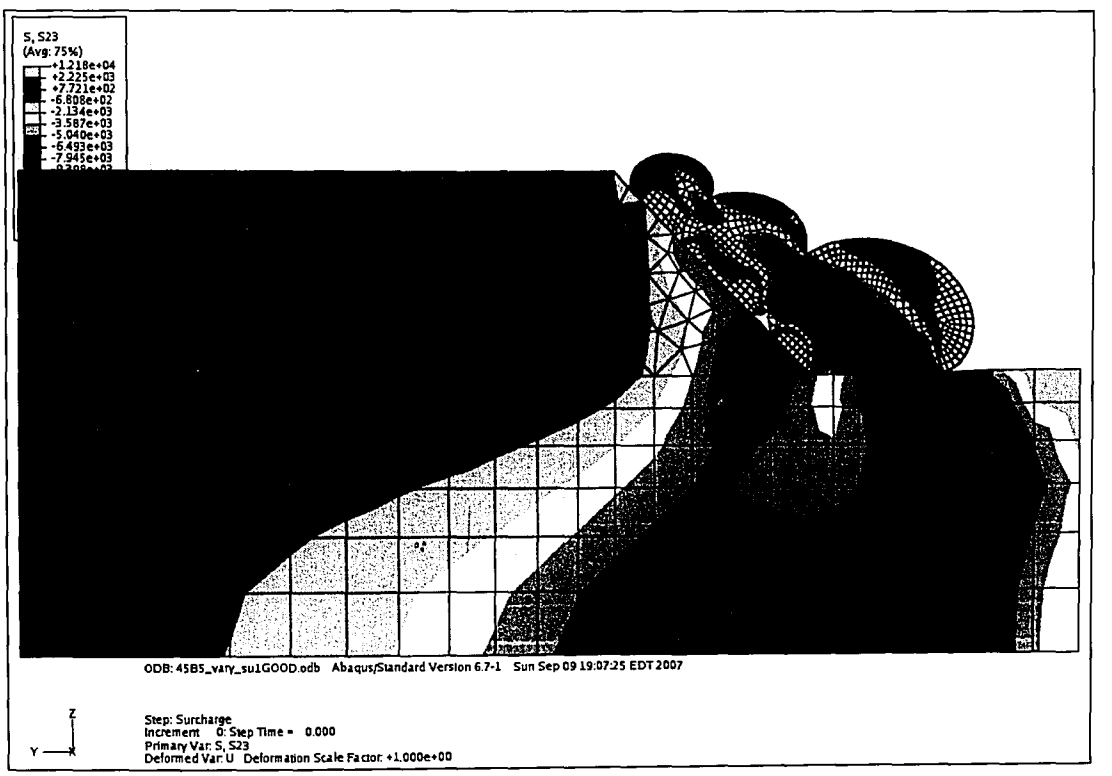

Figure 6.4.2.7. x-y shear stress contours for design 4.

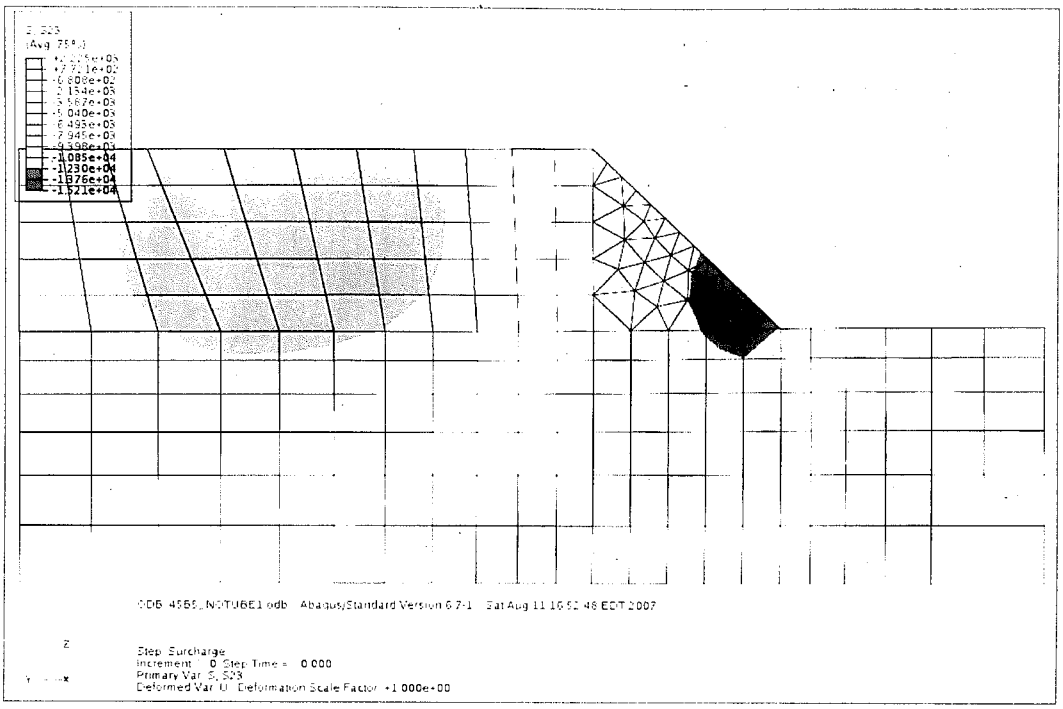

Figure 6.4.2.6. x-y shear stress contours for stable 45 degree slope.

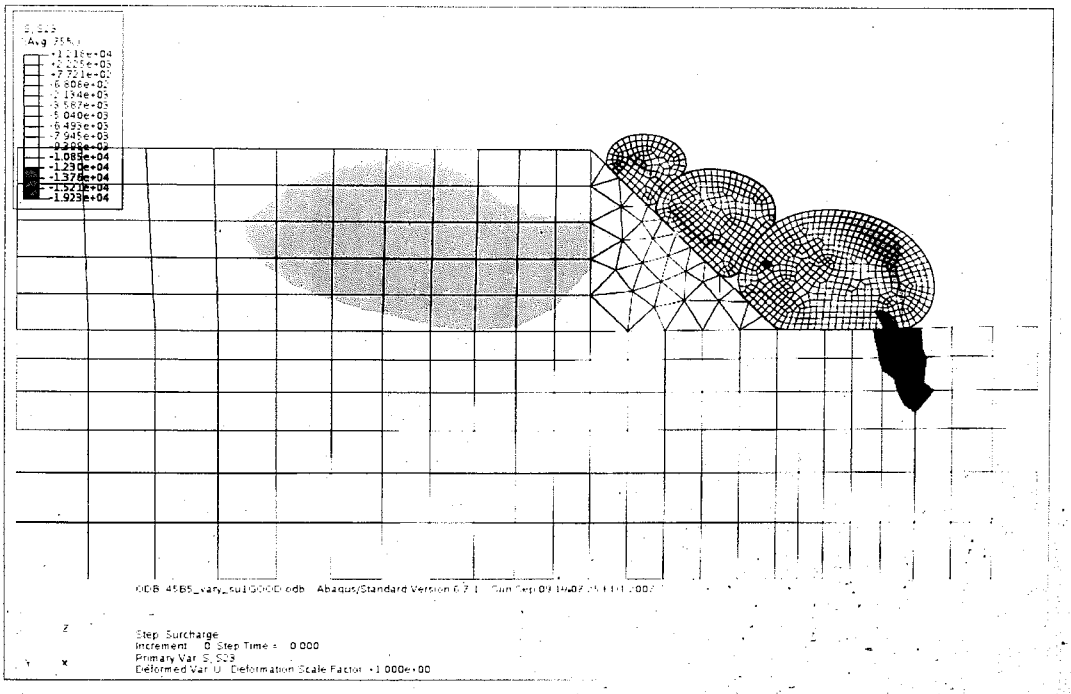

Figure 6.4.2.7. x-y shear stress contours for design 4.

According to Figures 6.4.2.6 and 6.4.2.7, design 4 improves the shear stresses around the slope. This was already shown with data in Table 6.4.2.1. Similar to the earlier models, a region below the bottom tube has an increase in shear stress due to the weight of the structure, but the stresses in the region behind the slope, particularly around the toe, are reduced. Higher plastic strains, higher movement, and lower shear stresses indicate that elastic strains are lower in the embankment for design 4. The deformation strain of the embankment is made up of elastic and plastic behaviour. Because the deformation is higher for design 4, the soil has yielded more causing plastic strains to increase.

Design 4, over all, can be considered a failure even though the stress state is reduced. The tubes cause the slope and structure to move as a whole to such an extent that in reality the slope would likely have failed.

6.5 Summary of Designs

Out of all of the designs investigated only design 1 appears to have improved slope stability. Design 1, however relied on an unrealistic restraint for the bottom tube. Based on results from all of the designs it appears that restraining lateral movement of the slope is just as important as minimizing vertical movement caused by the weight of the tubes. For a design to be successful in improving slope stability it must

have an effective method of restraining the bottom tube and each tube must be sized separately so that no tube is heavier than it has to be.

7 Consolidation

None of the models have considered consolidation behaviour of the material in the tubes. It is likely that consolidation would not only strengthen the tubes and the structure as a whole, but it would also alter the geometry. It was observed that if a fine-grained soil is used, tube height could be reduced by as much as 50% due to consolidation [15]. In this case, the tubes can be pumped full a second or third time to reach the desired height. On the other hand, it was stated that when sandy soils, with more than 50% of particles greater than sieve No. 200 were used in filling tubes, the desired tube height was achieved after pumping it full only once. The soil used in all of the ABAQUS models was based on Lebanon Sand [19] so it was assumed that the effects of including consolidation would be small. This was briefly investigated.

Consolidation behaviour was defined in ABAQUS and a short study was conducted on how this behaviour, if included, would affect the individual tubes' strength and deformation behavior. To model consolidation behaviour several new material properties were required. The permeability of the geo-textile was defined as 4×10^{-4} m/s [12]. This is a typical value for a non-woven needle punched geo-textile. An arbitrary value of 0.5 was selected as the initial void space ratio for geo-textile. A

three-dimensional pore pressure element was used in place of the three-dimensional stress element to model the soil within the tubes. In addition to the six displacement degrees of freedom, the pore pressure elements have a seventh degree of freedom for pore pressure.

The initial pore pressure was set as 12.36 kPa inside the tube. This is also the pumping pressure value that is used to inflate the membrane tubes in the sub-models. A pore pressure boundary condition is set at 12.36 kPa around the entire surface of the tube. The tube is first loaded with gravity. Next, in the consolidation step, the pore pressure boundary condition is reduced to zero effectively letting the pore pressure within the soil elements to dissipate therefore causing the tube contents to consolidate.

The first model was aimed only at observing the differences in geometry on a single tube that consolidation would cause. A model was created consisting of a single tube resting on a flat rigid surface (Figure 7.1). With the exception of including the consolidation behaviour, this tube had identical material properties and initial geometry as the tubes used in all other models. There were two load steps defined in the model: gravity and consolidation. The deformation caused by gravity alone would be representative of the behaviour of the tubes in all other models. The additional deformation as a result of consolidation would show how much of an effect it has on the tube geometry.

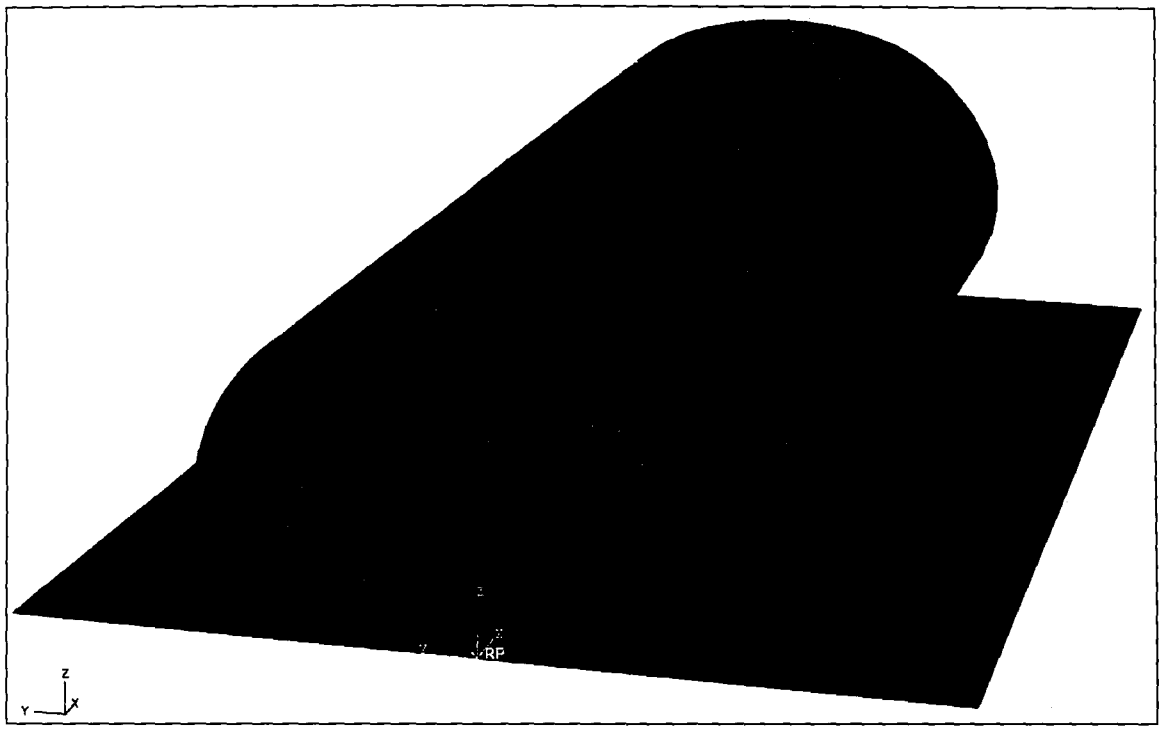

Figure 7.1. Consolidation model of single tube.

Deformations from both gravity and consolidation are small. Table 7.1 lists the height of the tube at the end of each load step.

Table 7.1. Tube Height in geometry consolidation model.

Step	Height (m)	Total Settlement (m)
Initial	1.402	--
Gravity	1.4	0.002
Consolidation	1.396	0.006

As indicated in Table 7.1, consolidation had a very small affect on geometry. The tube height is reduced by only 0.28%.

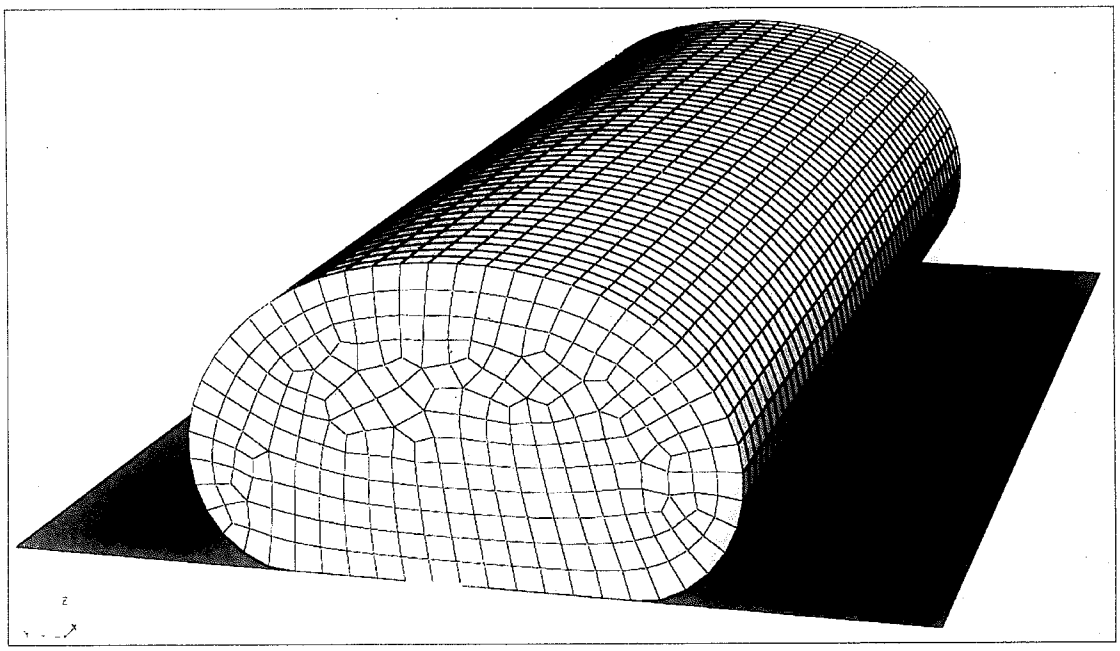

Figure 7.1. Consolidation model of single tube.

Deformations from both gravity and consolidation are small. Table 7.1 lists the height of the tube at the end of each load step.

Table 7.1. Tube Height in geometry consolidation model.

Step	Height (m)	Total Settlement (m)
Initial	1.402	--
Gravity	1.4	0.002
Consolidation	1.396	0.006

As indicated in Table 7.1, consolidation had a very small affect on geometry. The tube height is reduced by only 0.28%.

In order to investigate consolidation's effects on strength gain, two models, each consisting of two vertically stacked tubes was created. In one model no consolidation behaviour was defined and the stack was loaded with gravity one tube at a time, bottom tube first. In the other model, the bottom tube was allowed to consolidate before the gravity load on the top tube was applied. The weight of the top tube does not cause any further consolidation of the bottom tube in this model.

The material parameters and analysis procedures used to define the consolidation behaviour here were the same as the ones used in the first consolidation model aimed at investigating geometry changes. The goal of these two stacks was to observe the difference in strain that the bottom tube underwent when loaded by the top tube.

When observing strain behaviour it is useful to separate elastic and plastic strains. This allows one to see what type of yielding is occurring and how that yield surface may have moved due to consolidation. Figures 7.2 and 7.3 show maximum elastic strain contours in the tube stack. It is immediately clear that the strains in the consolidated tube are smaller than those in the unconsolidated tube. The maximum value seen in the centre of the unconsolidated tube is approximately 0.0028. The strain in the centre of the consolidated tube is around 0.0020. This is a 28 % difference. This is an indication that the consolidated tube could be up to 28% stiffer than the unconsolidated tube in certain regions.

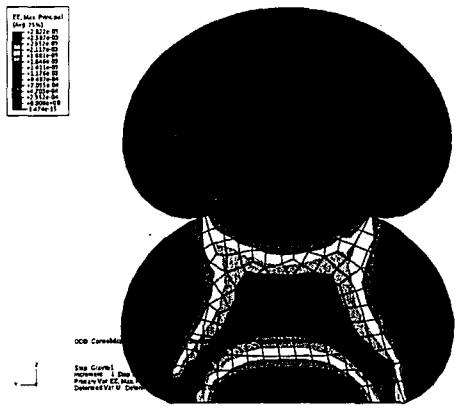

Figure 7.2. Elastic stains w/o Consolidation.

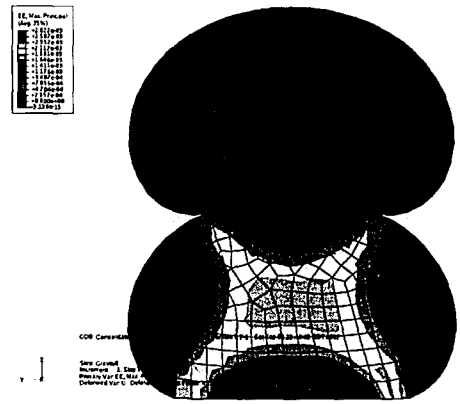

Figure 7.3. Elastic stains w/Consolidation.

After comparing the elastic strains, it is useful to also look at plastic strains. Figures 7.4 and 7.5 show maximum principle plastic strains in the tube stack. Again, it is clear right away that the unconsolidated tube has higher strains, particularly in the central region of the tube, as were the elastic strains. The maximum strain in the centre of the unconsolidated tube is approximately 0.015 and whereas the plastic strain in the centre of the consolidated tube is 0.008. This is a 53% difference.

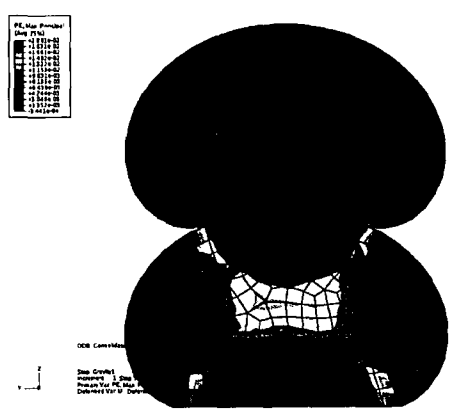

Figure 7.4. Plastic stains w/o Consolidation.

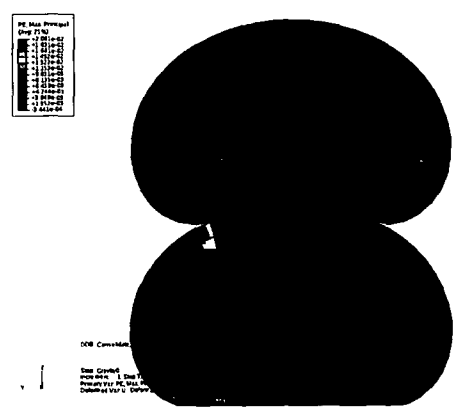

Figure 7.5. Plastic stains w/Consolidation.

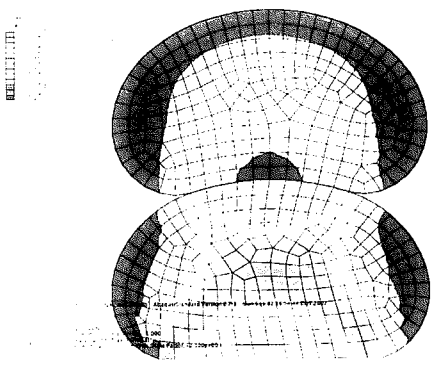

Figure 7.2. Elastic stains w o Consolidation.

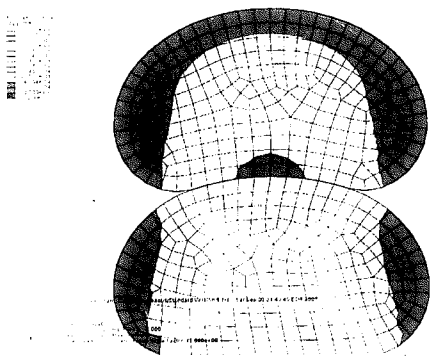

Figure 7.3. Elastic stains w Consolidation.

After comparing the elastic strains, it is useful to also look at plastic strains. Figures 7.4 and 7.5 show maximum principle plastic strains in the tube stack. Again, it is clear right away that the unconsolidated tube has higher strains, particularly in the central region of the tube, as were the elastic strains. The maximum strain in the centre of the unconsolidated tube is approximately 0.015 and whereas the plastic strain in the centre of the consolidated tube is 0.008. This is a 53% difference.

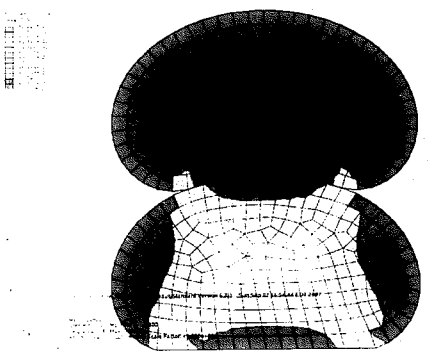

Figure 7.4. Plastic stains w o Consolidation.

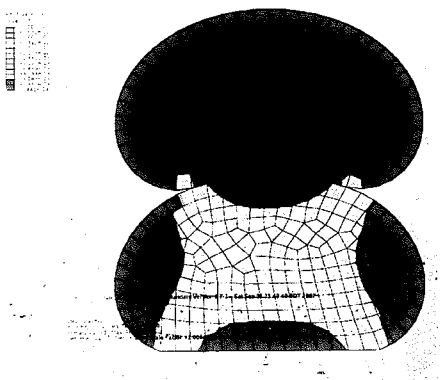

Figure 7.5. Plastic stains w Consolidation.

8 Conclusions

The primary goal of this research was to establish the necessary techniques needed to develop preliminary representative finite element models of stacked geotextile tubes as a soil retention structure. The goal was achieved by developing the following stepwise approach:

- Use of "sub-models" to build the final model. This allowed the final model to account for different phases with different behaviour in the tubes' construction. Past models have only considered either the liquid or solid form of the tube.
- Use of a multiple step-loading scheme. The appropriate loads were applied one by one in a particular order to capture the impact of actual in field processes. The order of the steps, combined with the boundary conditions, provides the numeric stability required by the ABAQUS solver. This was particularly important when using membrane elements.

The secondary goal of this model was to develop a three-tube stack formation design of geo-tubes as a slope stabilization structure. Multiple slope angles and surcharge load proximities were also considered. The results of these models do not directly incorporate a particular criterion for failure. Instead, the results of models of slopes with the tube stack and models of slopes without tubes that have a safety factor equal to one are compared .

The deformation behaviour of embankments with geotubes on them was different from the stable models without tubes. The effects the different stack designs had on the embankments were shown and the possible causes of slope stability or instability due to the geo-tubes were explored in discussion.

Design 1 reduced lateral movement of the slope as well as internal stresses and strains in the embankment. The problem with this design was that a flat rigid wall against the bottom tube, designed to prevent the bottom tube's lateral motion, was not realistic and would be impractical for construction. Design 1 did improve the slope's stability by reducing its lateral motion.

Design 2 consisted of the same stack as design one, but instead of a rigid wall restraining the bottom tube, a geotextile blanket was attached to the bottom tube and run up the slope underneath the other tubes. This design proved to be too challenging for accurate modelling with finite elements.

Design 3 used evenly spaced stakes to replace the rigid wall from design 1. Much data was collected on the performance of this design for two slope angles and various surcharge loads. It was observed that the stakes were much less effective at restraining the movement of the bottom tube. Because of this and the mass of the top two tubes, the embankment appeared to deform more with the tubes in place than without due to the excessive weight of the tubes. The x-y shear stresses and plastic strains were slightly reduced, in areas directly behind the slope surface.

Design 4 was intended to solve the problem of the top two tubes weighing down on the slope and causing more deformation by reducing their size. In order to model three tubes reaching the same height as design three, the bottom tube's size had to be increased disproportionately. This increase in mass of the bottom tube provided enough resistance to keep the stack stable without the stakes. The problem was that it was so massive that it caused higher vertical deformation. It was observed that vertical deformation coupled strongly with lateral movement, resulting in the entire slope deforming even more than that of design 3. Plastic strain was also higher.

Two models were created aimed at investigating the effects of consolidation behaviour of the geo-tube soil. These models showed that consolidation would have a minimal impact on tube geometry, less than 1%, but that it did noticeably reduce elastic and plastic strains within the tubes, increasing the tube strength. Overall, the effects were small enough that the initial assumption that consolidation would have little impact on model results was a valid one.

More work is needed to perfect a design. Design 4, even though leading to failure, indicates promise. It makes sense that the tubes should get smaller as they go up the slope not only to reduce the load on the slope and tubes below, but also because they are supporting less soil. The fact that the bottom tube did not need to be restrained by an outside component is also promising as it indicates a more stable structure. An improvement to design 4 might be using four tubes with the bottom tube restrained

by stakes. This would minimize weight on the upper half of the slope and reduce the size of the bottom tube needed for the structure to reach the required height.

An alternative perspective is to expect controlled slope deformation under the geo-tubes, so long the stability of the tube structure itself is not compromised. Overall, while the shear strength of the embankment may have been exceeded and there may have been plastic deformation, the slope will remain intact under the tube structure. It will still be underneath the stack of tubes and the tubes will not have slid away or overturned. In effect, the structure causes the embankment to re-establish a new state that is more stable. This theory would require a physical model to verify.

Finite element modelling has proven to be very useful tool as small design modifications can be made relatively quickly and their effects can be observed soon after. There are a number of modelling improvements that can be made in future work. The behaviour of the geotextile skin could be improved. The skin modelled here is, in effect, "bonded" to the surface of the solid tubes. In reality, the geotextile is a separate component of the tube interacting with the soil inside primarily through friction. The impact of this on geometry and stability is not known.

Modelling of the components restraining the bottom tube can also be improved. Deformable material embedded in the foundation would show realistic behaviour. It would eliminate the need for the assumption that they would not move when loaded. It would also allow for specific designs for these components to be developed.

Another aspect that could be improved lies in the interpretation of the results. If stress and strain results from the cap plasticity model could be directly input to a failure model, a better knowledge of the slope stability could be gained. This would allow a factor of safety to be assigned to any embankment with tubes on it, hence greatly improve the design process as it could be determined quickly and decisively whether or not the structure improves the slope's stability.

Vita

Mark Wayne McElroy Jr. was born May 10, 1983 in Wilmington, DE. The names of his parents are Mark Wayne McElroy Sr. and Amy Boyer McElroy. He graduated from Lehigh University in Bethlehem, PA with a Bachelor of Science in Civil Engineering in 2006. In January 2008 he received a Master of Science in Civil Engineering from Lehigh University. After completing graduate work in 2007, Mark will begin working as a structural engineer for Northrop Grumman at the Newport News Shipyard in Newport News, VA.

Cited References

[1] Adel, H. den, Hendrikse, C.S.H., Pilarczyk, K. (1996). "Design and Application of Geotubes and Geocontainers." *Geosynthetics: Applications, Design and Construction.* De Groot, Den Hoedt, & Termat (eds.). Balkema, Rotterdam.

[2] AASHTO. Standard Specifications for Highway Bridges, 17th Edition. Section 5.5.2, pg. 122. 2002.

[3] Breteler, M. and Pilarczyk, K. (1998). Dikes and Revetments. Chap. 16, "Alternative Revetments." A.A. Balkema, Rotterdam.

[4] Breteler, M.K., van Wijhe, H.J. (1994). "Stability of Geotubes and Geocontainers." *Report H 2029.* Delft Hydraulics, August.

[5] Cantre, S. (2002). "Geotextile Tubes-Analytical Design Aspects." *Geotextiles and Geomembranes*, Vol. 20, 305-319.

[6] Carroll, R.P. (1994) "Submerged Geotextile Flexible Forms Using Noncircular Cylindrical Shapes." *Geotechnical Fabrics Report*, Industrial Fabrics Association International, St. Paul, MN, 12(8), 4-15.

[7] Erchinger, H.F. "Geotextile Tubes Filled With Sand for Beach Erosion Control, North Sea Coast, Germany." *International Society For Soil Mechanics And Geotechnical Engineering, Committee TC9 – Geosynthetics Case Histories.* 102-103.

[8] "Geotube ® Brand Structures in Marine Engineering." Tencate Geotube ®. <http://www.geotubes.com/marine/marine_index.html>.

[9] Heerten, G., Jackson, A., Restall, S., Stelljes, K. (2000) "Environmental Benefits of Sand Filled Geotextile Structures for Coastal Protection." /International conference on geotechnical and geological engineering; GeoEng 2000, /November 19-24, Melbourne, Australia, Lancaster, v.2, 263.

[10] Kazimierowicz, K. (1994). "Simple Analysis of Deformation of Sand Sausages." *Fifth International Conference on Geotextiles, Geomembranes, and Related Products*, Singapore, 5-9 September. 775-778.

[11] Klusman, C. (1998). Two-Dimensional Analysis of Stacked Geosynthetic Tubes. Virginia Technical Institute. <http://scholar.lib.vt.edu/theses/available/etd-100698-115701/>.

[12] Koerner, R. Designing With Geosynthetics, Fifth Edition. Upper Saddle River, NJ: Pearson Prentice Hall, 2005.

[13] Landis, K. (2000). "Control Floods with Geotextile Cofferdams." *Geotechnical Fabrics Report*, Vol. 18, No. 3, 24-29.

[14] Leshchinsky, D. and Leshchinsky, O. (1996). "Geosynthetic Confined Pressurized Slurry (GeoCoPS): Supplimental Notes for Version 1.0," *Report TR CPAR-GL-96-1*, U.S. Army Corps of Engineers Waterways Experimental Station, Vicksburg, MS.

[15] Leshchinsky, D., Leshchinsky, O., Ling, H.I., and Gilbert, P.A. (1996). "Geosynthetic Tubes for Confining Pressurized Slurry: Some Design Aspects," *Journal of Geotechnical Engineering*, ASCE, Vol. 122, No. 8, 682-690.

[16] Liu, G.S. (1981). "Design Criteria of Sand Sausages for Beach Defenses." *International Association for Hydraulic Research: Summaries of Papers Proceedings*, New Dehli, India, 123-131.

[17] Moler, M., Freeman, M., Filz, G., Plaut, R. (2001). Pilot-Scale Test of Stacked Three-Tube Configuration of Water-Filled Tubs for Resisting Floodwaters. Virginia Technical Institute, Blacksburg, Virginia.

[18] Seay, Patricia, (1998). FiniteElement Analysis of Geotextile Tubes. Virginia Technical Institute. <http://scholar.lib.vt.edu/theses/available/etd-31498-131543/>.

[19] Shoop, S., Affleck, R., Janoo, V., Haehnel, R., Barrett, B. (2005). "Constitutive Model for a Thawing, Frost-Suseptible Sand." ERDC-CRREL TR-05-3, U.S. Army Cold Regions Research and Engineering Laboratory, Hanover, New Hampshire.

[20] Silvester, R. (1986). "Use of Grout-Filled Sausages in Coastal Structures." *Journal of Waterway, Port, Coastal, and Ocean Engineering*, 112(1), 95-114.

[21] Spelt, K. (2001) "Geotubes as the Core of Guide Dams for Naviduct at Enkhuizen, The Netherlands." /*Terra et Aqua*/, 83, 21-25.

END OF TITLE